UNIVERSITY OF CALIFORNIA, SAN DIEGO

Insights into the functionality and targeting of PKA regulatory subunit RIalpha

A dissertation submitted in partial satisfaction of the
requirements for the degree Doctor of Philosophy

in

Bioinformatics

by

Michele Elizabeth Day

Committee in charge:

Professor Susan S. Taylor, Chair
Professor Lynn F. Ten Eyck, Co-Chair
Professor Vineet Bafna
Professor Paul A. Insel
Professor Nicholas J. Schork

2008

The Dissertation of Michele Elizabeth Day is approved, and it is acceptable in quality and form for publication on microfilm and electronically:

_____

_____

_____

_____

Co-Chair

_____

Chair

University of California, San Diego

2008

DEDICATION

To my mom and brother.

And to my dad,

our guardian angel,

for whom I finished my degree.

TABLE OF CONTENTS

ABBREVIATIONS

AKAP. A-Kinase Anchoring Protein.

AKAR. A-Kinase Activity Reporter.

AKB. A-Kinase Binding domain.

AIF. Apoptosis-inducing factor.

ATP. Adenosine triphosphate.

Bis-Tris. Bis(2-hydroxyethyl)-imino-tris(hydroxymethyl)-methane.

BSA. Bovine serum albumin.

CBD. cAMP binding domain.

C-subunit. Catalytic subunit of PKA.

C-terminus. Carboxy-terminus.

cAMP. Adenosine 3',5'-Cyclic Monophosphate.

cGMP. Guanosine 3',5'-Cyclic Mononucleotide.

C. elegans. *Caenorhabditis elegans.*

CNC. Carney complex.

D-AKAP1. Dual A-Kinase Anchoring Protein-1.

D-AKAP2. Dual A-Kinase Anchoring Protein-2.

D/D. Dimerization/Docking domain.

Diamide. Diazene dicarboxylic acid bis-(*N,N*-dimethylamide).

DMEM. Dulbecco's Modified Eagle Medium.

DTT. Dithiothreitol.

E. coli. *Escherichia coli.*

EDTA. Ethylene diamine tetraacetic acid.

EEA1. Early endosomal antigen 1.

EGF. Epidermal growth factor.

EGTA. Ethylene glycol tetraacetic acid.

ER. Endoplasmic Reticulum.

FPLC. Fast Protein Liquid Chromatography.

GFP. Green fluorescent protein.

HEK 293. Human embryonic kidney 293 cells.

hnRNP. Heterogeneous nuclear ribonucleoproteins.

HPLC. High-pressure Liquid Chromatography.

Hsp90. Heat shock protein 90.

Ht31. Human Thyroid Anchoring Protein 31.

IBMX. Isobutylmethylxanthine.

IPTG. Isopropyl-β-D-thiogalactopyranoside.

IS. Inhibitor site.

kDa. Kilodaltons.

LB. Luria-Bertani broth.

LC3. Microtubule-associated protein 1A/1B-light chain 3.

LDH. Lactate dehydrogenase.

LTQ. Linear Trap Quadruple.

MEF. Mouse embryonic fibroblast.

MES. 2-(*N*-morpholino)ethanesulfonic acid.

$MgCl_2$. Magnesium chloride.

mRNA. Messenger Ribonucleic Acid.

MS. Mass Spectrometry.

mTOR. Mammalian Target of Rapamycin.

N-terminus. Amino-terminus.

NaCl. Sodium Chloride

NEM. N-ethylmaleimide.

NADH. Nicotinamide adenine dinucleotide.

NMR. Nuclear Magnetic Resonance.

NP-40. Nonidet P-40.

PARP. Poly (ADP-ribose) polymerase.

PBC. Phosphate binding cassette.

PBS. Phosphate Buffered Solution.

PBST. Phosphate Buffered Solution Tween-20

PDB. Protein Data Bank.

PKA. Protein Kinase A or cyclic AMP-Dependent Protein Kinase

PKI. Protein Kinase Inhibitor.

PMP70. 70-kDa peroxisomal membrane protein.

PP1. Protein Phosphatase 1.

PRKX. Protein kinase X.

PSC. Premature stop codon.

RFC 40. Replication Factor C 40.

RSK. p90 ribosomal S6 kinase.

R subunit. Regulatory subunit of PKA.

SDS-PAGE. Sodium dodecyl sulfate polyacrylamide gel electrophoresis.

SH3. Src-Homology 3 domain.

TAP. Tandem affinity purification.

TBS. Tris Buffered Saline.

TBST. Tris Buffered Saline Tween-20

Tris. Tris(hydroxymethyl)aminoethane.

YT. Yeast-tryptone broth.

LIST OF FIGURES

LIST OF TABLES

ACKNOWLEDGEMENTS

I would like to thank my advisor, Dr. Susan Taylor, for allowing me to work in her lab during my graduate career. Her high expectations motivated me to work diligently and think critically, allowing me to blossom as a scientist. Though at times it was difficult to meet her requirement of biweekly meetings, I thank her for forcing me to maintain up-to-date analyses of my data and figures because it made the writing process easier. I also want to thank Susan for providing input and editing several drafts of my dissertation.

I would like to thank my co-advisor, Dr. Lynn Ten Eyck. His open door policy encouraged me to discuss both work and personal issues freely. He always showed great support and optimism. I wish to express gratitude to the rest of my committee: Dr. Vineet Bafna, who provided insight and advice on the analysis of the mass spectrometry data; Dr. Paul Insel, who helped greatly with analysis of the cell biology portion; and Dr. Nicholas Schork, whose discussions helped me to see the meaning behind my work and its implications in the big picture. I also thank my committee for being readily accessible for multiple meetings throughout the years.

Much of this work could not have been possible without the help from others as well. I express the most gratitude to my baymate and mentor, Mira Sastri. She often put her own work aside to help me analyze and understand my data and to think about the next experiment. She also taught me a lot of the techniques used throughout my dissertation. Aside from work, she often gave me perspective through the tough times. I also thank Toni Koller, who often supported me in my meetings and helped to

troubleshoot much of the work in Chapters 3 and 4. Toni also ran all of the samples for mass spectrometry analysis, discussed in Chapters 2, 3, and 4. I thank Guido Gaietta for his cell biology expertise and for helping me make the live cell movies and taking the confocal pictures in Chapter 5. I appreciate the time Mason Mackey spent searching for that one correlated cell and for taking the EM pictures in Chapter 5. I am grateful to Guy Perkins for his analysis of the EM pictures and pointing out multivesicular bodies. I thank Dennis Young at the UCSD Cancer Center Flow Cytometry Shared Resource for help with the cell cycle analysis in Chapter 6.

Many people who cannot be forgotten provided great moral support and/or insight on my work (though apologies to anyone I did forget to include): CJ, Ganesh A., David B., Angie, Jaume, Peter, Manjula, Mike D., Chris E., Sarma, Nina, Ken, Ganesh I., Francis, Mike K., Frank, Rebecca, Robert, Tim, Jon, Elaine, Sventja, Jian, and Jie. Special thanks to Gary Thompson who always saw the best in me and kept me company during late nights in the lab on countless occasions. I also thank Carolyn Huttenmaier, Jan Lenington, Mary Ellen Perry, and Juniper Pennypacker for their encouraging words along with their administrative assistance.

Much appreciation to people that helped with proofreading portions, if not most, of the dissertation: Ken Humphries, Mira, Chris Eggers, Chris Benner, Jie Yang, Kasey Hutt, Guido, and Mason. Thanks to Kristine Briedis for help with formatting.

Of course, life is not all work and no play. Thanks to the many friends outside of work who made life fun throughout the years: Alix, Rita, Kasey, Kristine, Eugene, Neha, Lydia, Coleman, Rebecca, Sventja, Mira, and Manjula.

Most importantly, I want to thank the people in my life who continually show unconditional love and support that make me smile everyday: Mom, Dad, little brother, David, and boyfriend, Chris Benner. My parents, who always believed in me, inspired me to pursue a higher education beyond college and taught me to be optimistic in any situation. My brother, David, takes the role of an older brother by watching out for me and pampering me whenever he's around. Though often unspoken, I appreciate my little Chris for letting me take out my frustrations on him so that I maintained composure in front of everyone else.

Chapters 2 and 3, in part, will be submitted for publication. Day, M.E., Koller, A., and Taylor, S.S. Analysis of disulfide bonds in PKA RIalpha dimers reveals the loss of wild-type RIalpha homodimers in the presence of Carney complex-associated mutant RIalpha. The dissertation author was the primary investigator and author of this work.

Chapter 4, in part, will be submitted for publication. Day, M.E., Koller, A., Sastri, M., and Taylor, S.S. AKAP220 is a dual A-kinase anchoring protein with high affinity for the RIalpha subunit of PKA. The dissertation author was the primary investigator and author of this work.

Chapter 5, in part, will be submitted for publication. Day, M.E., Gaietta, G., Mackey, M., Perkins, G., and Taylor, S.S. Novel targeting of the RIalpha subunit of PKA, disassociated from C-subunit, is mediated by protein kinase anchoring proteins. The dissertation author was the primary investigator and author of this work.

VITA

2001 B.A., Molecular & Cell Biology – Biochemistry & Molecular Biology, University of California, Berkeley. Berkeley, California

2004 Teaching Assistant, BIMM 184 Computational Molecular Biology, University of California, San Diego. La Jolla, California

2006 Teaching Assistant, BENG 203 Genetic Circuits and Modeling Pathways, University of California, San Diego. La Jolla, California

2008 Ph.D., Bioinformatics, University of California, San Diego. La Jolla, California

PUBLICATIONS

Day, M.E., Koller, A., and Taylor, S.S. *Analysis of disulfide bonds in PKA RIalpha dimers reveals the loss of wild-type RIalpha homodimers in the presence of Carney complex-associated mutant RIalpha*. (Manuscript in preparation)

Day, M.E., Koller, A., Sastri, M., and Taylor, S.S. *AKAP220 is a dual A-kinase anchoring protein with high affinity for the RIalpha subunit of PKA*. (Manuscript in preparation)

Day, M.E., Gaietta, G., Mackey, M., Perkins, G., and Taylor, S.S., *Novel targeting of the RIalpha subunit of PKA, disassociated from C-subunit, is mediated by protein kinase anchoring proteins*. (Manuscript in preparation)

Conference Posters

Day, M., Koller, A., Kannan, N., and Taylor, S.S., *A PKA "SNP"et – Regulation to Disease.* FASEB Summer Research Conference, 2007.

Day, M., Koller, A., Kinderman, F., and Taylor, S.S., *Deciphering the Role of Disulfide Bonds in RIalpha*. Experimental Biology Conference, 2008.

ABSTRACT OF THE DISSERTATION

Insights into the functionality and targeting of PKA regulatory subunit RIalpha

by

Michele Elizabeth Day

Doctor of Philosophy in Bioinformatics

University of California, San Diego, 2008

Professor Susan S. Taylor, Chair

Professor Lynn F. Ten Eyck, Co-Chair

Regulatory subunits (R) of cAMP-dependent protein kinase (PKA) are differentially expressed and carry out various functions. Two general classes exist, RI and RII, as well as α and β isoforms within each class. Though the four isoforms share the same general domain organization, they are not functionally redundant. RIα is embryonically lethal in mice and cannot be compensated for by the other R

isoforms. A change in RIα expression levels, higher or lower, is implicated in diseases, such as Carney complex (CNC).

CNC is an autosomal dominant syndrome that is associated with RIα mutations, most of which are not expressed, resulting in a haploinsufficiency of RIα. I studied two mutations among the few that do get expressed, RIα R74C and RIα(1-303). RIα R74C results in a mutation in the linker region, while RIα(1-303) results in a truncation in the cAMP binding domain. My goals were to characterize these mutants in *E. coli* (Chapter 2) and in mammalian cells (Chapters 3 and 5) and to search for novel binding partners of RIα (Chapter 4).

Purified RIα(1-303) showed a four-fold increase in PKA activation and RIα R74C dimers had a tendency to form disulfide-bonded tetramers. TAP-tagged constructs of RIα and RIα R74C were engineered and expressed in mammalian cells to make stable cell lines. Using diagonal gel electrophoresis, I showed that both constructs of TAP-tagged RIα formed heterodimers with endogenous RIα. No homodimers of endogenous RIα were observed when RIα R74C was expressed, which could explain the CNC phenotype. These stable cells were also used to study the RIα interactome. Using various affinity methods followed by mass spectrometry analysis, I discovered an A-kinase anchoring protein (AKAP), AKAP11, which binds with unusually high affinity to RIα.

When RIα was overexpressed, it formed puncta, which were dependent on the disassociation from C-subunit and were reversible. In addition, RI-specific AKAPs abolished the puncta formation. Using indirect immunofluorescence and correlated

light and electron microscopy, these puncta were found to localize to multivesicular bodies.

In summary, I have identified an effect on the interchain disulfide bonding in RIα, putative binding partners for RIα, as well as a novel way of targeting RIα.

Chapter 1:

Introduction

1.1: cAMP-dependent protein kinase

Eukaryotes have developed highly specific and exquisitely sensitive signal transduction systems by which external information, such as by hormones or growth factors, is converted into intracellular information that regulates the internal workings of the cell. One example that has been well-characterized, the cyclic AMP (cAMP)-dependent signaling pathway, serves as a paradigm of signal transduction. The identification of cAMP as a second messenger [1] subsequently led to the discovery of cAMP-dependent protein kinase (PKA) [2] with regulatory (R) subunits [3].

In the cAMP-dependent signaling pathway, extracellular ligands, such as adrenocorticotropin, glucagon and adrenaline, bind to G-protein coupled receptors, inducing a conformational change that activates the α subunit of G proteins via a GTP:GDP exchange mechanism. The GTP-bound activated α subunit binds to and activates adenylyl cyclase, which catalyzes the conversion of ATP to cAMP. Increases in cellular concentrations of cAMP directly activate PKA [Figure 1.1].

PKA is a serine/threonine kinase that recognizes the substrate consensus motif: R-R-X-S/T-Y, where X is any amino acid and Y is a large hydrophobic amino acid. PKA is known to phosphorylate a plethora of proteins and thus has several functions in the cell, including regulation of glycogen, sugar, and lipid metabolism. In its inactive state, it is a tetramer composed of dimeric R subunits bound to two catalytic subunits (C-subunits), also known as a holoenzyme. A-Kinase Anchoring Proteins (AKAPs) bind to the R subunits and target the holoenzyme and/or the free R subunit to distinct areas of the cell.

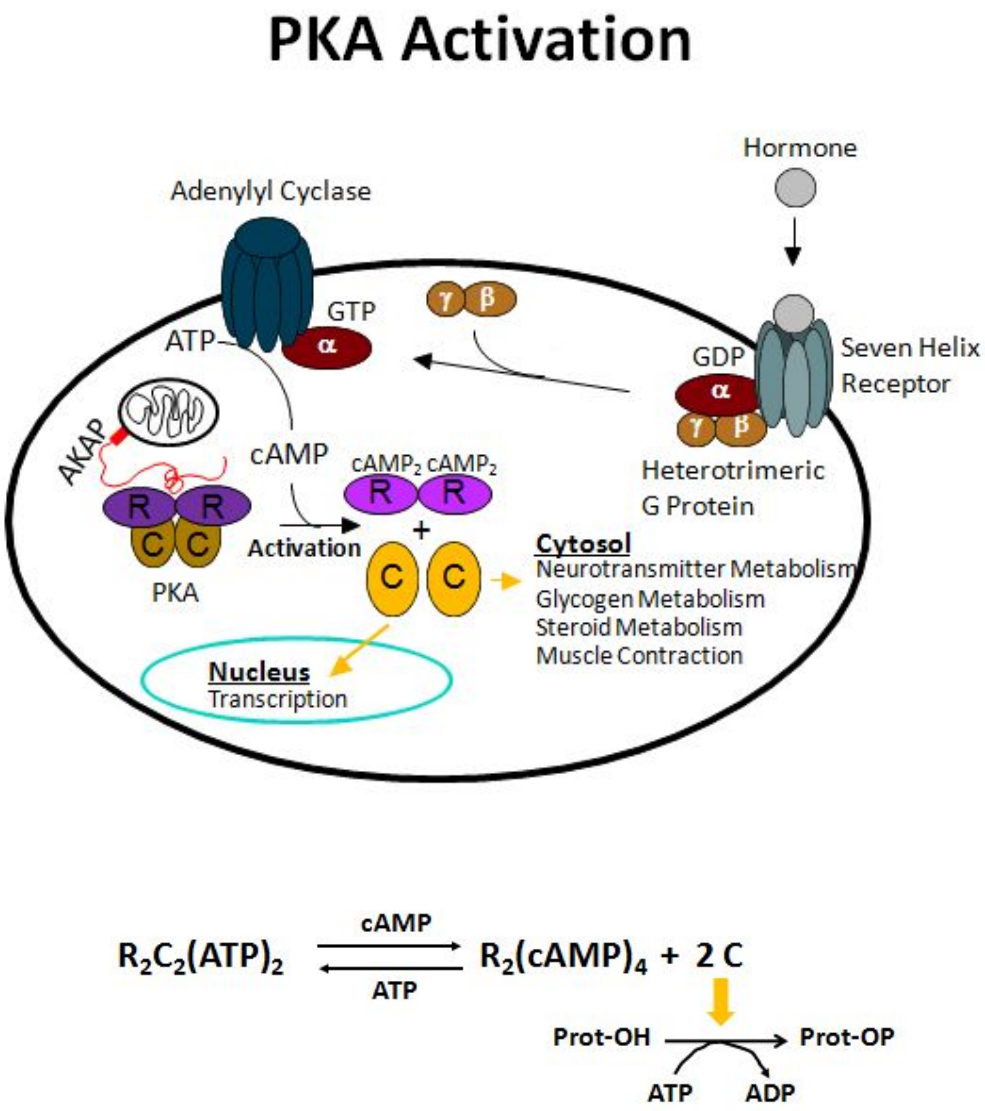

Figure 1.1: Increased levels of cAMP lead to the activation of PKA.

Extracellular signals, such as hormones, lead to the activation of adenylyl cyclase which results in increases in cellular levels of cAMP. In the inactive state, PKA consists of a holoenzyme complex of two R subunits (shown in purple) bound to two C-subunits (shown in yellow). The holoenzyme can be targeted to different subcellular locations through the binding of AKAPs (shown in red). cAMP bind to the R subunits and cause their disassociation from C-subunits. The released C-subunits phosphorylate their substrates (Prot-OH in the equation) in different parts of the cell. The regulation of PKA activation is summarized by the equation.

The allosteric activation of PKA is uniquely regulated by the inhibitory R subunits that are also the primary receptors for cAMP. In the absence of cAMP, each R subunit binds with high affinity to C-subunits and renders them inactive. In addition to being inhibited by R subunits, PKA is regulated in cells by the heat-stable protein kinase inhibitor (PKI), which is insensitive to cAMP [4]. When PKI, which also contains a nuclear export signal, binds with high affinity to the C-subunit, it actively transports the C-subunit out of the nucleus [5].

1.2: Regulatory subunit properties and differences

There exist two general classes of R subunits, RI and RII [6], which can be further resolved at the genetic level into four separate gene products: RIα [7], RIβ [8], RIIα [9], and RIIβ [10]. RI and RII share the same general domain structure: an N-terminal domain (D/D domain) which is required for dimerization and for docking to specific locations through AKAPs, followed by a disordered linker region that contains a C-subunit recognition site (IS), and finally two tandem and homologous cAMP-binding domains at the C-terminus [Figure 1.2].

Despite the shared domain structure and sequence similarities, there are significant differences between the R subunits. An evolutionary tree built from a multiple sequence alignment of the R isoforms clearly shows that the RI isoforms evolved differently from the RII isoforms [Figure 1.3]. The R isoforms differ in their localization in that the RI subunits are mainly found in the cytoplasm, whereas the RII subunits, which can bind to AKAPs with higher affinity, are typically localized in

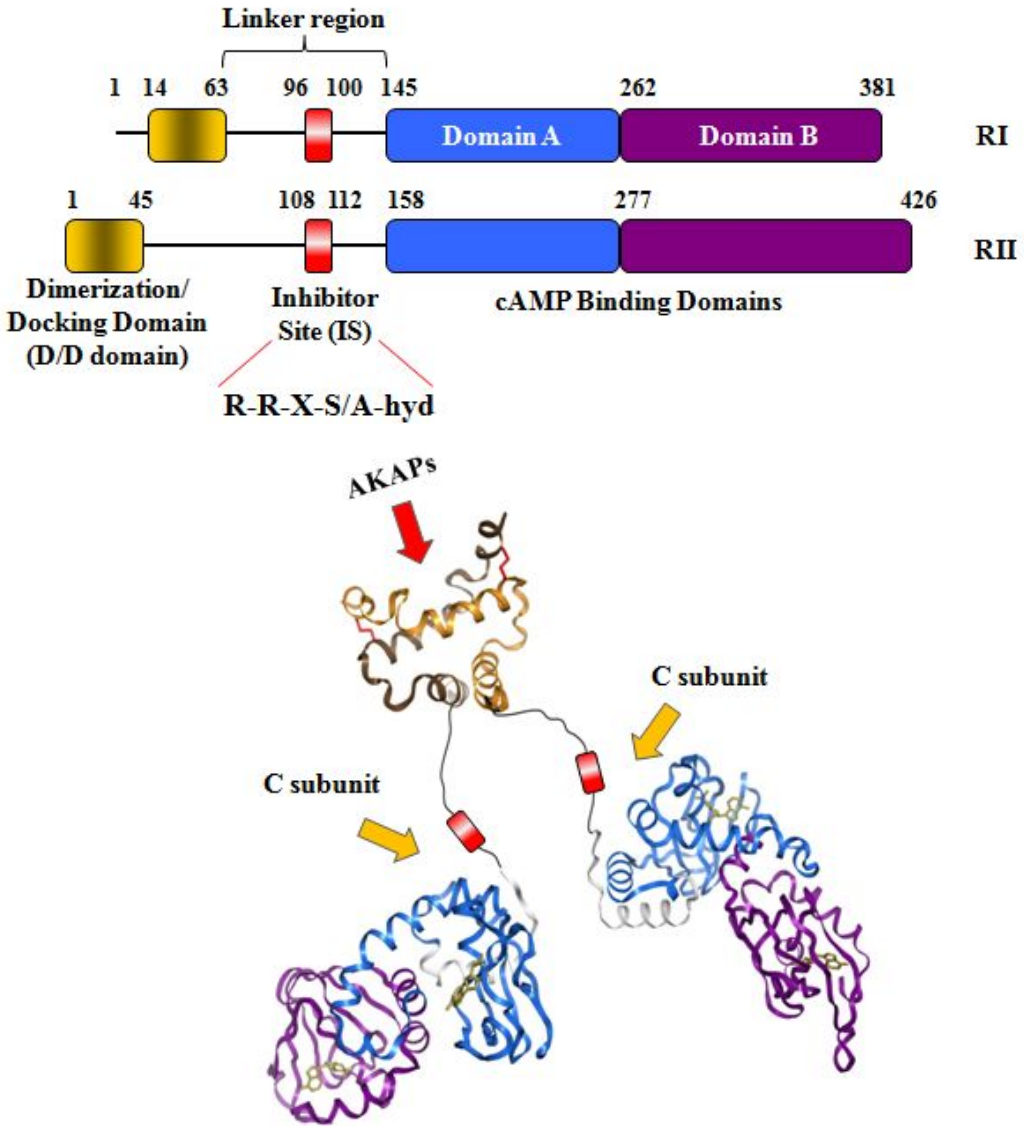

Figure 1.2: RI and RII subunits share similarities in sequence and domain organization.

RI and RII subunits share a similar domain organization with an N-terminal D/D domain (which bind to AKAPs) and two tandem cAMP binding domains (which bind to cAMP and C-subunit) at the C-terminus. A schematic representation of the spatial domains organization is illustrated in the bottom picture. The D/D domain [11] and cAMP binding domains [12] are separated by a linker region, which contains the inhibitor site (IS), shown in red. Typically RI is distinguished from RII by the PKA phosphorylation motif in the IS. In the RI isoforms, the site of phosphorylation is an alanine or glycine, making this segment a pseudosubstrate inhibitor. In the RII isoforms, this site is a serine that is phosphorylated by PKA and functions as a substrate inhibitor of PKA.

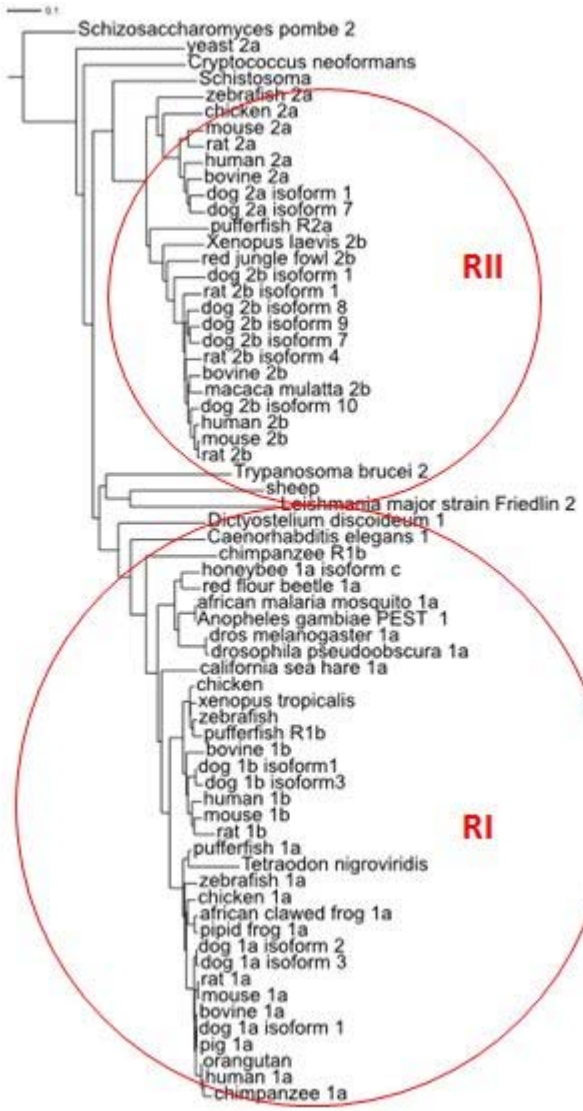

Figure 1.3: Phylogenetic analysis of the R subunits.

Sequences of R subunits from different organisms were obtained by Psi-Blast [13] using human RIα as the query sequence and a BLOSUM62 weight matrix. Sequences were identified as RI if it had an alanine or glycine at the PKA phosphorylation site or as RII if it had a serine. Multiple sequence alignments were performed using T-coffee [14], ClustalX [15], and MUSCLE [16] . A phylogenetic tree of the alignments, rooted using the *S. pombe* sequence, was visualized with the program, Interactive Tree of Life [17].

discrete particulate fractions in association with either membranous organelles or the cytoskeleton [18]. However, both RI and RII isoforms have been observed in the nucleus of rat hepatoma cells through post-embedding immunogold labeling techniques [19]. RI isoforms show higher sensitivity to cAMP activation than RII [20], but both isoforms show an allosteric mechanism of activation [21, 22]. For RIα, the cooperative activation pathway is highly ordered. In the presence of cAMP, one molecule of cAMP binds to the cAMP binding B domain in RIα, allowing access of one molecule of cAMP to bind to the A domain, thus leading to the release and activation of C-subunit. RI subunits also require ATP and two magnesium ions for tight interaction with C-subunit, unlike RII subunits which are autophosphorylated [23, 24].

RI and RII isoforms show the highest variability in the linker region. The linker region contains a PKA phosphorylation consensus motif, which serves as a docking and recognition site for the C-subunit. This consensus sequence (IS) inhibits the C-subunit. Differences in this motif sequence can be used to distinguish between the two isoforms of the R-subunit. In the RI isoforms, the serine at the site of phosphorylation in RII is changed to an alanine or glycine, making this segment a pseudosubstrate inhibitor. In the RII isoforms, the serine at this site is phosphorylated by PKA and thus functions as both a substrate and an inhibitor of PKA [25]. Many motifs lie in the linker region of RIα [Figure 1.4]. RI isoforms also have a putative SH3 binding motif, which has been shown to bind to Growth factor receptor-bound protein 2 (Grb2), one of the unique binding partners to RIα [26]. RI isoforms have a

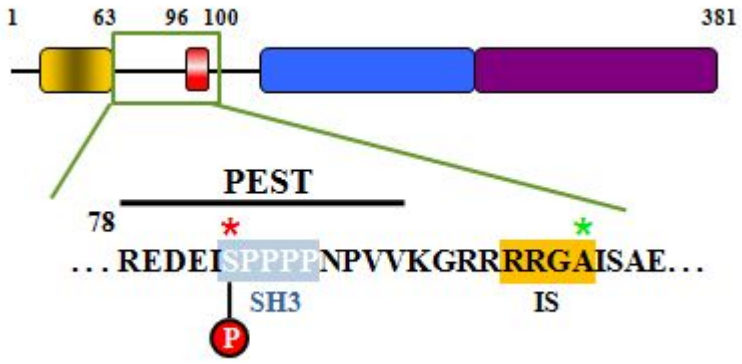

Figure 1.4: Motifs in the linker region of RIα.

Several motifs exist in the linker region of RIα. A PEST sequence (residues 78-91) is exposed upon cAMP binding. Within the PEST sequence is a constitutive phosphorylation site (red asterisk above S) as well as a putative SH3 binding domain, highlighted in blue. C-terminal to the PEST sequence lies the inhibitory site (IS), where the PKA phosphorylation site is an alanine (green asterisk above A) instead of a serine found in RII subunits.

PEST sequence, which upon cAMP binding, is exposed and is predicted to contribute to its degradation in Aplysia (sea slug) nervous tissue [27]. RI also has a constitutive phosphorylation site first identified *in vivo* almost 30 years ago [28] and recently mapped near the SH3 binding domain and within the PEST sequence [29]. However, the function of this modification has yet to be determined.

RI and RII also show differences in their D/D domain. Although the D/D domain structure for both RIα and RIIα form an anti-parallel four-helix bundle, they differ in the docking surface to which the amphipathic helices of AKAPs can bind [Figure 1.5]. The RIα D/D forms a more compact docking module with a deep cleft, while RIIα D/D has a shallow hydrophobic groove across its surface [11]. Another difference in the D/D domain is the presence of cysteines in RI isoforms that are not found in RII isoforms [Figure 1.6A]. These cysteines form intermolecular anti-parallel disulfide bonds [Figure 1.6B and C]. The RI isoforms can interact with each other, forming a heterodimer of RIα:RIβ [30]. On the other hand, heterodimers of RIIα:RIIβ have not been reported.

Though the cysteines do not affect the dimerization of the RI isoforms [31, 32], their presence has been reported to correlate with the subcellular location of RI. For example, Boeshans *et al.* discovered a higher extent of disulfide bond formation in membrane-associated RIα compared to soluble RIα in bovine cardiac tissue [29]; although, they suspected that the disulfide bonding was not the cause for the membrane localization. Another recent report showed a more substantial correlation

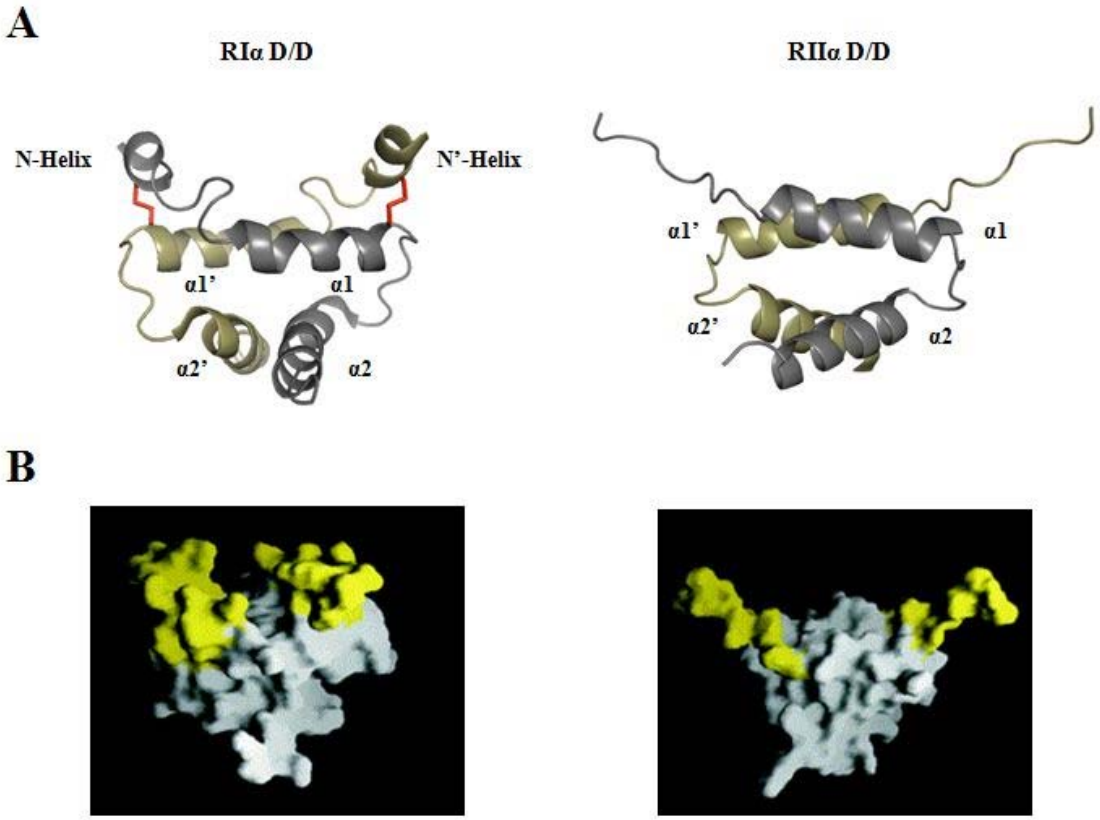

Figure 1.5: NMR structures of RI and RII D/D domains reveal isoform-specific features.

(A) The RIα D/D domain (left) forms an anti-parallel, four-helix bundle similar to the RII isoforms. However, RI isoforms contain a unique, interchain disulfide bond and an additional N-terminal helix, labeled here as the N-Helix [11]. Disulfide bonds between cysteines are shown in red. The RIIα D/D domain (right) forms a stable helical core flanked by flexible N-terminal tails, which are the greatest source of variation in the NMR ensemble [33].

(B) GRASP surface rendition of RIα (12–61) (left) and RIIα (1–44) (right) are shown. The isoform-specific N-terminal region is shown in yellow. This figure was taken from a previous publication from our lab [11].

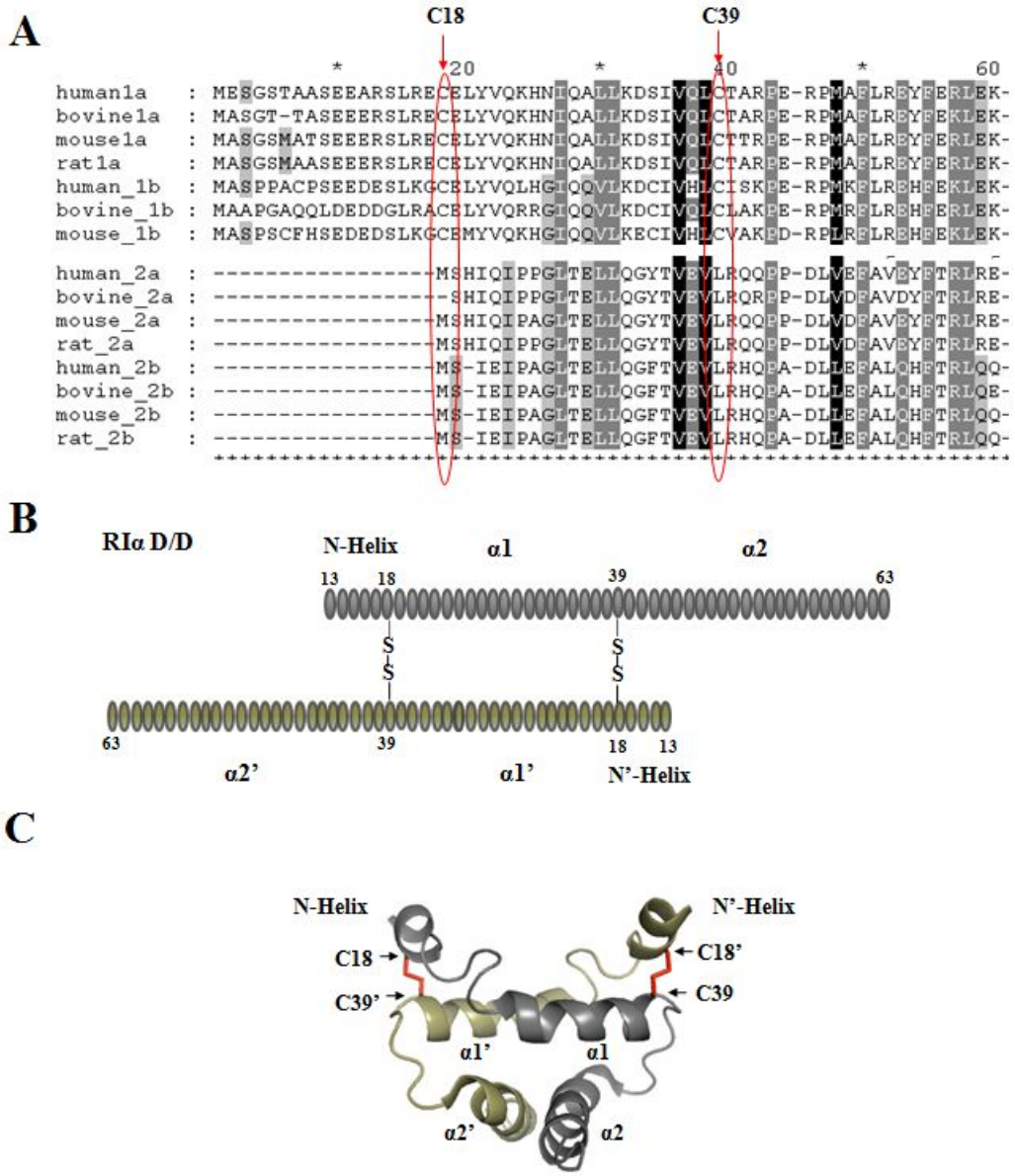

Figure 1.6: Cysteines present in RI isoforms, but not RII isoforms, form disulfide bonds.

(A) An alignment of the D/D domains from human, bovine, mouse, and rat R isoforms is shown. The RIα sequences have two cysteines, RIβ have four cysteines, and RII isoforms have none.

(B) The two pairs of cysteines in RIα are known to form antiparallel disulfide bonds.

(C) The cysteines are indicated by black arrows in the NMR structure of the RIα D/D domain.

between localization and disulfide bond formation. The authors found that in cardiac myocytes under conditions of oxidative stress, RIα is disulfide-bonded and translocates from the cytoplasm to the nucleus [34]. Structural differences in the D/D domain can result in different binding partners and is thus another mechanism for achieving specificity. One group reported that in HEK 293 cells, the second subunit of the Replication Factor C complex (RFC40) depends on RIα to bring it into the nucleus [35]. These authors previously showed the direct binding of RFC40 to RIα in a C-subunit-independent manner [36]. They also showed that RFC40 binds to the N-terminus of RIα. Though not confirmed in the paper, the authors deduced that due to differences in the docking surfaces between RI and RII, this interaction is RIα-specific; however, a specific AKAP binding motif has not been identified in RFC40.

1.3: A-kinase anchoring proteins

The D/D domains bind to a specific amphipathic helix motif that is embedded within each AKAP. Though AKAPs make up a structurally diverse protein family with >50 members [37], they share an ability to bind to R subunits via this amphipathic helix. Most of the AKAPs have been identified by gel overlay assays and are specific for RII subunits. However, some AKAPs, such as AKAP1 (D-AKAP1) [38] and AKAP10 (D-AKAP2) [39], bind to both RI and RII subunits. Although these AKAPs have dual specificity, AKAP1 has been shown to bind more tightly to RII isoforms (K_D=0.5 nM and 2.1 nM for RIIα and RIIβ, respectively) than RIα (K_D=185 nM) [40]. AKAP1 does not bind to RIβ. AKAP10 was also shown to bind more

tightly to RIIα (K_D=2 nM) than RIα (K_D=48 nM) [41]. These interactions with AKAPs allow the R subunits to localize to different compartments of the cell.

1.4: Non-redundancy of R subunits

The R subunits are also not functionally redundant. Deletion of RIβ results in defects in hippocampal function. An analysis of the protein extracts from the hippocampus of RIβ knockout mice showed an increase in RIα protein levels with no change in C-subunit or RII isoforms [42]. Deletion of RIIα showed no gross organ dysfunction [43], while deletion of RIIβ resulted in a lean phenotype with elevated body temperature and metabolic rates [44]. Western blot analyses of white adipose tissue from wild type and RIIβ mutant mice showed a complete loss of RIIβ in the mutant mice along with a 3-4-fold increase in RIα protein levels and approximately 43% reduction in C-subunit levels. However, the RIα mRNA levels in both wild-type and RIIβ mutant mice were identical [45]. Another study showed an interesting outcome from RIIβ knockout mice – a decreased sensitivity to increased ethanol consumption, likely because normal PKA activity was disrupted in brain regions involved with mediating ethanol reward [46]. Only the deletion of RIα subunit showed the extreme phenotype of embryonic lethality in mice by E10.5 [47], unless the C-subunit was also deleted [47]; however these RIα and Cα knockout mice were not viable and displayed developmental defects later in life. These same authors had previously shown that overexpression of the C-subunit in NIH 3T3 cells produced an increase in RIα levels with no change in RII subunits levels [48]. Thus, RIα is the

only isoform that can compensate for excess C-subunit activity, suggesting a tightly coordinated regulation between RIα and C-subunit that is crucial for normal development.

1.5: Involvement of RIα in cellular processes

RIα has been mapped to chromosome 17 and it has also been shown to control the expression of other genes. In 1991, two independent studies verified that the tissue-specific extinguisher locus encoded RIα, which acted to downregulate the expression of seven other genes in the liver [49, 50]. The RIα mRNA has 11 exons [Figure 1.7]. Although a single gene, *PRKAR1A*, encodes RIα, two distinct, alternately spliced RIα mRNAs (RIα 1a and RIα 1b) exist that derive from transcription from two different start sites in the first non-coding exons (1a and 1b). Solberg *et al.* demonstrated that these two mRNAs, which encode the same protein, were subject to differential regulation by cAMP [51]. Its expression has been shown to vary in different tissue and cell types as well [49, 52]. The aforementioned paper, as well as the Genomics Institute of the Novartis Research Foundation (GNF) website (https://biogps.gnf.org/), both show that one of the lowest levels of RIα mRNA expression is seen in liver [Figure 1.8]. This differential expression results in different PKA phenotypes.

RIα has been shown to be involved in cell cycle progression. Microtubules, a main component of the cytoskeleton, participate in many processes that take place during the cell cycle. Imaizumi-Scherrer *et al.* showed that RIα was associated with

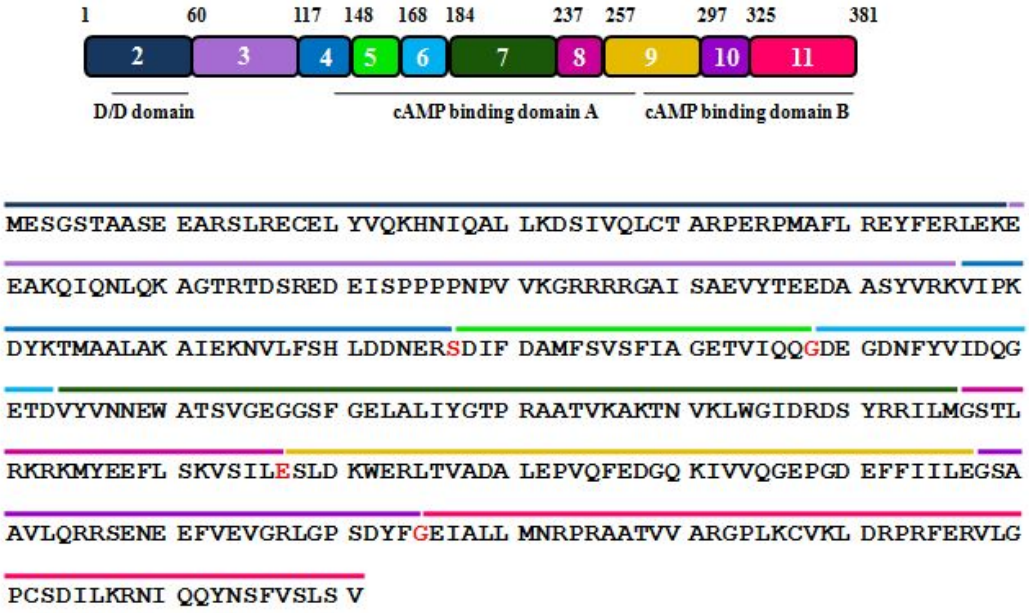

Figure 1.7: Gene structure of *PRKAR1A.*

The gene, *PRKAR1A,* encodes the RIα protein. *PRKAR1A* expresses 11 exons. The exon structure with its associated domains is shown. Residues in red indicate amino acids encoded across a splice junction.

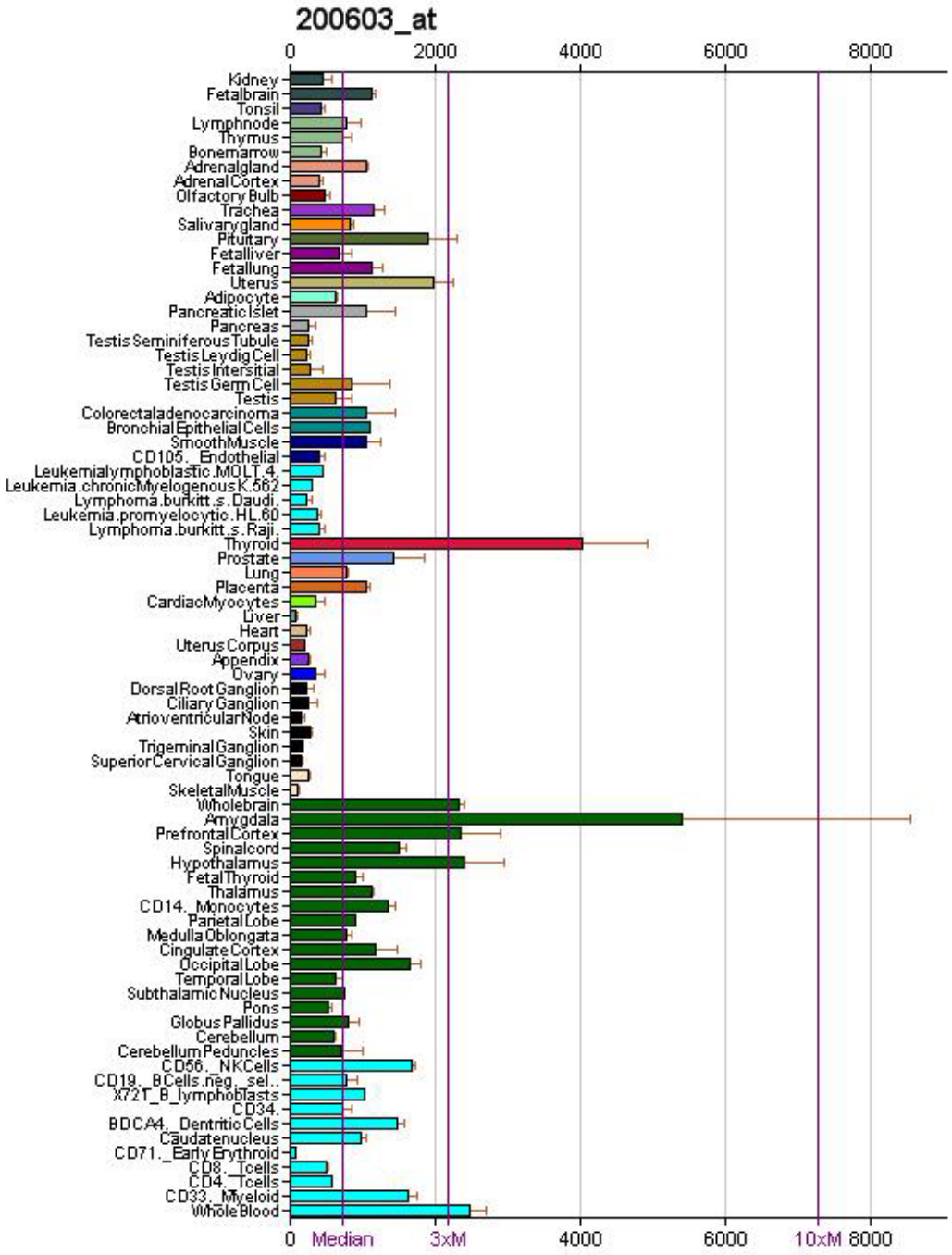

Figure 1.8: RIα mRNA shows differential expression in various tissues.

The GNF website (https://biogps.gnf.org/) allows one to see the expression of an mRNA of interest across different tissues. RNA expression levels were examined using Affymetrix gene chips. RIα is expressed in most tissues, but is expressed the lowest in liver.

microtubules during the entire cell cycle, stronger during the phases of mitosis and weaker during interphase [53]. Furthermore, Tortora *et al.* showed that downregulation of RIα blocked S phase entry of MCF-10A cells [54]. In Chinese-hamster-ovary (CHO) cells, Tortora *et al.* showed that downregulation of RIα resulted in growth arrest and accumulation in the G0/G1 phase of the cell cycle, while overexpression of RIα resulted in growth advantages and accumulation in S phase [55]. Taken together, these results show strong evidence that RIα is involved in the control of cell cycle progression and cell growth.

The involvement of RIα in other parts of cell growth has also been suggested. Autophagy is a tightly regulated process by which cells degrade their cytoplasmic components through fusion with lysosomal compartments. Autophagy is a normal part of cell growth and development and is a mechanism by which a starving cell reallocates nutrients. PKA has been reported to be involved in autophagy in yeast through its phosphorylation of Atg1 [56]. Atg1 is a serine/threonine kinase that is required for vesicle formation in autophagy and has a human ortholog, ULK1. These authors previously found that PKA activity inhibits the formation of autophagosomes [57]. More recently, an independent study reported the association of RIα with autophagosomes and a defect in autophagy associated with a deficiency in *Prkar1a,* the gene encoding RIα in mice [58].

1.6: Involvement of RIα in disease

RIα has been implicated in a variety of diseases [59-61]. One example is breast cancer. Breast cancer is a common disease that affects about one in ten women in the United States. A comparison of RI and RII subunits expression in breast tissues from normal versus breast cancer patients showed a significantly higher overexpression of RI subunit than RII [62]. The authors also showed a positive association between the level of cell proliferation and RI expression. Cells that expressed more RIα showed an enhanced growth rate. This proliferation can be reversed using antisense RIα [63]. Specifically, Nesterova *et al.* showed that downregulation of RIα by a 21-mer antisense oligonucleotide correlated with a decrease in RIα protein levels and an increase in RIIβ protein levels. The antisense also delayed the first tumor appearance and is being evaluated as an antitumor drug, called GEM231, in human phase I studies [64, 65]. These preclinical studies demonstrated synergistic antitumor activity when GEM231 was combined with docetaxel, an anti-mitotic chemotherapy medication used in the treatment of breast cancer.

While it is the overexpression of RIα that is associated with breast cancer, it is the underexpression of RIα that results in systemic lupus erythematosus, a condition characterized by chronic inflammation of various tissues [66], and also Carney complex [67]. Carney complex (CNC), which can be caused by mutations in *PRKAR1A*, the gene encoding RIα, is a multisystem tumorous disorder that is transmitted as a Mendelian autosomal dominant trait. It is characterized by cardiac

myxomas, spotty pigmentation, endocrine overactivity, and schwannomas. To date, approximately 500 patients with CNC from all races and with equal distribution between the sexes are listed in the National Institutes of Health-Mayo Clinic (NIH-MC) registry [68]. The genes responsible for CNC have been mapped to chromosomes 2 and 17. In some CNC families, Kirschner *et al*. identified mutations in *PRKAR1A*, the responsible gene on 17q22-24 [67]. Most of these mutations result in premature stop codons due to mRNA degradation through nonsense-mediated mRNA decay (NMD) and consequently, a 50% reduction in the amount of the predicted protein product.

NMD is a quality control pathway for cells to degrade mRNAs that prematurely stop translation. Thus, with these NMD-degraded mRNAs, half as much mRNA would in theory encode for truncated proteins. NMD is avoided when a termination codon is located less than 50-55 nucleotides upstream of the final exon junction [69]. NMD would be especially important for regulating the expression of multimeric proteins where expression of a truncated and functionally compromised subunit could lead to the formation of heterodimers.

1.7: Significance of this study

Though PKA has been extensively studied for decades, the role of RIα, independent of the C-subunit in cells has not been well-characterized. Since it is the only isoform whose deletion results in embryonic lethality and the only one that has been pursued as an anti-cancer drug target, RIα is an important isoform to study.

Using biochemical, cell biology, and proteomic techniques, I have provided data that sheds new light on the role of RIα in a C-subunit independent manner. In Chapter 2, I describe the purification and characterization of two CNC-related RIα mutants in *E. coli*. In Chapter 3, wild-type RIα, CNC-related RIα mutants, and other well-characterized RIα mutants were overexpressed in mammalian cells. I demonstrate the dimerization of mutant RIα in the presence of wild-type RIα and develop tools for analyzing the disulfide-bonded state of RIα. Through these tools, I discovered a novel disulfide bond in one of the CNC mutants. In Chapter 4, I discuss the proteomic techniques that have been developed to probe the RIα interactome in cells and describe a novel RIα AKAP. Lastly, Chapter 5 describes the association of overexpressed RIα with multivesicular bodies.

Chapter 2:

Biochemical characterization of two Carney complex-related RIα mutants

2.1: Introduction

As discussed in Chapter 1, four isoforms of the regulatory subunit exist in cells (RIα, RIβ, RIIα, and RIIβ). All the isoforms share the same general domain organization with a dimerization/docking domain (D/D) at the N-terminus, followed by an inhibitor site, and two tandem cAMP binding sites, referred to here as CBD A and CBD B. Each CBD has a non-contiguous α subdomain that is linked to an 8-stranded β sandwich [Figure 2.1]. The hallmark feature of the CBDs is the Phosphate Binding Cassette (PBC), located between β6 and β7, where the ribose phosphate of cAMP is anchored.

One unique feature that distinguishes the RI isoforms from the RII isoforms is the site of phosphorylation in the inhibitor site. Another is the pair of cysteines in the D/D domain of RIα, C18 and C39 (numbering in *H. sapiens*). Although the cysteines readily form interchain disulfide bonds between the two antiparallel strands [70], disulfide bonds are not required for the dimerization [32]. When either or both were mutated to alanine, the dimer remained intact based on analytical gel filtration and native gel electrophoresis. Though the cysteines are not important for the dimerization, they have been shown to correlate with the localization of RIα in cells. Boeshans *et al.* initially showed that membrane-bound RIα from bovine cardiac tissue had a higher extent of disulfide bond formation than cytoplasmic RIα [29]. Brennan *et al.* later showed that in adult rat ventricular myocytes under oxidizing conditions, RI translocated from the cytoplasm to the nucleus, implying a correlation between disulfide bond formation and localization [34].

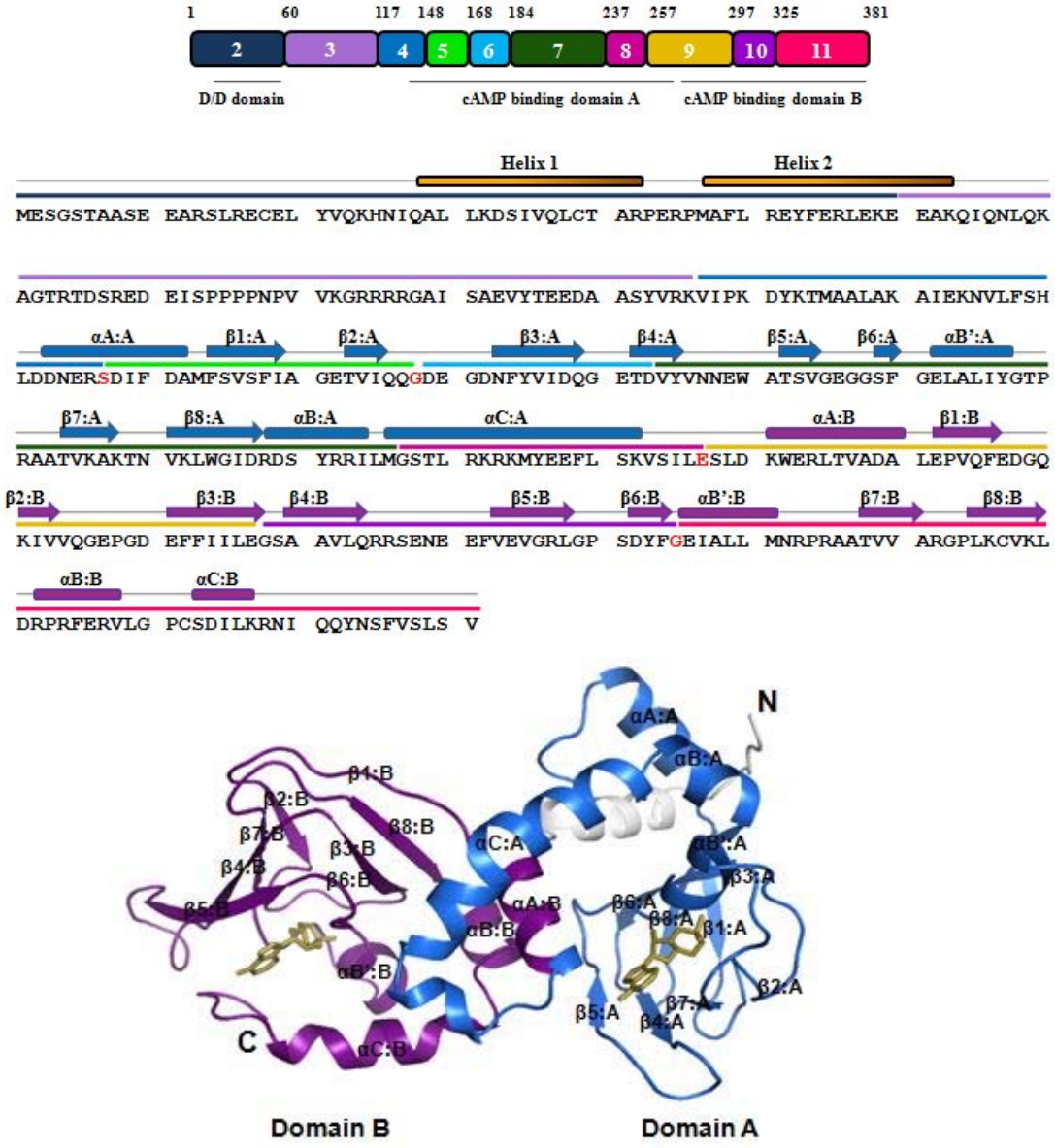

Figure 2.1: Secondary structure of RIα.

The *PRKAR1A* exons are shown with their domains and respective secondary structures. RIα is composed of two helices at the N-terminal D/D domain. The two tandem cAMP binding domains at the C-terminus, domain A in blue and domain B in purple, each consist of an eight stranded β barrel that acts as a pocket for cAMP, shown in yellow. For nomenclature, the three helices in domain A are named αA:A, αB:A, and αC:A. The corresponding helices in domain B are labeled αA:B, αB:B, and αC:B. Each β strand is likewise designated as β1:A, β2:A … β8:A in domain A and β1:B, β2:B … β8:B in domain B. This structure is from PDB ID: 1RGS [12].

The importance of RIα expression levels has been well documented. Overexpression of RIα is associated with breast cancer, where women with breast cancer had a higher level of RI subunit expression than RII [62]. A decrease in the expression of RIα has also shown negative phenotypes. RIα is the only isoform that is embryonically lethal in knockout mice [47], most likely due to the lack of compensatory expression from the other R isoforms. Lowered expression of RIα has been linked to diseases, such as systemic lupus erythematosus (SLE) [66] and Carney complex (CNC) [71]. In SLE T cells, the expression of RIα is decreased by about 20%, while in CNC, the reduction is about 50%.

The decrease in RIα expression in CNC patients is a result of mutations in the gene expressing RIα, *PRKAR1A*. Most of the mutations result in a premature stop codon (PSC) that is recognized by nonsense-mediated mRNA decay (NMD) surveillance. NMD will find PSCs that have been introduced by either nonsense or frameshift mutations in any coding exon, with the exception of the ones in the final or penultimate exons. Since most of the *PRKAR1A* mutations are PSCs, the mRNA gets degraded through NMD, resulting in haploinsufficiency and consequently, half the normal levels of RIα. The fact that a decrease in the level of RIα expression is sufficient to cause CNC emphasizes the importance of balancing RIα expression levels.

The CNC mutations known as of Summer 2008 [71-73], are listed in Tables 2.1-2.3. The nomenclature for the mutations is according to the guidelines listed by the human genome variation society (http://www.hgvs.org/mutnomen/). "c." refers to

Table 2.1: CNC mutations that resulted in point mutations.

Point mutations are listed with their corresponding exon locations and resulting amino acid change. Nonsense mutation means the point mutation results in a stop codon. Whether the mRNA gets expressed is also displayed. Taken from NCBI, the coding DNA reference sequence was NM_002734, while the protein reference sequence was NP_002725. Nucleotide 1 is the A of the ATG-translation initiation codon. The mutations highlighted in yellow were used in these studies. Some mutations escaped nonsense-mediated mRNA decay (NMD) by being a point mutation. Most of the point mutations were in the cAMP binding domains. One mutation evaded NMD surveillance even though it was a premature stop codon. Mutations that were expressed are labeled in their respective domains with a red asterisk.

Mutations (cDNA)	Exon	Mutation consequence	mRNA expressed
Point			
c. 1 A>G	2	abolish initiator ATG	+
c. 26 G>A	2	missense: p. S9N	+
c. 82 C>T	2	nonsense	-
c. 124 C>T	2	nonsense	-
c. 220 C>T	3	missense: p. R74C	+
c. 289 C>T	3	nonsense	-
c. 438 A>T	4	missense: p. R146S	+
c. 497 C>T	5	nonsense	-
c. 547 G>T	6	missense: p. D183Y	+
c. 638 C>A	7	missense: p. A213D	+
c. 682 C>T	7	nonsense	-
c. 786 GG>CT	9	nonsense	-
c. 865 G>T	9	missense: p. G289W	+
c. 910 C>T	10	nonsense: p. Q304stop	+

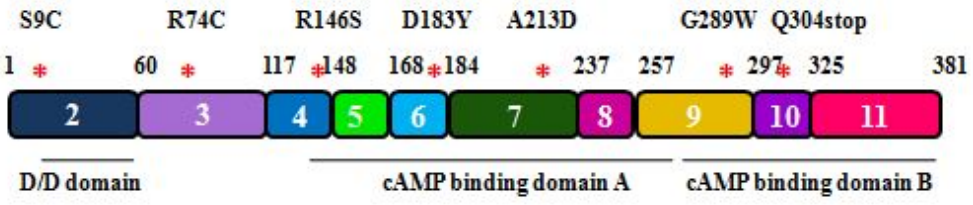

Table 2.2: CNC mutations that result in frameshift mutations.

The mutations that resulted in frameshifts are displayed with their corresponding exon location. Most frameshifts resulted in a premature stop codon (PSC), but one, resulted in the deletion of an exon, which eliminated the linker region with inhibitor site. Since the frameshift did not result in a PSC, the mutation escaped NMD surveillance. Another mutation evaded NMD because the PSC was in the penultimate exon and 22 nucleotides upstream of the last exon-exon boundary. This PSC eliminated the PBC in CBD B. The mutations, highlighted in red, are drawn beneath the table.

Mutations (cDNA)	Exon	Mutation consequence	mRNA expressed
Frameshift			
c. 101_105delCTATT	2	PSC	-
c. 491_492delTG	5	PSC	-
c. 531_534delTGAT	6	PSC	-
c. 566 AA>CAC	7	PSC	-
c. 694insT	7	PSC	-
c. 712insAA	8	PSC	-
c. 623delG	6	PSC	-
c. 758_759delTC	7	PSC	-
c. 52_53delTG	2	PSC	-
c. 588insGG	7	PSC	-
c. 658_659delAA	7	PSC	-
c. 545insC	6	PSC	-
c. 619delT	7	PSC	-
c. 623insA	7	PSC	-
c. 804insT	9	PSC	-
c. 951delA	10	PSC	+
c. 528_531delGATT	6	PSC	-
c. 528insTATGATCAATC	6	PSC	-
c. 178_348del171	3	Δ-exon 3	+

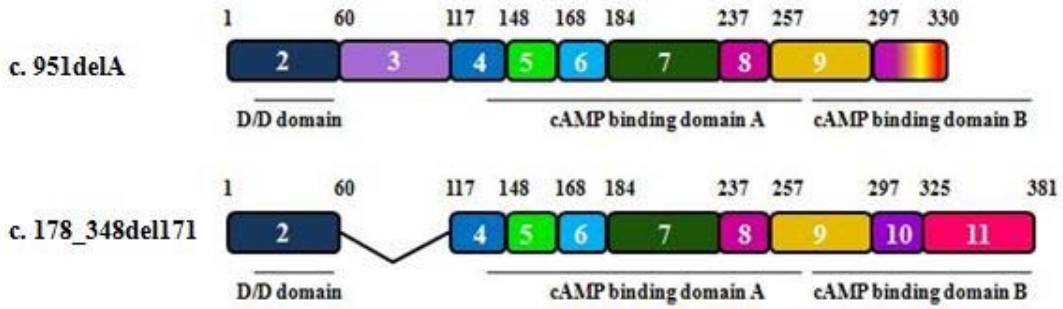

Table 2.3: CNC mutations that are located at the introns.

The mutational consequences of CNC-associated mutations in introns are listed. The intron number is listed and a "+" is the position at the start of that intron whereas a "-" is the position at the end of that intron. Most of the mutations resulted in NMD, but one escaped by causing the deletion of an exon. The result of this mutation is shown beneath the table. The PBC from CBD A is completely removed.

Mutations (cDNA)	Mutation consequence	mRNA expressed
Splice site		
IVS1-2 A>G	unsure	-
IVS3+1 G>C	cryptic splice	-
IVS5-9del(CTCTTTTA)	exon skipping	-
IVS8+3 G>A	cryptic splice	-
IVS4+1 G>A	splicing/frameshift/PSC	-
IVS5+1ins(T)	splicing/frameshift/PSC	-
IVS6-17 T>A	splicing/frameshift/PSC	-
IVS4-1 A>G	splicing/frameshift/PSC	-
IVS5 +3 A>C	splicing/frameshift/PSC	-
IVS8+5 G>C	splicing/frameshift/PSC	-
IVS6-1del(GGTCTA)	Δ-exon 7	+
IVS5+1 G>A	splicing/frameshift/PSC	-

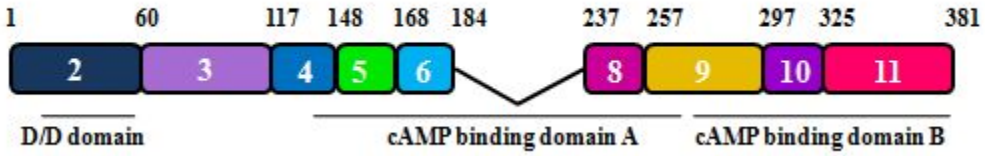

the coding DNA sequence, while "p." stands for protein sequence. A few gene mutations, c. 910 C>T, c. 220 C>T, IVS6-1del(GGTCTA), and c. 951delA were shown to escape NMD by one group in 2004 [71]. More recently, another study showed additional mutations that escape NMD [73].

Table 2.1 lists the point mutations. Most of the point mutations that are expressed are located in the cAMP binding domains, indicated as asterisks in the exon structure beneath the table. Table 2.2 lists the CNC mutations that result in a frameshift. Only two of the mutations were known to be transcribed into mRNA. c. 951delA resulted in a change of amino acids that starts from position 317 and ends with a premature stop codon at position 330 (top exon picture). This mutation, which eliminates the second PBC, escapes NMD because the PSC is located in the last exon. c. 178_348del171 results in a deletion of exon three which eliminates most of the linker region as well as the inhibitor site (bottom exon picture). Table 2.3 lists the CNC mutations that are located at the introns. The only mutation to be expressed into an mRNA results in deletion of exon 7. This deletion removes the PBC in the CBD A.

Two mutations, highlighted in Table 2.1, were chosen for this project: c. 220 C>T and c. 910 C>T. c. 220 C>T translates into missense mutation, R74C, and is known to be expressed in patients [71]. R74C lies in the linker region before the inhibitor site [Figure 2.2]. c. 910 C>T is 63 nucleotides upstream of the last exon-exon boundary. Though the mRNA was shown to be expressed, the truncated protein was not detected [71], most likely because it was rapidly degraded. We thus studied how the protein would behave if it were stable. c. 910 C>T introduces a PSC in the

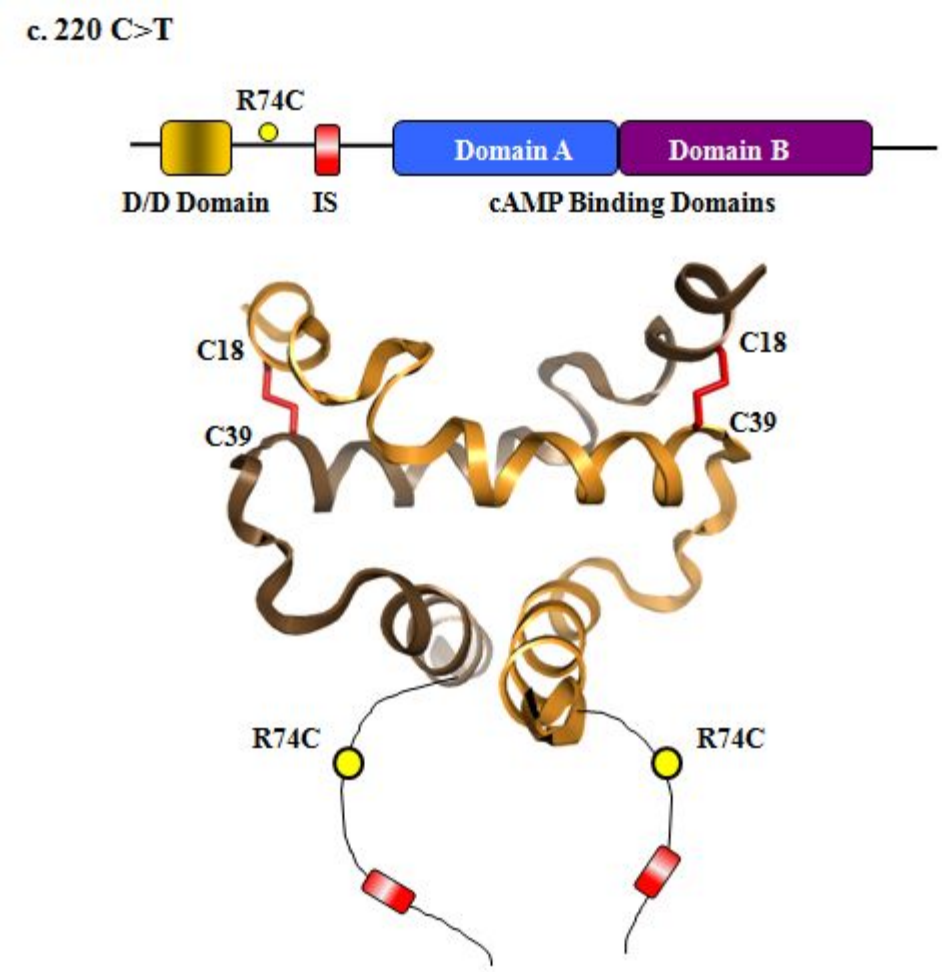

Figure 2.2: R74C is located in the linker region of RIα.

The domain organization of RIα is presented with the missense mutation, indicated by a yellow ball. R74C lies upstream of the inhibitor site, within the linker region. The NMR structure of the D/D domain (PDB ID: 2EZW) [11], shown on the bottom, highlights the N-terminal disulfide bonds as red lines. The linker region of RIα is quite flexible and its structure has not been solved. The location of R74C is drawn in as an example of where it would lie, spatially.

penultimate exon and results in a truncation in CBD B that eliminates the PBC [Figure 2.3]. From here on, this truncated protein will be called RIα(1-303).

The significance of the mutations escaping NMD remains unclear. Therefore, we undertook studies to correlate the genotype and phenotype of RIα mutations. Since R74C introduced an extra cysteine, it was important to characterize its effects on disulfide bond formation as well as its effects on protein function. RIα(1-303) created a truncated protein that lacked the CBD B, which we hypothesized, would affect PKA activation. We therefore expressed and purified these mutant proteins *in vitro* and looked at their effects on PKA activation. We found that the truncated protein showed a change in PKA activation while R74C did not. We then expressed the R74C protein under non-reducing conditions to study its effects on the disulfide bonding of RIα and demonstrated the formation of a disulfide-bonded tetramer.

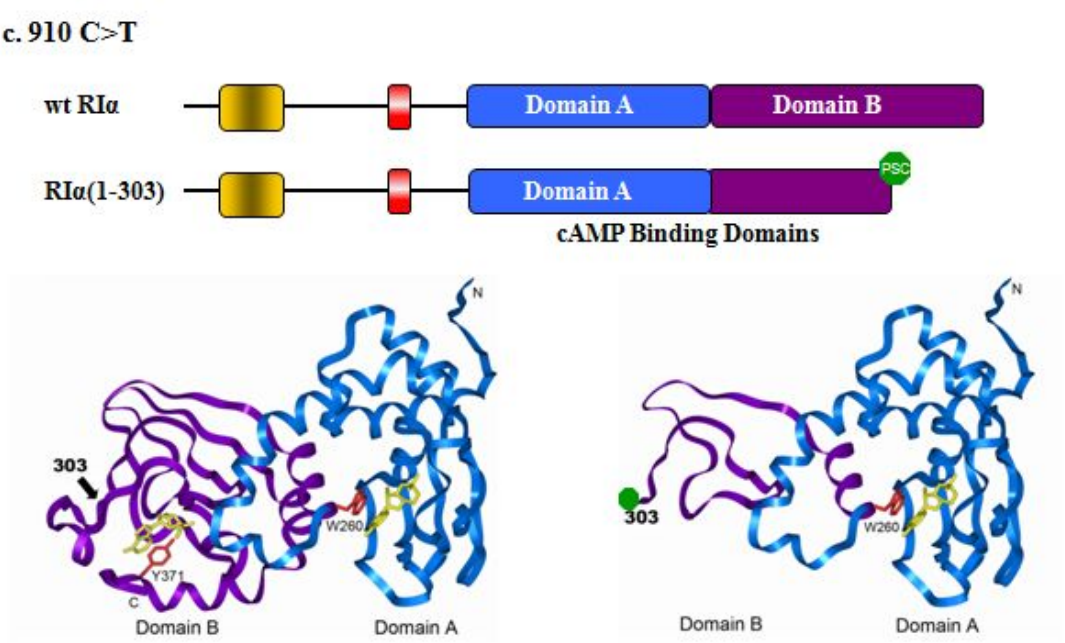

Figure 2.3: RIα(1-303) removes the cAMP binding site in the second cAMP binding domain.

c. 910 C>T results in a premature stop codon in the penultimate exon. The protein that would be expressed from this mutation introduces a stop codon before the cAMP binding site in cAMP binding domain B. On the top, the domain organization of wild-type RIα is displayed with that of RIα(1-303). On the bottom, the crystal structure of 1RGS [12] is shown, with (on the right) and without the truncated mutation (on the left). cAMP binding domain A is in blue while cAMP binding domain B is in purple. The stop codon is drawn in green.

2.2: Experimental Procedures

Antibodies. Mouse monoclonal RIα antibody was purchased from Transduction Laboratories. Rabbit polyclonal RIα antibody (in-house) was developed in our lab. Other RIα antibodies, commercially purchased and developed in our lab, were screened but did not work.

Cloning, expression, and purification of bovine RIα. Truncated bovine RIα(1-303) was isolated by PCR and the amplified cDNA subcloned into the BamHI-HindIII site of pRSET (Invitrogen). The single site mutation, R74C, was introduced by QuikChange mutagenesis (Stratagene). All constructs were verified by sequencing. This vector has an IPTG-inducible promoter and ampicillin resistance.

The clones were transformed into BL21(DE3) *E. coli* (Novagen) and grown in YT media with 100 μg/mL ampicillin. Cells were grown at 37°C, shaken at 225 rpm, and induced at A_{280} = 0.6-0.8 with 0.5 mM IPTG. Following induction, cells were allowed to grow for 6 additional hours at 24°C before harvesting. Pellets from a 6 L culture were resuspended in lysis buffer (200 mM MES (pH 6.5), 100 mM NaCl, 2 mM EGTA, 2 mM EDTA, 5 mM DTT, and protease inhibitors), then lysed with a French pressure cell and centrifuged. After centrifugation, the supernatant was precipitated with 45% ammonium sulfate for 1 hour. The ammonium sulfate solution was centrifuged and the pellet resuspended in lysis buffer and then bound to 8-AEA cAMP Sepharose resin (Sigma) at 4°C overnight. The resin was then washed with

lysis buffer, followed by one wash with lysis buffer containing 700 mM NaCl, and then washed once more with lysis buffer using a Kontes flex-column.

The protein was eluted with elution buffer (200 mM MES (pH 5.5), 100 mM NaCl, 2 mM EGTA, 2 mM EDTA, 5 mM DTT, 40 mM cGMP, and protease inhibitors). Elutions were pooled and injected onto an S200 gel filtration column (GE Healthcare). Gel filtration was performed in final buffer consisting of 50 mM MES (pH 5.8), 200 mM NaCl, 2 mM EDTA, 2 mM EGTA, and 5 mM DTT.

Cloning, expression, and purification of human RIα. Human RIα was subcloned from pCMV-SPORT6 (Invitrogen) into the BamHI-HindIII site of pRSET (Invitrogen). The single site mutation, R74C, was introduced by QuikChange mutagenesis (Stratagene). All constructs were verified by sequencing.

The clones were transformed into BL21-CodonPlus(DE3)-RIPL *E. coli* (Stratagene) and grown in YT media with 100 µg/mL ampicillin and 50 µg/mL chloramphenicol. Cells were grown at 37°C, shaken at 225 rpm, and induced at A_{280} = 0.6-0.8 with 0.5 mM IPTG. Following induction, cells were allowed to grow for 4 additional hours at 24°C before harvesting. The protein was purified as described above, except no DTT was included. Elutions were loaded onto an S200 analytical gel filtration column (GE Healthcare), where final gel filtration buffer consisted of 50 mM MES (pH 5.8), 200 mM NaCl, 2 mM EDTA, and 2 mM EGTA.

Expression checks. Human RIα clones were transformed into BL21(DE3) *E. coli* (Novagen) and grown in YT media with 100 µg/mL ampicillin. Cells were grown at 37°C, shaken at 225 rpm, and induced at A_{280} = 0.8 with 0.5 mM IPTG. Following induction, cells were allowed to grow for 2-24 additional hours at 24°C. Samples (100 µl) were taken at different time points, resuspended in sample buffer, and sonicated.

Oxidation of purified RIα. RIα was oxidized by incubating with 5 mM diamide for 10 minutes at room temperature.

Measurement of apparent molecular weights. Low molecular weight proteins (chymotrypsinogen A, ovalbumin, and albumin) and high molecular weight proteins (aldolase and catalase) from the Gel Filtration Calibration Kit (GE Healthcare) were dissolved to 5 µg/µl in gel filtration buffer to a final volume of 500 µl. These samples were applied to the S200 analytical gel filtration column (GE Healthcare) using the same protocol as that for the RIα R74C protein. Elution volumes for each sample were recorded. Blue Dextran 2000, used to calculate the void volume, was dissolved to 1 µg/µl in gel filtration buffer. K_{av} values for each protein was calculated using the equation

$$Kav = \frac{Ve - Vo}{Vt - Vo}$$

where V_e = elution volume for the protein

V_o = elution volume for Blue Dextran 2000

V_t = total bed volume

For the S200 analytical gel filtration column, the V_t is 23.5 mL. K_{av} values for each protein standard (on the linear scale) were plotted against the corresponding molecular weight (on the logarithmic scale) and a line was drawn that best fits the points. Apparent molecular weights for the R74C peaks were calculated using this calibration curve.

Western blot analysis. Western blot analysis was performed by separating proteins on a 4-12% Bis-Tris polyacrylamide, NuPAGE gel (Invitrogen). Proteins were then transferred to nitrocellulose (Bio-Rad), blocked for 1 hour at 24°C with 5% milk. Milk was made in TBST (Tris-buffered saline containing 0.1% Tween 20) for in-house antibody and made in PBST (Phosphate-buffered saline containing 0.05% Tween 20) for the antibody from Transduction Laboratories. After blocking, the blots were incubated overnight at 4°C with primary antibody (1:1000 dilution in TBST milk for in-house and 1:1000 dilution in PBST for Transduction Laboratories). Blots were then washed 4 times for 5 minutes each with TBST (in-house) or PBST (Transduction laboratories) and incubated with horseradish peroxidase-conjugated secondary antibodies (Amersham Biosciences, 1:5000 dilution for mouse, 1:10,000 dilution for rabbit), diluted in TBST milk, for 1 hour. Following 4 washes for 5 minutes each with TBST, blots were incubated with Super-Signal West Pico chemiluminescent substrate (Pierce) for 1 minute and then exposed to HyperFilm (Amersham Biosciences) for 2–30 minutes.

Native gel electrophoresis. Purified samples from Figure 2.4C were run on an 8% Tris-Glycine gel (Invitrogen) at 25°C for 6 hours at 80V and stained with Coomassie.

Purified protein samples from Figure 2.12A were run on a 4-16% Bis-Tris polyacrylamide, NativePAGE gel (Invitrogen) at 4°C for 1 hour at 150 V followed by 1.5 hours at 250 V (Blue Native PAGE protocol, Invitrogen). Coomassie G-250 was used to convert the proteins to a net negative charge, while still maintaining the native state without any protein denaturation, so that molecular masses could be estimated.

Holoenzyme formation. The C-subunit was expressed and purified in *E. coli*, as previously described [74]. The full length bovine RIα protein was mixed with wild-type C-subunit in a 1.2:1 molar ratio, while the truncated RIα protein was mixed with wild-type C-subunit in a 1:1.2 molar ratio. The complexes were dialyzed in holoenzyme buffer (10 mM MES (pH 6.5), 50 mM NaCl, 0.5 mM ATP, 5 mM $MgCl_2$, and 5 mM DTT) at 4°C overnight. Holoenzyme was purified using the S200 gel filtration column, as described above.

Holoenzyme of human RIα:C-subunit was formed *in situ*, as described below.

PKA activation assay. For Figure 2.6, a coupled spectrophotometric assay was used to measure PKA activation constants (K_a). Holoenzyme (30 nM) was incubated with 100 nM - 36.5 mM cAMP for 5 minutes, then added to assay mix (100 mM MOPS (pH 7), 10 mM $MgCl_2$, 1 mM phosphoenolpyruvate, 1 mM ATP, 15 U/mL lactate dehydrogenase, 7 U/mL pyruvate kinase, and 0.2 mM NADH) and placed in a cuvette.

Kemptide (0.2 mM) was added directly to the cuvette and the activity of free C-subunit was measured by following the decrease in absorbance at 340 nm due to oxidation of NADH.

A modified spectrophotometric assay was used to measure the apparent activation constants (EC50) in Figure 2.14. Holoenzyme was first formed *in situ* by incubating 7 nM of C-subunit and 8.4 nM of R subunit in assay mix (same as above except MOPS was replaced with 25 mM HEPES (pH 7) and 75 mM KCl) for 15 minutes on ice. For reduced protein, R subunit was incubated with 100 mM DTT for 15 minutes on ice prior to holoenzyme formation. Holoenzyme solution (145 μL) was then aliquoted into each well in a 96-well clear bottom untreated Costar plate (Corning) using multichannel pipettes. 2-fold dilutions of cAMP ranging from 4 - 4096 nM were added to each well and incubated for 10 minutes at 25°C. The reaction was initiated with 0.2 mM Kemptide and continuous decrease in absorbance at 340 nm was monitored using a GeniosPro microplate reader (Tecan).

Data points from both assay methods were analyzed using Prism 5 software (GraphPad). Each point was tested in triplicate or quadruplicate.

Mass spectrometry analysis of disulfide bonds. RIα (50 pmol) was resuspended in 0.1 M ammonium bicarbonate and digested with 250 ng trypsin overnight at 37°C. Digests (2 pmol) were analyzed on the LTQ, as described in Chapter 4. 6+, 5+ and 4+ ions were manually checked for correlation with all possible combinations of cysteine-cysteine peptides.

2.3: Results

Expression and characterization of CNC mutants. Two of the CNC mutants that escape NMD were chosen for this study: RIα R74C and RIα(1-303). To characterize the biochemical effects of these mutations, we expressed them in *E. coli* and purified them using a cAMP affinity column. The proteins were eluted using cGMP and further purified, in the presence of DTT, using a gel filtration column. R74C behaved the same as wild-type RIα and purified as a dimer, indicated by the single peak from the gel filtration column [Figure 2.4A] and its similarity in mobility under non-denaturing conditions [Figure 2.4C]. Additionally, R74C can form a complex with C-subunit [Figure 2.4B]. A native gel of the mutant holoenzyme showed that it ran the same as wild-type RIα holoenzyme while the free R74C protein migrated a little faster than free wild-type RIα [Figure 2.4C].

To make the truncated protein, residues 1-303 were subcloned into pRSET. RIα(1-303) also eluted as a single peak from the gel filtration column, consistent with a dimer [Figure 2.5A]. While RIα(1-303) expressed at a significantly lower level in *E. coli*, it still formed a complex with C-subunit, as evidenced by an SDS-PAGE gel which showed bands for both C-subunit and RIα(1-303) [Figure 2.5B].

Since the major role of the regulatory subunit is to act as an inhibitor of PKA catalytic subunit, one question was whether these mutations affect the interaction between the R and C-subunits and/or the activation of the holoenzyme. To answer this question, the activity of PKA was measured using the coupled spectrophotometric activity assay. The results from Figure 2.6 showed no difference in activity for the

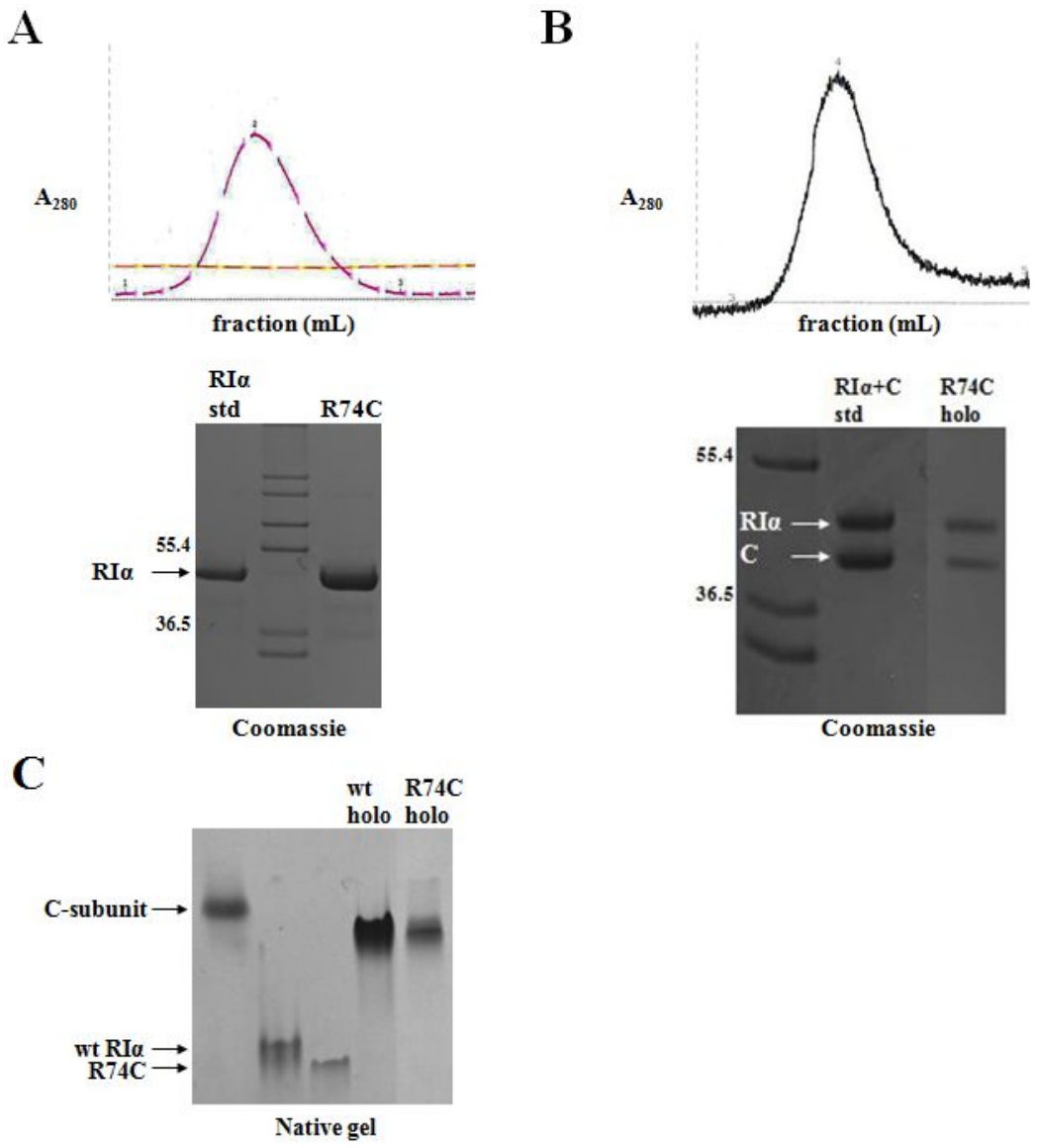

Figure 2.4: R74C purified as a dimer and formed a complex with C-subunit.

(A) R74C purified as a single peak from gel filtration, in the presence of DTT. An SDS-PAGE gel of the purified protein, stained with Coomassie, is below the graph.

(B) R74C formed a complex with C-subunit as evidenced by the SDS-PAGE gel of the purified holoenzyme, stained with Coomassie, shown beneath the curve.

(C) A native gel, which keeps the protein in its native conformation, showed wild-type RIα with slightly slower mobility than R74C. Similar mobilities between wild-type RIα holoenzyme and R74C holoenzyme were seen. The holoenzyme showed a slightly faster mobility than the free C-subunit.

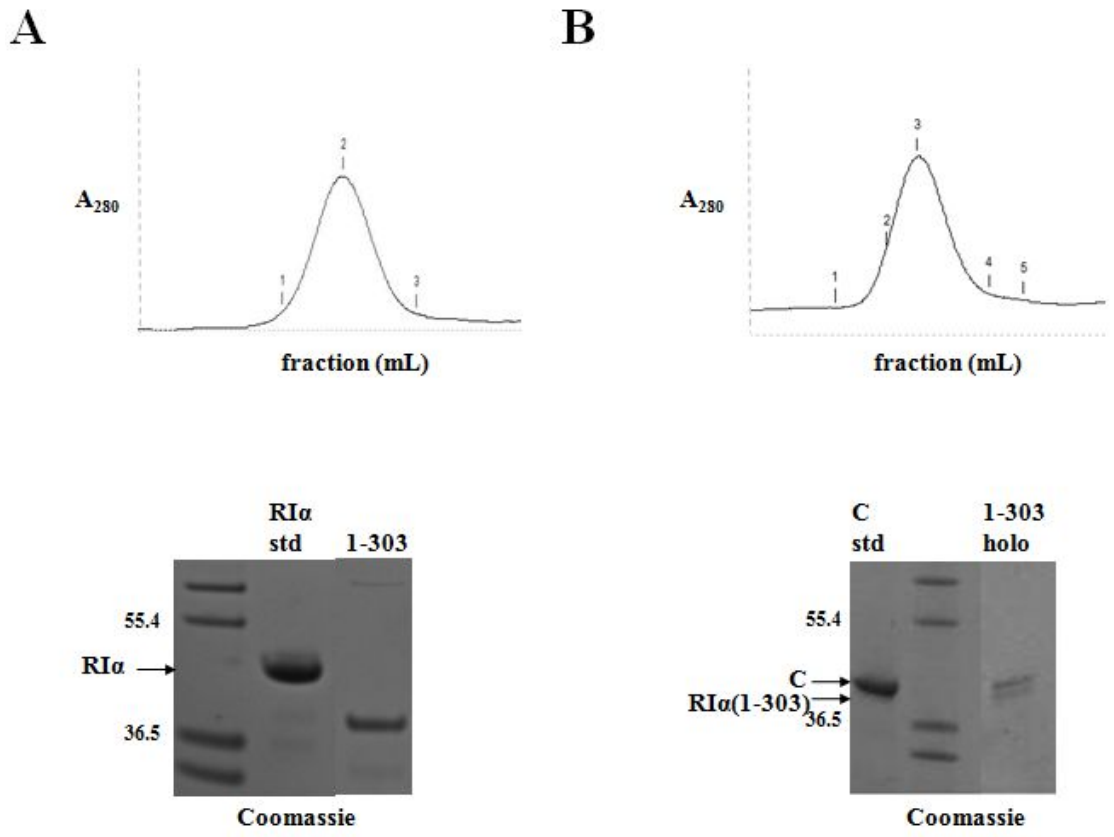

Figure 2.5: RIα(1-303) purified as a dimer and formed a complex with C-subunit.

(A) The purification of RIα(1-303) from gel filtration resulted in a single peak. The protein was run on an SDS-PAGE gel and stained with Coomassie. As expected, the RIα(1-303) protein was smaller in size at about 33 kDa, while wild-type RIα was 43 kDa.

(B) RIα(1-303) formed a complex with C-subunit to make holoenzyme. The holoenzyme on an SDS-PAGE gel, stained with Coomassie, is shown. In the lane loaded with RIα(1-303) holoenzyme, the top band is C-subunit and the bottom band is RIα(1-303).

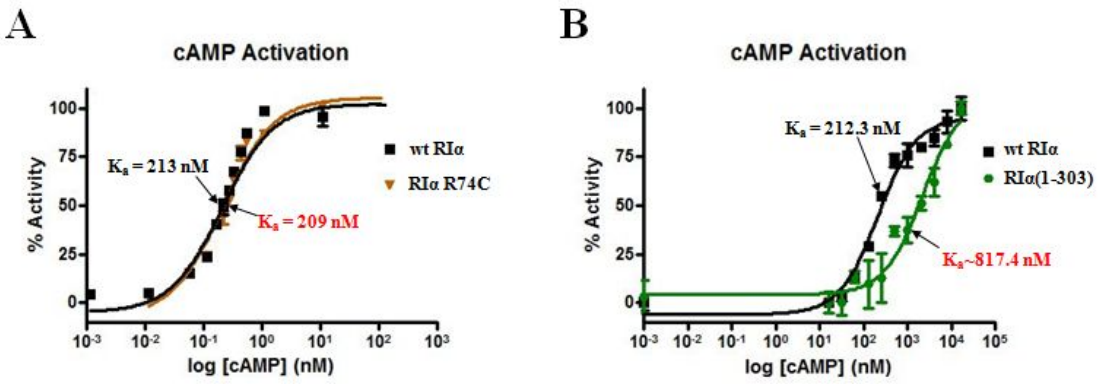

Figure 2.6: R74C holoenzyme showed no change in PKA activation, while RIα(1-303) holoenzyme showed a higher PKA activation constant.

Binding curves were fit using GraphPad Prism 5 software; error bars indicate the standard error of the mean.

(A) R74C holoenzyme, orange curve, showed a similar activation constant (K_a= 209 nM) compared to wild-type RIα holoenzyme, black curve (K_a= 213 nM).

(B) RIα(1-303) holoenzyme, green curve, showed a higher activation constant (K_a=818 nM) than wild-type RIα holoenzyme, black curve (K_a= 213 nM).

R74C mutation (K_a= 213 nM and 209 nM for wild-type RIα and R74C, respectively); however, RIα(1-303) required a higher concentration of cAMP to activate the C-subunit (K_a=818 nM).

Disulfide bonds in RIα. Though no change in PKA activation was found for the R74C mutant protein, the additional cysteine could affect the N-terminal disulfide bonding. At first, the differential recognition of antibodies to RIα made it very confusing to interpret disulfide bonding. However, after testing a number of antibodies for RIα, produced both commercially and within our lab, we found two antibodies that could clearly distinguish between oxidized and reduced protein populations. One antibody, commercially available from Transduction Laboratories (TL), preferentially recognized the reduced (non-disulfide bonded) population. The other antibody, produced within our lab (in-house), only recognized the oxidized (disulfide-bonded) population [Figure 2.7].

Purified RIα samples were run on SDS-PAGE gels either without DTT (non-reducing) to maintain the disulfide bond or with DTT (reducing) to disrupt the disulfide bond. Additionally, a sulfhydryl-specific oxidizing agent, diamide, was used to trap disulfide-bonded dimers. The non-reducing gel, stained with Coomassie, revealed a mixed population of RIα. In lane 1, without diamide, a mixed population of RIα with and without disulfide bonds was present. In lane 2, with diamide present, only the oxidized population existed. In a reducing gel, stained with Coomassie, only the reduced population of RIα (no disulfide bonds) is present. Western blots of these

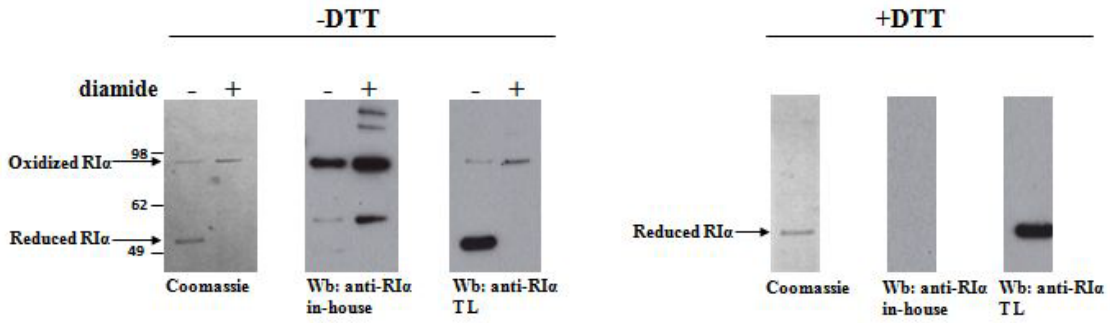

Figure 2.7: Antibodies can be used to distinguish the disulfide-bonded population from the non-disulfide bonded population on a Western blot.

RIα purified from *E. coli* was used to assess the recognition of two different antibodies for the oxidation state. Diamide was used to trap all of the RIα into the oxidized state. From a gel stained with Coomassie, the entire population of RIα can be visualized. Without diamide, both the oxidized and reduced state existed, while in the presence of diamide, only the oxidized state formed. A Western blot probed with in-house antibody showed recognition of the oxidized state only. Meanwhile, a Western blot probed with commercial antibody, Transduction Laboratories (TL), showed preferential recognition of the reduced state. As a control, the proteins were completely reduced with DTT. The same preferential recognition from the antibodies was seen.

gels showed the preferential recognition of the antibodies. The sample treated with diamide had multiple bands above the oxidized RIα, likely due to aggregation from the oxidizing conditions. Since the two antibodies were so distinct in their recognition, the two antibodies could be mixed together to give the advantage of visualizing both populations in a single gel.

Expression of human RIα. Not only was the choice of antibody important for interpretation of results, but using RIα from the right species mattered as well. Though human and bovine RIα showed 97% sequence similarities, there are some key differences, especially in the D/D domain [Figure 2.8A]. The second residue is a glutamic acid in the human sequence and an alanine in the bovine sequence; therefore, the methionine in the bovine sequence is cleaved off when the protein is expressed [75], while it is not cleaved off in the human protein. The bovine sequence is also one residue shorter than the human sequence so the numbering of residues is off by two. We chose to use human RIα in order to interpret the results in relation to Carney complex, a human disease. From now on, all residue numbering will be according to the human sequence, unless otherwise stated.

The sequence variations between species also influenced the level of expression in *E. coli*. Previously, our lab has characterized and expressed bovine RIα in BL21(DE3). However, when human RIα was expressed in this *E. coli* strain, a minimal amount of protein was detected. A different strain of *E. coli*, BL21-CodonPlus, was tested for optimal expression. The BL21-CodonPlus(DE3)-RIPL

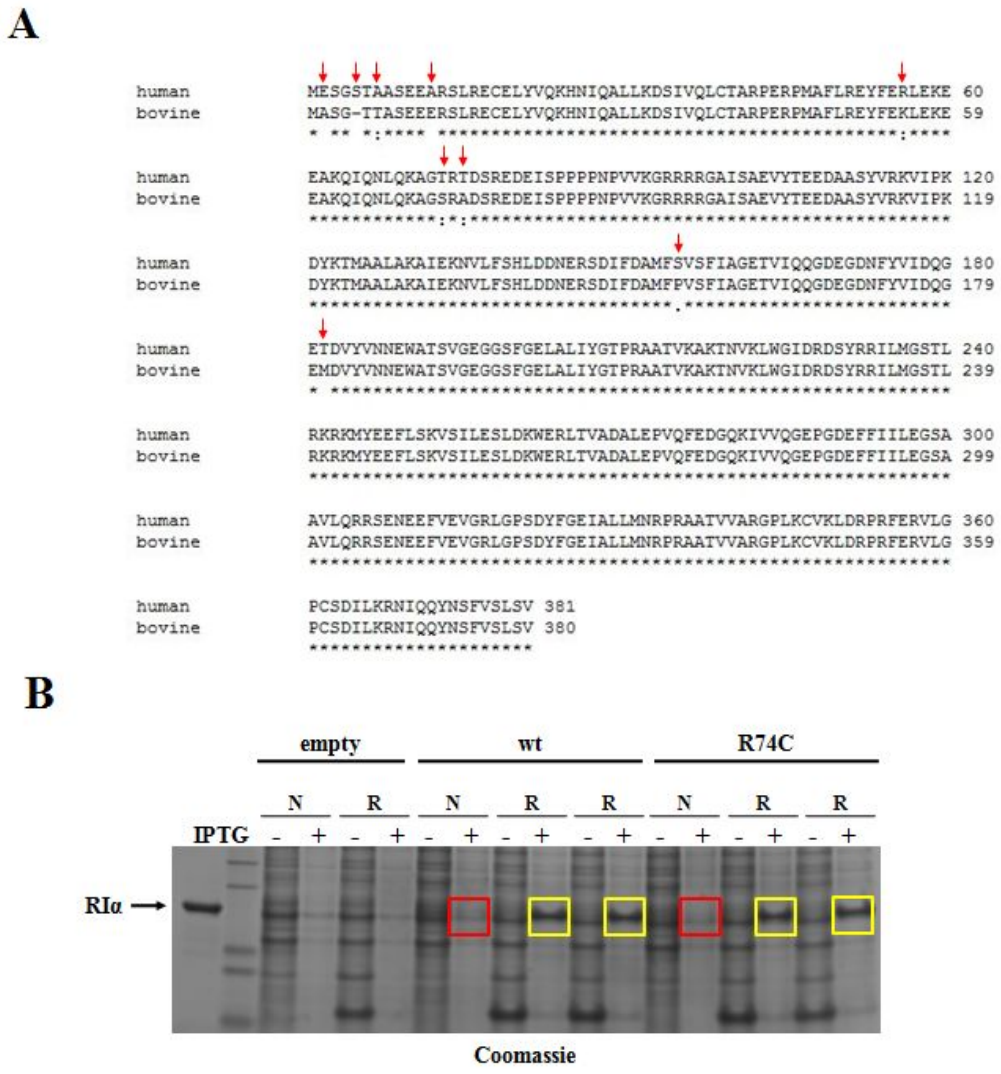

Figure 2.8: Variations in sequence result in different levels of expression in *E. coli*.

(A) Sequence comparison of human and bovine RIα revealed nine sites of amino acid differences. Human RIα has an extra residue in addition to the expression of its start codons. Because bovine RIα has an alanine in its second position, the start codon does not get expressed.

(B) Human RIα was expressed in both BL21-DE3 (N) and BL21-CodonPlus (R) cells. IPTG was used to induce the expression. The red squares indicate protein expressed from BL21-DE3 cells, while yellow squares indicate protein expressed from BL21-CodonPlus cells. The SDS-PAGE gel, stained with Coomassie, showed that a much greater amount of expression was seen from the CodonPlus cells. Two cultures each of wild-type RIα and R74C, expressed in CodonPlus cells, were used.

cells rescue expression of heterologous proteins from organisms that have either AT- or GC-rich genomes by containing extra copies of the *argU*, *ileY, proL*, and *leuW* tRNA genes, which frequently limit translation of heterologous proteins in *E. coli*. Whole cell lysates of protein expressed in the conventional BL21, labeled as 'N', were run on an SDS-PAGE gel alongside protein expressed in CodonPlus cells, labeled as 'R', and stained with Coomassie [Figure 2.8B]. A significant difference in expression was clearly visible, where human RIα expressed better in the CodonPlus cells than the conventional BL21 cells.

Analysis of cysteines. We next used the mixture of the two antibodies (from above) to study the disulfide bonds. In bovine RIα, it has been shown that the N-terminal cysteines have variation in their anchoring to AKAPs: C37 is essential for anchoring while C16 is not [32]. Furthermore, residues surrounding the cysteines have previously been shown to affect the stability of the disulfide bonds. Despite the presence of two disulfide bonds, the regions surrounding the disulfide bonds are not rigid, as revealed by the multiple conformations computed in the NMR ensemble [Figure 2.9]. It was proposed that the disulfide bonds are stabilized by the presence of two neighboring aromatic side chains, Tyr19 and His23, through S-π electron interactions [11]. We asked whether R74C would also act to disrupt the stabilized disulfide bond. We predicted the different possible disulfide bond formations that could occur with the additional cysteine [Figure 2.10A] and made single site mutations in full length human RIα. R74C could form a disulfide bond with itself or with either

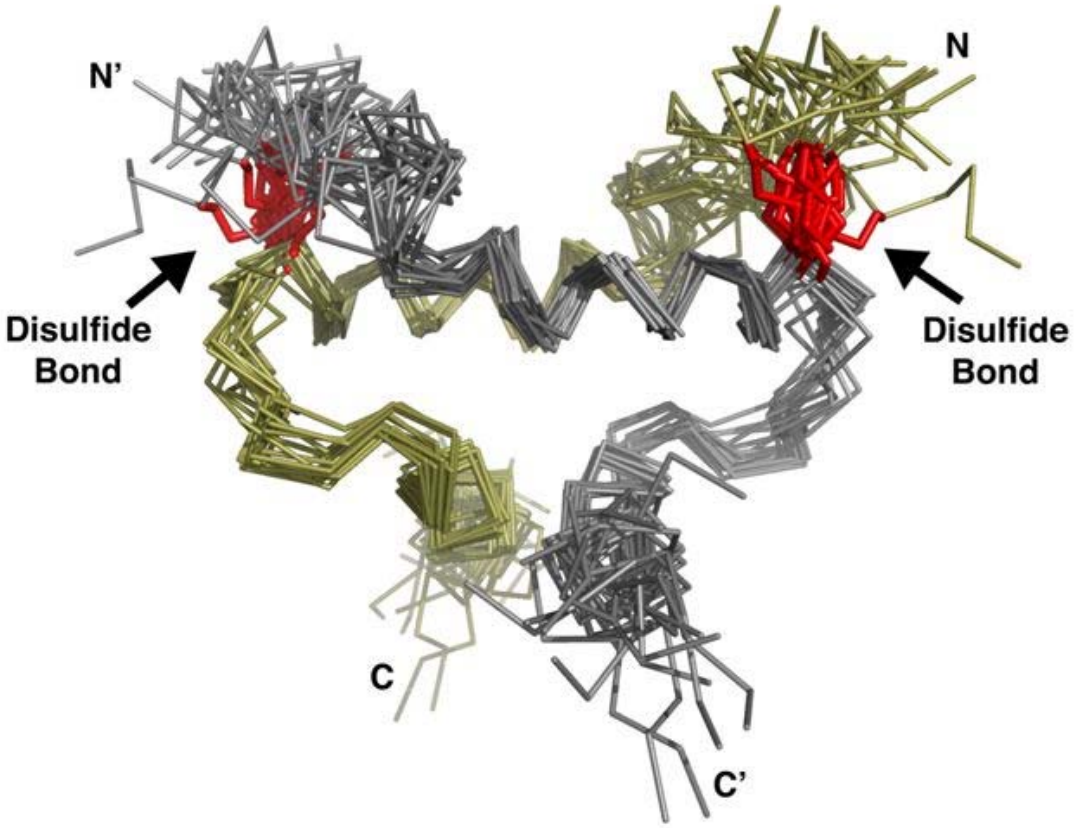

Figure 2.9: The NMR ensemble reveals multiple possible conformations for the region surrounding the disulfide bond.

The NMR ensemble of the RIα D/D domain, 2EZW [11], revealed multiple possible conformations for this region. Disulfide bonds, shown in red, do not rigidify the molecule, but instead provide a hinge point for the helix to move about.

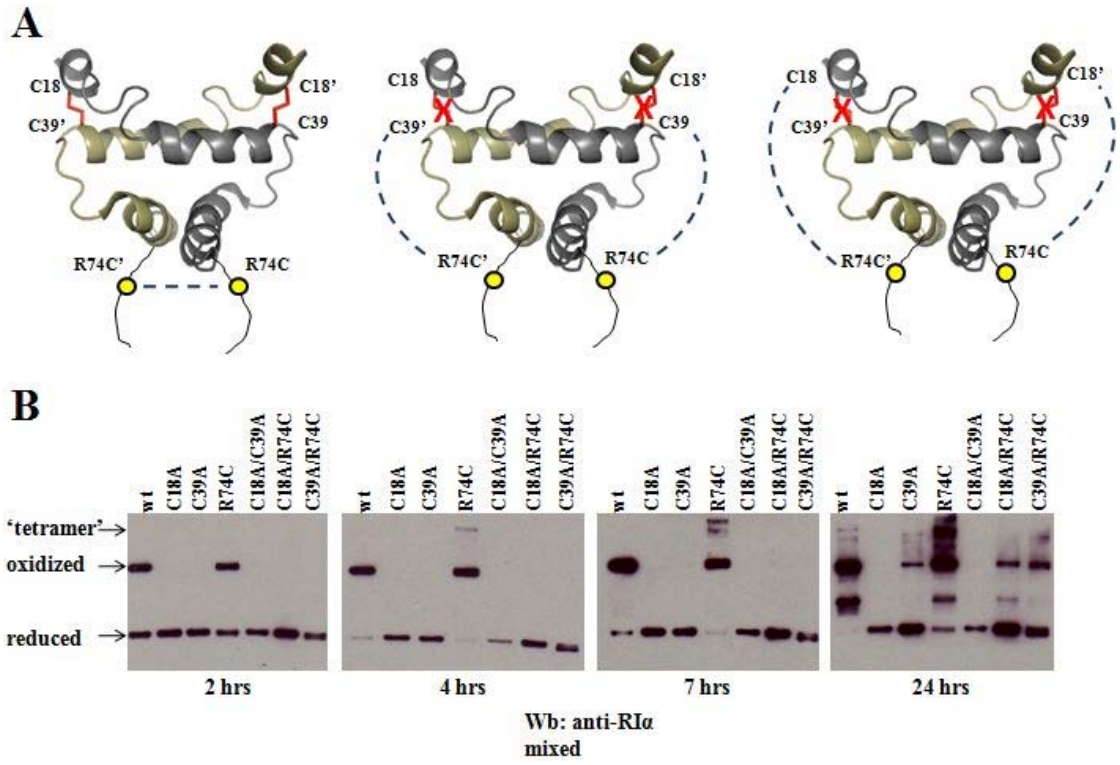

Figure 2.10: Mutational analysis of cysteines revealed differences in disulfide bond formations.

(A) The multiple combinations of disulfide bonds with the additional cysteines are shown. A disulfide bond could form between the additional cysteines. Alternatively, a disulfide bond could form between C74 and either of the N-terminal cysteines.

(B) A Western blot of wild-type and mutant RIα protein from *E. coli* whole cell lysates is shown. Samples were collected after different lengths of expression and run under non-reducing, denaturing conditions. The expression level of oxidized wild-type RIα increased over time, while the reduced form decreased. Mutations of either or both N-terminal cysteines resulted in the abolishment of disulfide bonds, except at the 24 hour time point. R74C introduces an additional cysteine which produced a small population of "tetramers" after 4 hours. We assumed the tetrameric state formed because of a disulfide bond between two dimers.

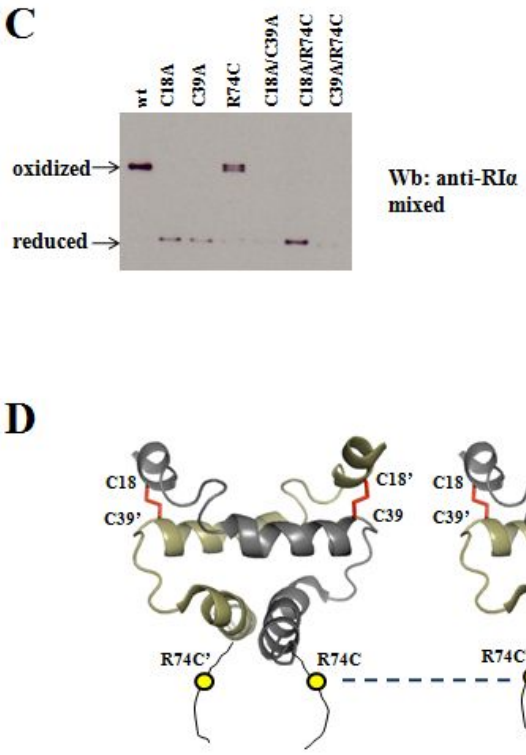

Figure 2.10: Mutational analysis of cysteines revealed differences in disulfide bond formations, Continued.

(C) The samples from the 4 hour time point in (B) were run for a longer period on an SDS-PAGE gel under non-reducing conditions. A Western blot of the gel showed two different dimer populations in the R74C protein.

(D) A tetramer could form through a disulfide bond between the additional cysteine from two R74C dimers.

of the N-terminal cysteines. Single alanine mutations were made at C18 and C39, and a single cysteine mutation was introduced at R74. Double mutations were also made: C18A/C39A, C18A/R74C, and C39A/R74C. The ability of these mutations to form disulfide-bonded dimers was assessed by a Western blot of the proteins expressed in *E. coli* for 2, 4, 7, and 24 hours [Figure 2.10B]. The non-reducing SDS-PAGE gel at the 2 hour time point showed the majority of the protein population in the oxidized state for wild-type RIα, in other words, as a disulfide-bonded dimer. This oxidized dimer was still present with the addition of the R74C mutation, indicating that the extra cysteine did not disrupt the N-terminal cysteine bonds. As expected, the double mutation, C18A/C39A, completely abolished any disulfide bond in wild-type RIα and the oxidized form of RIα was not rescued with addition of the R74C mutation. When these samples were run for a longer period [Figure 2.10C], a separation of the oxidized band from the R74C sample revealed a doublet. This doublet was likely due to two populations that migrate differently, one where the disulfide bonding was just like wild-type and one where a third intermolecular disulfide bond formed between the two additional cysteines [Figure 2.10A, left-most cartoon]. Moreover, a faint higher molecular weight band was detected with the R74C mutation [Figure 2.10B], which was likely due to a "tetramer" or dimer of RIα dimers. A cartoon of this "tetramer" is shown in Figure 2.10D. Taken together, these results provide evidence that both N-terminal cysteines were essential for the disulfide-bonded RIα. With any of the cysteine to alanine mutations, the oxidized form of RIα could not form; however, when expressed for 24 hours, additional aggregation was seen and this was especially

apparent with the R74C mutant. At this time point, the wild-type RIα was almost entirely disulfide-bonded.

R74C forms two protein populations. The wild-type RIα and R74C proteins were then purified from *E. coli* using a cAMP affinity column followed by gel filtration chromatography, where proteins are separated based on size. Wild-type RIα purified as a single population, corresponding to a dimer, while R74C showed two peaks, labeled P1 and P2 [Figure 2.11A]. The peak fractions of wild-type RIα and R74C were run under non-reducing and reducing conditions and stained by Coomassie [Figure 2.11B]. Under non-reducing conditions, an oxidized and a reduced population were seen, whereas with DTT present, all of the proteins were now reduced. A Western blot was also run to detect any population with low concentrations [Figure 2.11C]. The oxidized form of P1and P2 ran as a doublet while oxidized wild-type RIα ran as a single band. The P1 fraction contained greater amounts of a high molecular weight population and lower amounts of the reduced protein, compared to the P2 fraction.

To clarify the two distinct R74C populations, a native gel was run so that protein conformations could be maintained [Figure 2.12A]. Wild-type RIα and R74C Peak 2 showed similar mobility to bovine RIα. Based on this result and the similar elution volumes between the wild-type RIα and R74C P2, R74C Peak 2 was deduced to be in a dimer conformation. On the other hand, R74C Peak 1 had a slower mobility, indicative of a different oligomerization state.

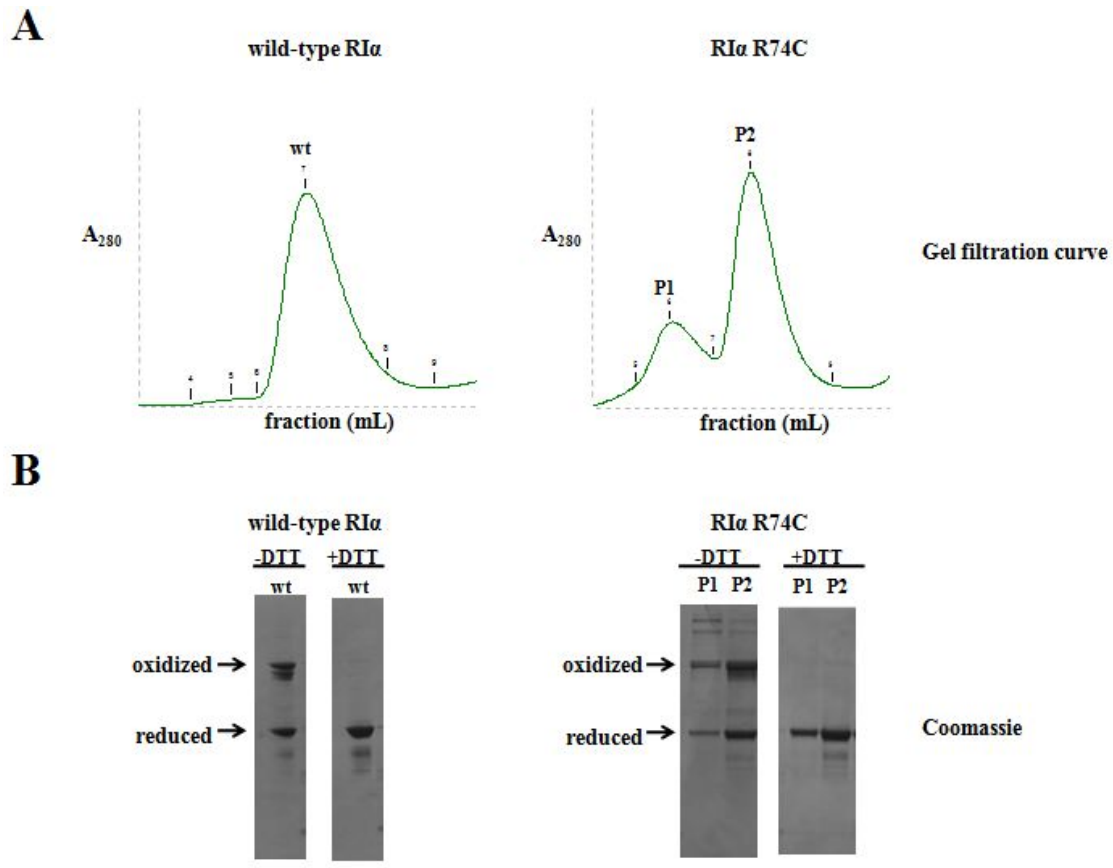

Figure 2.11: Purification of R74C revealed two populations.

(A) Wild-type RIα and R74C expressed from BL21-CodonPlus cells were purified using a cAMP affinity column, followed by gel filtration. The resulting gel filtration curve is shown. Wild-type RIα purified as a single peak, while R74C purified as two peaks.

(B) The peak samples from gel filtration were run under non-reducing and reducing conditions on an SDS-PAGE gel, stained by Coomassie. Wild-type RIα formed both oxidized and reduced dimers. R74C P1 and P2 fractions also formed both oxidized and reduced dimers. In addition, faint bands in the P1 fraction indicated possible tetrameric formation.

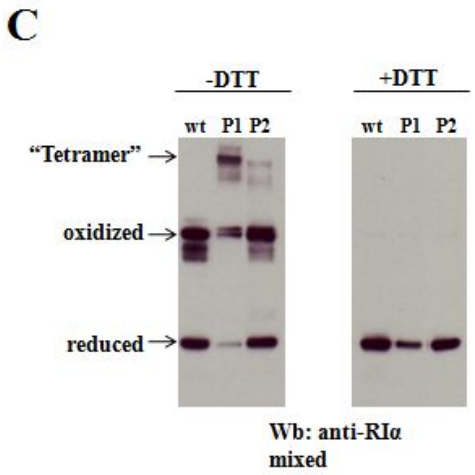

Figure 2.11: Purification of R74C revealed two populations, Continued.

(C) The peak samples from gel filtration were run under non-reducing and reducing conditions on an SDS-PAGE gel and examined by a Western blot. Both wild-type RIα and R74C P2 showed oxidized and reduced dimers. R74C P1 showed oxidized dimers and higher molecular weight proteins. All proteins were in the reduced state in the presence of DTT.

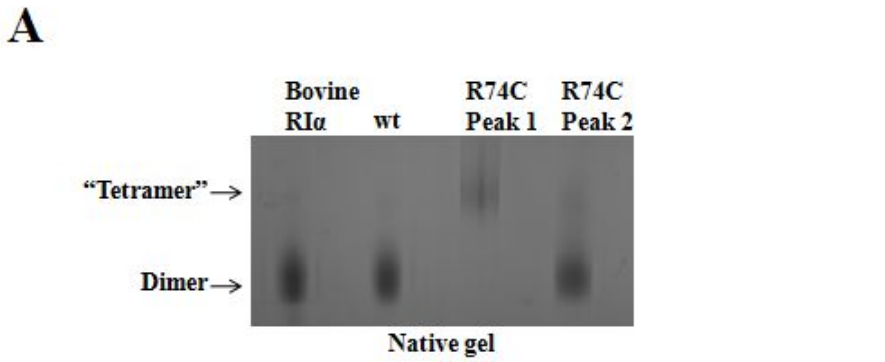

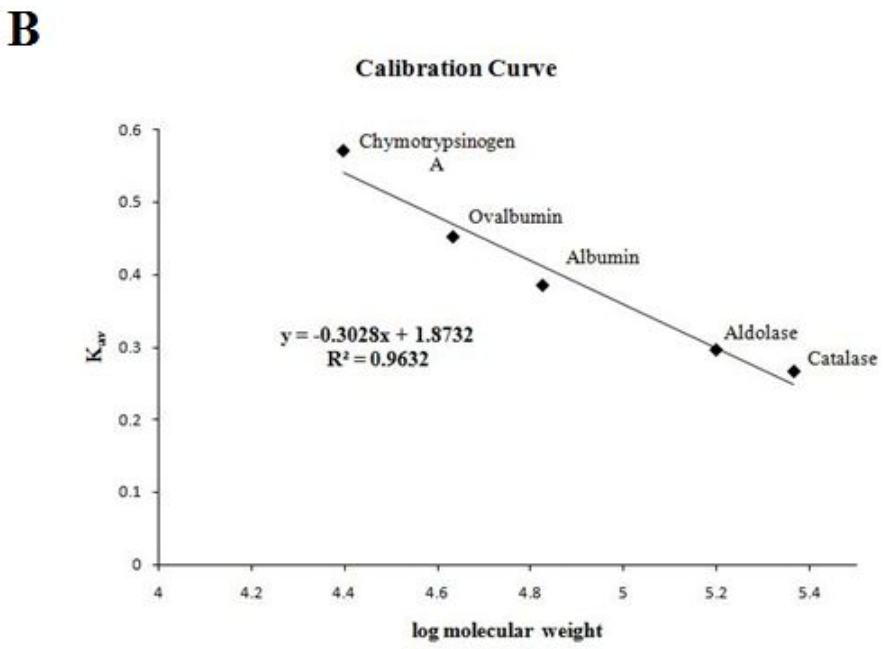

Sample	K_{av}	log mw	apparent mw (kDa)	expected mw (kDa)
R74C P1	0.18	5.6	398	172
R74C P2	0.29	5.2	159	86

Figure 2.12: R74C protein can form disulfide-bonded tetramers.

(A) Native gel electrophoresis was performed on the samples to determine their oligomerization state. Bovine RIα, known to be a dimer, was used as a control. Human wild-type RIα and R74C Peak2 showed the same mobility as bovine RIα, therefore they were in a dimer conformation. R74C Peak1 displayed a slower mobility, indicative of a different conformation.

(B) Using a calibration curve, the apparent molecular weights for the two R74C protein populations were calculated. R74C P1 was about two times larger than R74C P2. Since R74C P2 was a dimer, R74C P1 was deduced to be a tetramer.

Analytical gel filtration was used to estimate the difference in apparent molecular weight between the two R74C peaks. Protein markers in the range of 25-232 kDa were used to make a calibration curve [Figure 2.12B]. The apparent molecular weights for R74C P1 and P2 were 398 kDa and 159 kDa, respectively. It is known that the R subunit runs with a higher molecular weight on a gel filtration column due to its asymmetrical non-globular shape. However, since the apparent molecular weight of R74C P1 was a little over twice the size of R74C P2, we conclude that R74C P1 was likely a tetramer.

An analysis of the R74C peaks by mass spectrometry revealed a disulfide bond between residues C74 and C74 [Figure 2.13]. One peak, at m/z 770.3, eluted as a 6+ and 3+ ion in the oxidized R74C sample [Figure 2.13A]. The 6+ ion was not found in the reduced sample. When the oxidized R74C sample was run through tandem mass spectrometry, a peak was detected at m/z 918.75 that constituted the 4+ ion of two peptides linked by a cysteine-cysteine bond, one peptide being the full length peptide and the second being the b13 fragment [Figure 2.13B]. The bond between residues C74 and C74 was also identified independently through an algorithm that identifies linked peptides [personal communication, Dr. Nuno Bandeira].

Functional analysis of R74C. Similar to the studies at the beginning of this chapter, the effect of oxidized RIα on holoenzyme activation can be determined. The purified wild-type RIα and R74C peaks were each complexed with purified C-subunit *in situ* and assayed for a change in cAMP sensitivity. The R74C P1:C-subunit complex

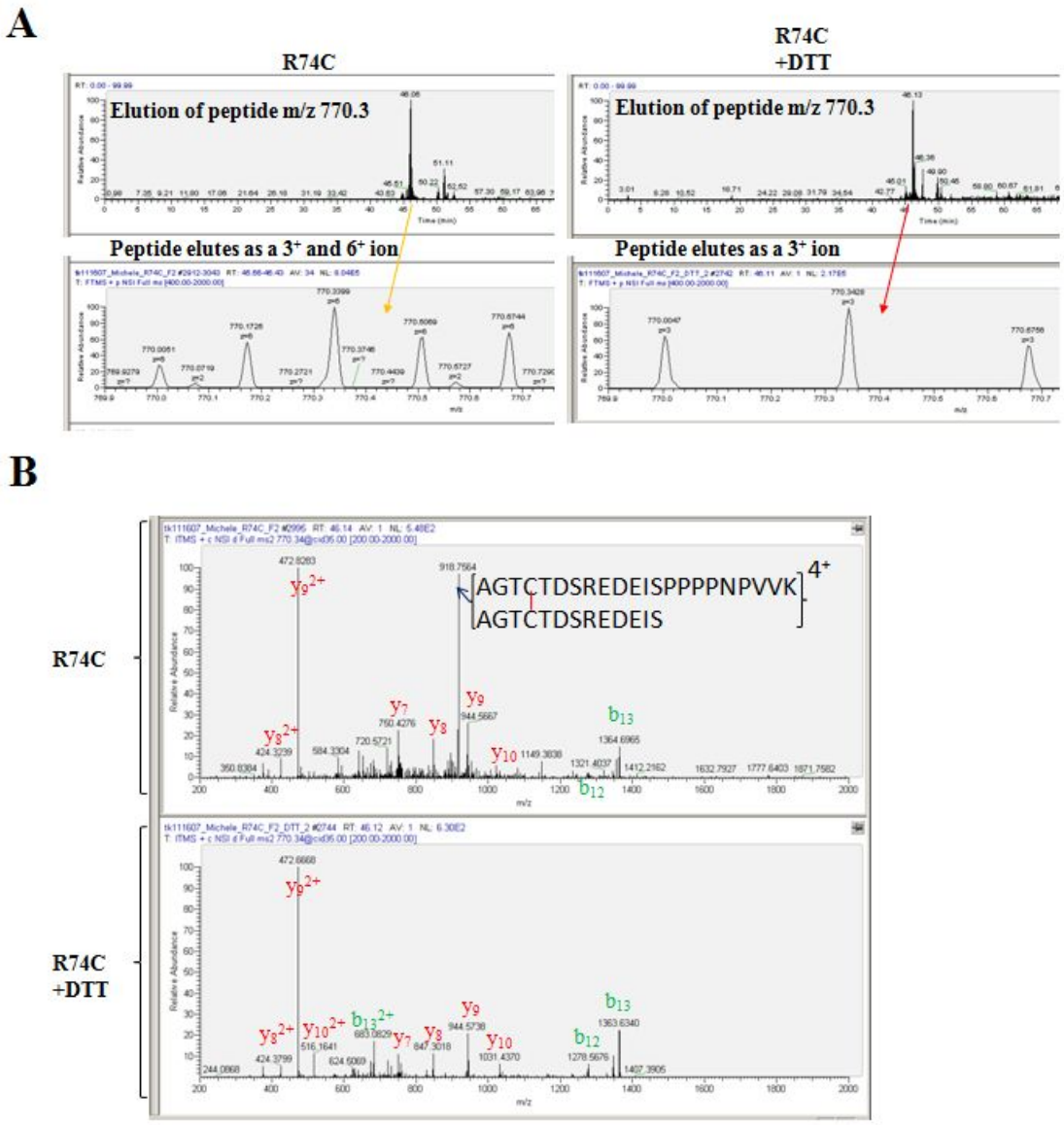

Figure 2.13: Mass spectrometry analysis of R74C sample revealed a bond between the two C74 residues.

(A) One peak, at m/z 770.3, eluted as both a 3+ and 6+ ion in the R74C sample without DTT, but eluted as a 3+ ion in the R74C sample with DTT.

(B) The samples were then analyzed by tandem mass spectrometry and revealed a peak that eluted as a 4+ ion at m/z 918.75. This peak constituted the 4+ ion of two peptides linked by a cysteine-cysteine bond, one peptide being the full length peptide and the second being the b13 fragment. This peak was not detected in the sample with DTT.

showed a slightly higher activation constant than either the wild-type RIα or R74C P2 holoenzyme [Figure 2.14]. When R74C P1 was reduced before forming a complex with C-subunit, the activation constant was about the same as both wild-type RIα and R74C P2 holoenzyme.

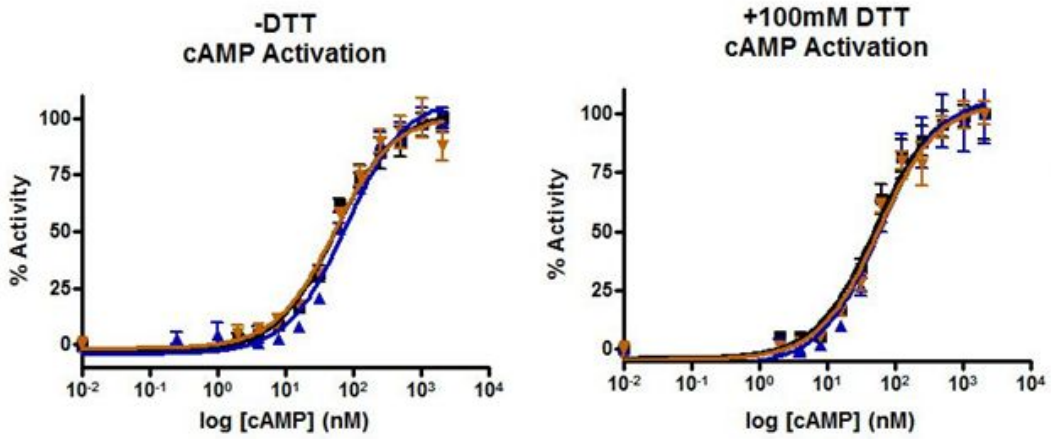

	EC50 -DTT	EC50 +DTT
■ wt RIα	53.9 ± 1.2	50.1 ± 1.2
▲ R74C P1	78.1 ± 1.1	59 ± 1.3
▼ R74C P2	52.3 ± 1.2	56 ± 1.2

Figure 2.14: Tetrameric R74C holoenzyme showed a slightly higher activation constant.

The effect of dimeric and tetrameric R74C on PKA activation by cAMP was measured. Wild-type RIα and R74C P2 holoenyzme showed similar apparent activation constants (EC50). R74C P1 holoenzyme showed a slightly higher EC50. In the presence of DTT, the EC50 of R74C P1 decreased to those seen from wild-type and R74C P2.

2.4: Discussion

RIα has been studied extensively in its roles as an inhibitor of the C-subunit of PKA as well as its involvement in disease. However, to date, the mechanism of *PRKAR1A* involvement in Carney complex is unknown. For this study, we chose two mutations that evade NMD and studied their effects *in vitro*: RIα R74C and RIα(1-303). R74 is a highly conserved residue among mammalian RIα, while the RIα(1-303) truncated protein results in the deletion of the second cAMP binding site, cutting the structure off at the β4-β5 loop.

It has been shown that RIα exists as a dimer when purified from *E. coli* [76] and its biochemical properties both alone and with the C-subunit have been well-studied. We wanted to first determine whether these Carney complex-related mutants were capable of forming functional dimers. We found that both of these mutants were functional dimers and both formed a holoenzyme complex with the C-subunit [Figures 2.4, 2.5]. The R74C holoenzyme showed a similar activation constant compared to wild-type RIα holoenzyme when the activation was carried out in the presence of DTT [Figure 2.6]. However, in the absence of DTT, a slightly higher activation constant was observed [Figure 2.14]. This difference in activation could indicate that the extra cysteine caused the holoenzyme to form a slightly tighter complex.

The activation of the RIα holoenzyme is highly cooperative [21]. cAMP binds to the PBC in CBD B, which opens up the structure, allowing a second molecule of cAMP to bind to the PBC in CBD A. The RIα(1-303) holoenzyme needed more cAMP for PKA activation. Its activation constant increased by about 4-fold compared

to wild-type RIα holoenzyme. With the deletion of the cAMP binding site in CBD B, it was likely that cAMP had more difficulty in accessing the PBC in CBD A.

The mutation of R74 to C in RIα could result in two possibilities when expressed in cells. One possibility is that it could affect the pre-existent disulfide bonds; however, this was not the case [Figure 2.10B]. Alternatively, it could form an intermolecular disulfide bond. This formation of an external disulfide bond is what we observed with purification of R74C under non-reducing conditions. Under non-reducing purification conditions, R74C formed a tetramer [Figure 2.12], which when in complex with C-subunit, showed that a slightly higher amount of cAMP was needed for its activation [Figure 2.14].

Although the change in PKA activation *in vitro* was not dramatic, this change with the R74C mutation in structural conformation could display significant effects in mammalian cells. The higher amounts of cAMP needed for PKA activation could imply that the C-subunit stays in an inactive state when cells express the R74C mutant, thus inhibiting it from phosphorylating its downstream substrates. Diminished PKA activity has already been implicated in diseases, such as systemic lupus erythematosus [66]. Moreover, in knockout mice, the loss of Cα subunit and hence lowered PKA activity, showed neonatal lethality or growth retardation [77]. Furthermore, the tetrameric conformation could affect AKAP binding which would lead to different targeting in cells. Therefore, future studies are needed to determine if this change occurs in mammalian cells and we address these questions in Chapter 3.

2.5: Acknowledgements

We would like to thank CJ Allison, Sventja von Daake, and Jie Yang for suggestions regarding the purification of human RIα. We also thank Mike Deal for providing purified C-subunit. We would also like to thank Adrian Saldanha for advice on using the multiplate reader for the PKA activation assay. Thanks to Nina Haste and Jian Wu for help with making the structure figures. This work was supported by the NIH/NCI Growth Regulation & Oncogenesis Training Grant and the UCSD Bioinformatics Program.

Chapter 2, in part, will be submitted for publication. Day, M.E., Koller, A., and Taylor, S.S. Analysis of disulfide bonds in PKA RIalpha dimers reveals the loss of wild-type RIalpha homodimers in the presence of Carney complex-associated mutant RIalpha. The dissertation author was the primary investigator and author of this work.

Chapter 3:

Characterization of RIα mutants in mammalian cells

3.1: Introduction

By expressing RIα mutants in *E. coli*, we saw that Carney complex (CNC)-related RIα mutants can behave differently from wild-type RIα [Chapter 2]. However, to understand how RIα mutants contribute to disease, it is essential to express them in mammalian cells, which is the focus of this chapter.

Most of the CNC-related mutations result in a haploinsufficiency of RIα because of a premature stop codon that signals nonsense-mediated mRNA decay (NMD) surveillance. However, many of the mutations evade NMD and are expressed [Chapter 2, Tables 2.1-2.3]. Using our knowledge of RIα along with the results from Chapter 2, we can predict the biochemical effects of the other mutations. For example, one mutation, S9C, could result in a change in disulfide bond formation at the N-terminus or could affect the dimerization, similar to what we saw with the R74C mutation. Another mutation, RIα Δ61-116, which eliminates the linker region and disrupts C-subunit binding, would result in constitutively active PKA. Another CNC mutation, A213D, is located in the phosphate binding cassette (PBC) of the first cAMP binding site (CDB A) and would likely lead to a defect in cAMP binding. The A317frameshift, which changes the residues after residue 316 and causes a truncation immediately before the PBC in the second cAMP binding site (CDB B), could be similar to our findings with RIα(1-303) and need a higher amount of cAMP for PKA activation. Most of these mutations were very recently reported [73], but we assume that all of them will adversely affect the functionality of RIα. Unlike the other mutations that result in a haploinsufficiency, these mutations would likely result in

same levels of total RIα expression. However, assuming equal levels of expression and binding affinities between wild-type RIα and mutant RIα, a majority of the RIα dimers would consist of the mutant homodimers and heterodimers, reducing the wild-type RIα homodimer to levels even lower than that seen from haploinsufficiency, which may be how these mutations that evade NMD still result in Carney complex.

The natural occurrence of RIα heterodimers has already been reported [30]. A little over a decade ago, Tasken *et al.* reported that RIα can form a heterodimer with RIβ. Combining their data from *in vitro* dimerization of recombinant RIα and RIβ subunits with their Western blot analysis of homogenates from a human neoplastic B cell line (Reh cells) led them to deduce that the RIα:RIβ heterodimer formed quite easily [30]. The fact that they saw almost all of the RIβ subunits involved in a RIα:RIβ heterodimer complex suggests that this heterodimer forms more readily than a RIβ homodimer. More recently, using a yeast two-hybrid assay, Carlson *et al*. confirmed that RIα:RIβ heterodimers could form and suggested that the heterodimers could bind to D-AKAP1 [78]. This binding was in contrast to the RIβ homodimers that did not interact with D-AKAP1 [40]. Thus, the heterodimers could interact in novel ways with known AKAPs and thus potentially affect its targeting in cells.

Expression of a mutant RIα with wild-type RIα could also form heterodimers that are functionally different from either wild-type or mutant RIα homodimer. If only mutant RIα homodimers form, then the amount of wild-type RIα homodimers would reduce by 50%, which could be similar to the effects of haploinsufficiency of RIα. On the other hand, if mutant RIα heterodimers and homodimers form, as we predict they

would, then the amount of wild-type RIα would now be reduced by 75%, which would actually be worse than the effects from haploinsufficiency.

For this study, we investigated the outcome of co-expressing mutant RIα subunits with wild-type RIα in mammalian cells. We engineered GFP-tagged constructs of RIα to facilitate visualization. HEK 293 cells stably expressing mutant RIα were used to track the heterodimerization and to detect novel binding partners. We used diagonal electrophoresis to decipher the protein composition of the dimers and found novel dimers forming in the cells stably expressing R74C.

3.2: Experimental Procedures

Antibodies. RIα antibodies from Chapter 2 were used. Rabbit polyclonal anti-calmodulin binding peptide was purchased from Millipore.

Cloning for expression in mammalian cells. Bovine RIα and human RIα were subcloned into the HindIII-KpnI site of pEGFP C2 vector (Clontech). Human RIα was subcloned into BamHI-HindIII site of pNTAP (Stratagene). Truncated RIα (1-303, 1-246, 1-93, and 93-379) was isolated by PCR and the amplified cDNA subcloned. Single site mutations were introduced by QuikChange mutagenesis.

Cell culture conditions. HeLa and HEK 293 cells were obtained from the American Type Culture Collection. Cells were maintained in DMEM supplemented with 10% fetal bovine serum (HyClone), 2 mM GlutaMax (GibcoBRL), and 100 units/mL penicillin and streptomycin (GibcoBRL) under 8% CO_2. Stable cells were maintained in the same media as above, but with an additional 500 μg/mL geneticin (Gibco). Transient transfections were carried out by Fugene 6 (Roche) one day prior to analysis. Procedure for imaging the GFP transfections is described in Chapter 5.

Generation of stable cell lines. Stable cell lines of HEK 293 were generated by transfection with Lipofectamine 2000 (Invitrogen) and selected accordingly for genetecin resistance. Stable expressors were chosen from a Western blot, which was probed with anti-calmodulin binding peptide to find TAP expression.

Whole cell lysis. Mammalian cells were harvested in PBS and lysed by resuspension in lysis buffer (50 mM Tris (pH 7.0), 150 mM NaCl, 1 mM EDTA and 1.0% NP-40) for 10 minutes on ice.

Two dimensional gel electrophoresis. Samples were resolved on a 4-12% Bis-Tris polyacrylamide, NuPAGE gel (Invitrogen). After non-reducing electrophoresis, the entire lane containing the resolved proteins was excised and incubated in SDS sample buffer containing 100 mM DTT (to reduce any disulfide bonds present between proteins) for 15-30 minutes. The slice was rotated 90° and laid horizontally on top of a large format 1.5-mm thick 4-12% Bis-Tris polyacrylamide, NuPAGE gel (Invitrogen) for reducing gel electrophoresis. At this stage, proteins that were linked by a disulfide bond were separated and resolved from one another, allowing them to migrate further down the gel at their true molecular weight in the second dimension. Gels were stained with colloidal Coomassie Blue G stain then destained in 20% methanol to visualize the proteins. To enhance detection of lowly expressed proteins, the destained gels were then rinsed in double distilled water for 10 minutes with gentle agitation and silver stained using the SilverQuest Silver Staining Kit (Invitrogen). Gels were also analyzed by Western blot, as described in Chapter 2. When RIα antibodies were mixed, the primary antibodies were diluted in PBST without milk.

Pull-down experiments. Stable cells were grown on Nunc dishes and harvested at 80% confluency in PBS. Cells were lysed in 50 mM Tris (pH 7.0), 150 mM NaCl, 1

mM EDTA and 1.0% NP-40 by three freeze-thaw cycles. Lysates were bound to streptavidin resin for 2 hours and proteins were eluted with streptavidin elution buffer which contains biotin (Stratagene).

Hydrogen peroxide treatment. Stable cells were grown on Nunc dishes and treated with 100 μM hydrogen peroxide for 5 minutes at 37°C prior to harvesting. Cardiac myocyte cells were grown on glass coverslips and treated with 100 μM hydrogen peroxide for 10 minutes at 37°C prior to immunofluorescence staining.

Immunofluorescence staining. Cells were fixed in 4% paraformaldehyde for 15 minutes at room temperature, then blocked in 10X blocking buffer (0.2% Triton X-100, 1% BSA, 0.4% glycine, 1% fish gelatin, and 1% Normal Donkey Serum) for 20 minutes at room temperature. Primary antibody (in-house anti-RIα) was diluted (1:50) in 1X blocking buffer and left on cells overnight at 4°C. Wash steps before and after antibody incubations were performed using 1X blocking buffer. Donkey anti-rabbit FITC (Jackson ImmunoResearch) was used as secondary antibody at a dilution of 1:100 in 1X blocking buffer and left on cells for 1 hour at room temperature. Cells were fixed with 4% paraformaldehyde for 15 minutes, washed with 1X Dulbecco's PBS (Mediatech), and then washed with double deionized water three times. Hoechst stain (1:1000 dilution in water) was added to the plates for 20 minutes at room temperature and washed away with water. Epifluorescent images were acquired at room temperature on Zeiss Axiovert 200M, using 40x 1.3 oil objective.

3.3: Results

Expression of CNC mutants in mammalian cells. Since Carney complex patients have heterozygous expression of wild-type and mutant RIα, the expression of RIα mutants was investigated in mammalian cells. RIα is mostly cytosolic, but this localization may change with certain mutations. RIα constructs were cloned into a GFP-tagged expression vector, where the GFP was at the C-terminus. The GFP constructs engineered for this chapter are shown in Figure 3.1A and most were transiently transfected into HeLa cells [Figure 3.1B]. The GFP vector alone was used as a control. Both wild-type RIα and R74C were diffuse in the cytoplasm with a faint punctate pattern. The significance of these puncta will be discussed in further detail in Chapter 5. This punctate pattern was not displayed in the cells transfected with RIα(1-303) or RIα(1-246), though these proteins were diffuse in the cytoplasm. RIα(1-303) was excluded from the nucleus while RIα(1-246) also showed strong nuclear localization. RIα(1-246) has the entire CBD B deleted and was used as a control for comparison with RIα(1-303) which is missing only part of CBD B, including the PBC. We did not pursue the localization of RIα(1-246) further.

Heterodimer formation between RIα and mutant RIα. We wanted to determine whether dimerization between R74C and wild-type RIα could occur in mammalian cells. Because RIα can form disulfide-bonded dimers, we have a mechanism to visualize the dimers on a denaturing gel in the absence of DTT. HeLa and HEK 293 cells were first transiently transfected with GFP-tagged RIα constructs and

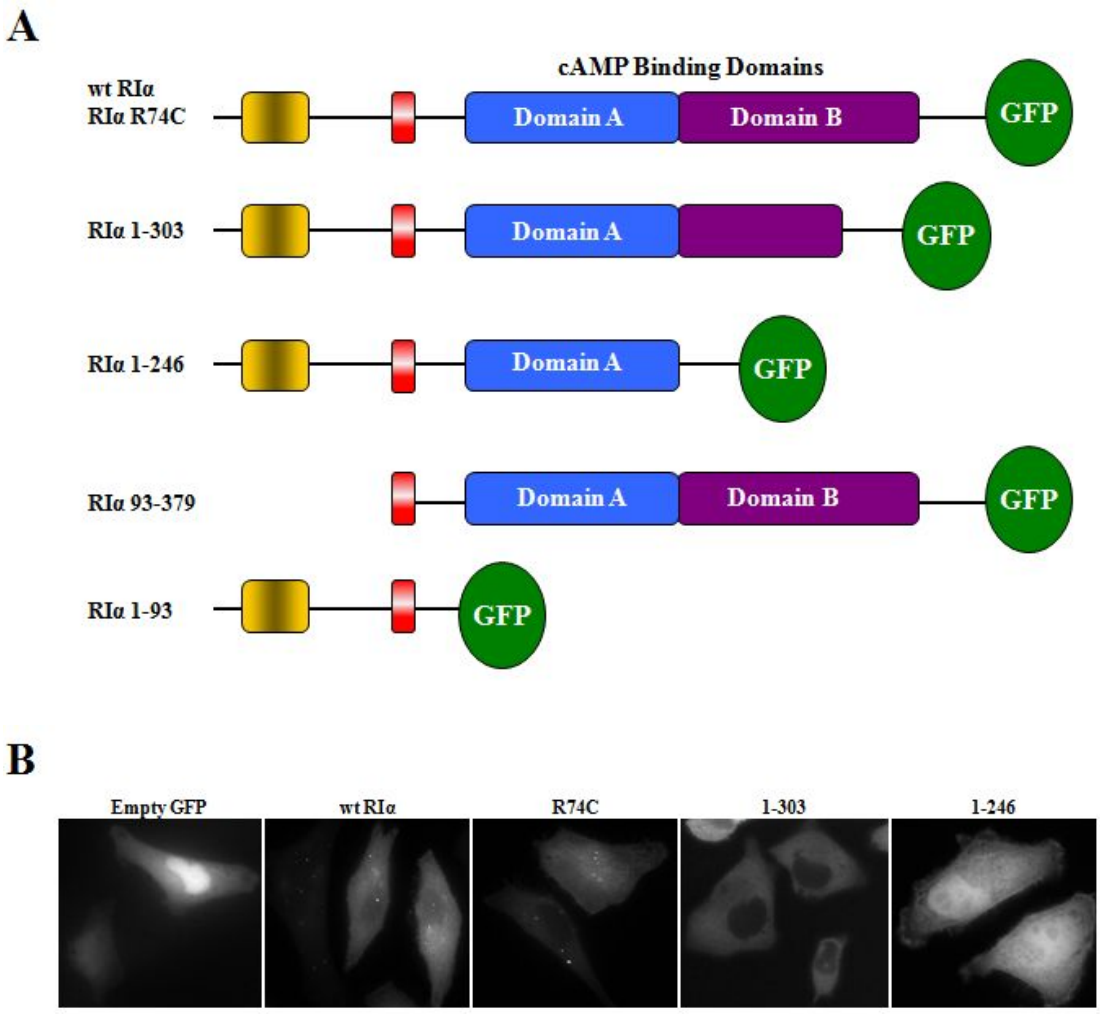

Figure 3.1: GFP-tagged RIα constructs showed different localizations.

(A) Constructs of RIα were cloned into GFP-tagged expression vector. GFP was expressed at the C-terminus.

(B) GFP-tagged constructs were expressed using transient transfection in HeLa cells. As a control, empty GFP showed diffuse localization everywhere. Wild-type RIα and R74C showed diffuse localization in the cytoplasm and was mostly excluded from the nucleus. A faint punctate pattern was noticed. RIα(1-303) and RIα(1-246) showed a diffuse pattern without the puncta. RIα(1-303), but not RIα(1-246), was excluded from the nucleus.

dimerization was assessed using a Western blot on the cell lysates run under both non-reducing and reducing conditions [Figure 3.2A and B]. From the Western blot under non-reducing conditions, multiple bands, corresponding to both the homodimers and heterodimers were observed. In the untransfected HeLa cells, endogenous RIα was in both the oxidized and reduced states. On the other hand, only the reduced form of endogenous RIα was detected in HEK 293 cells. In the transfected HeLa cells, five bands were identified: oxidized and reduced RIα GFP, oxidized and reduced endogenous RIα, and a heterodimer of RIα GFP:endogenous RIα. Similarly, in the transfected HEK 293 cells, four bands were identified: oxidized and reduced RIα GFP, reduced endogenous RIα, and a heterodimer of RIα GFP:endogenous RIα. Thus, mutant RIα can form a heterodimer with endogenous RIα in both HeLa and HEK 293 cells. Under reducing conditions, only the reduced forms of RIα GFP and endogenous RIα existed.

Since the RIα antibody is known to cross-react weakly with RIβ, the band detected above the endogenous RIα in HeLa cells under reducing conditions was speculated to be RIβ [Figure 3.2A, right panel]. The levels of this RIβ band were comparable to that of the endogenous RIα band in both the untransfected cells and the cells transfected with wild-type RIα GFP. However, in the HeLa cells transfected with mutant RIα GFP, the RIβ band was not seen. These results suggest multiple things. First, the RIα and RIβ heterodimers exist in these cells. We would have expected to see a band corresponding to this heterodimer in the gel run under non-reducing conditions. However, as will be discussed in the next section, the

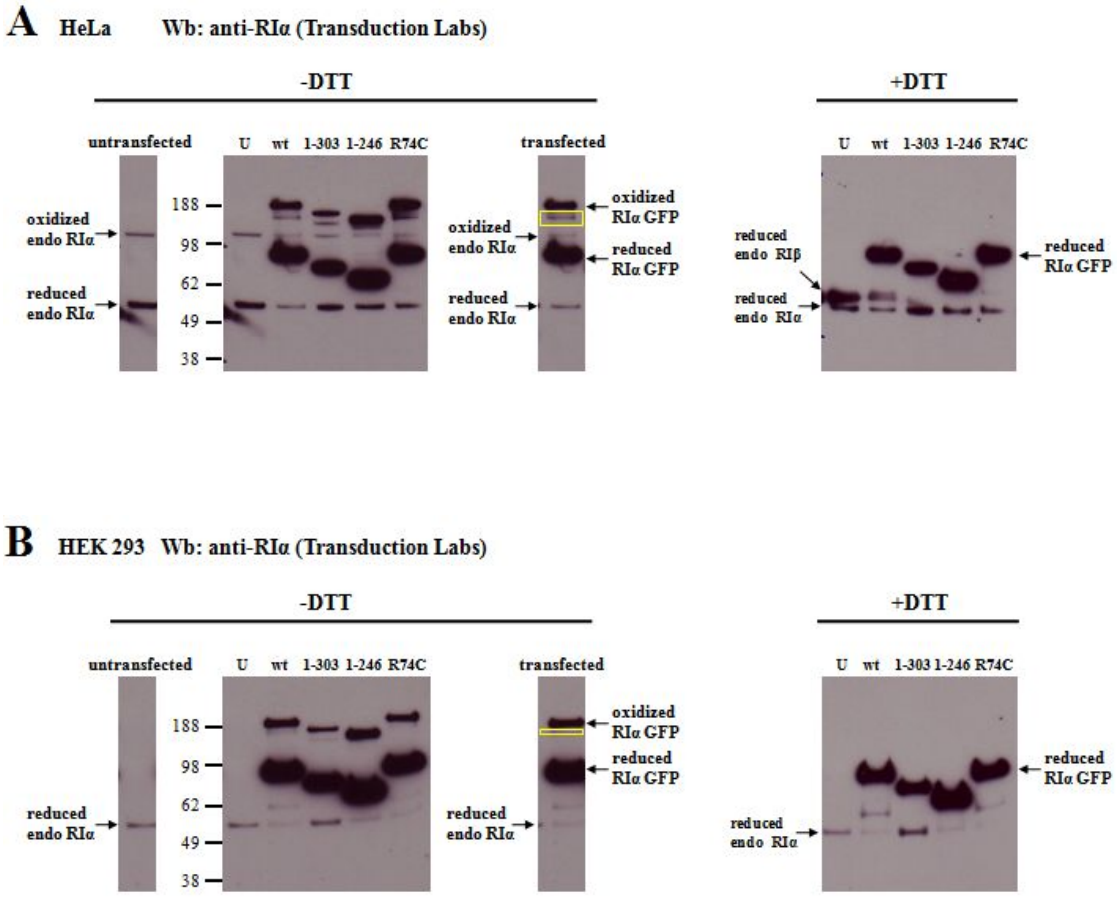

Figure 3.2: GFP-tagged RIα in HeLa and HEK 293 cells formed heterodimers.

HeLa (A) and HEK 293 cells (B) were transiently transfected with GFP-tagged RIα constructs. A Western blot of the cell lysates (10 µg total protein) revealed multiple protein populations from each transfection. Untransfected cells are marked as 'U'. The different protein populations are marked on strips to the left and right of the full-size Western blot. Heterodimers of GFP-tagged RIα:endogenous RIα, indicated by yellow squares, were detected. Under reducing conditions, only reduced forms of GFP-tagged RIα and endogenous RIα were present so the heterodimers seen under non-reducing conditions were due to cysteine bonds. The band above the endogenous RIα in the Western blot of HeLa cells is assumed to be RIβ that was picked up from cross-reactivity of the antibody. Thus, heterodimers of RIα:RIβ also formed but were quickly degraded in the cells transfected with mutant RIα.

commercially available antibody used for this Western did not accurately reflect the amount of disulfide-bonded dimers. Second, the RIα:RIβ heterodimers that formed in the cells transfected with mutant RIα were most likely mutant heterodimers which were quickly degraded.

Dimerization is not due to the GFP tag. The question arose whether the dimerization of RIα GFP in these SDS-PAGE gels was from RIα or from GFP itself. However, the results from Figure 3.3A and B proved that the dimerization is not due to the GFP tag. HEK 293 cells were transiently transfected with the GFP-tagged construct of RIα(93-381), which lacked the D/D domain. Without this D/D domain, RIα(93-381) itself cannot dimerize. A Western blot of these cells showed only a reduced form of RIα(93-381) GFP; hence, the dimerization is not due to GFP. To confirm the recognition of oxidized RIα GFP, the same two antibodies that were discussed in Chapter 2 were used. Again, the commercial antibody from Transduction Laboratories preferentially recognized the reduced form [Figure 3.3A], as indicated by the intensity of these bands compared to the corresponding ones in the blot probed with in-house antibody [Figure 3.3B]. Furthermore, the reduced endogenous RIα was detected with the commercial antibody, but not the in-house antibody. However, the in-house antibody was able to detect the reduced form of RIα GFP, most likely due to their high levels of expression.

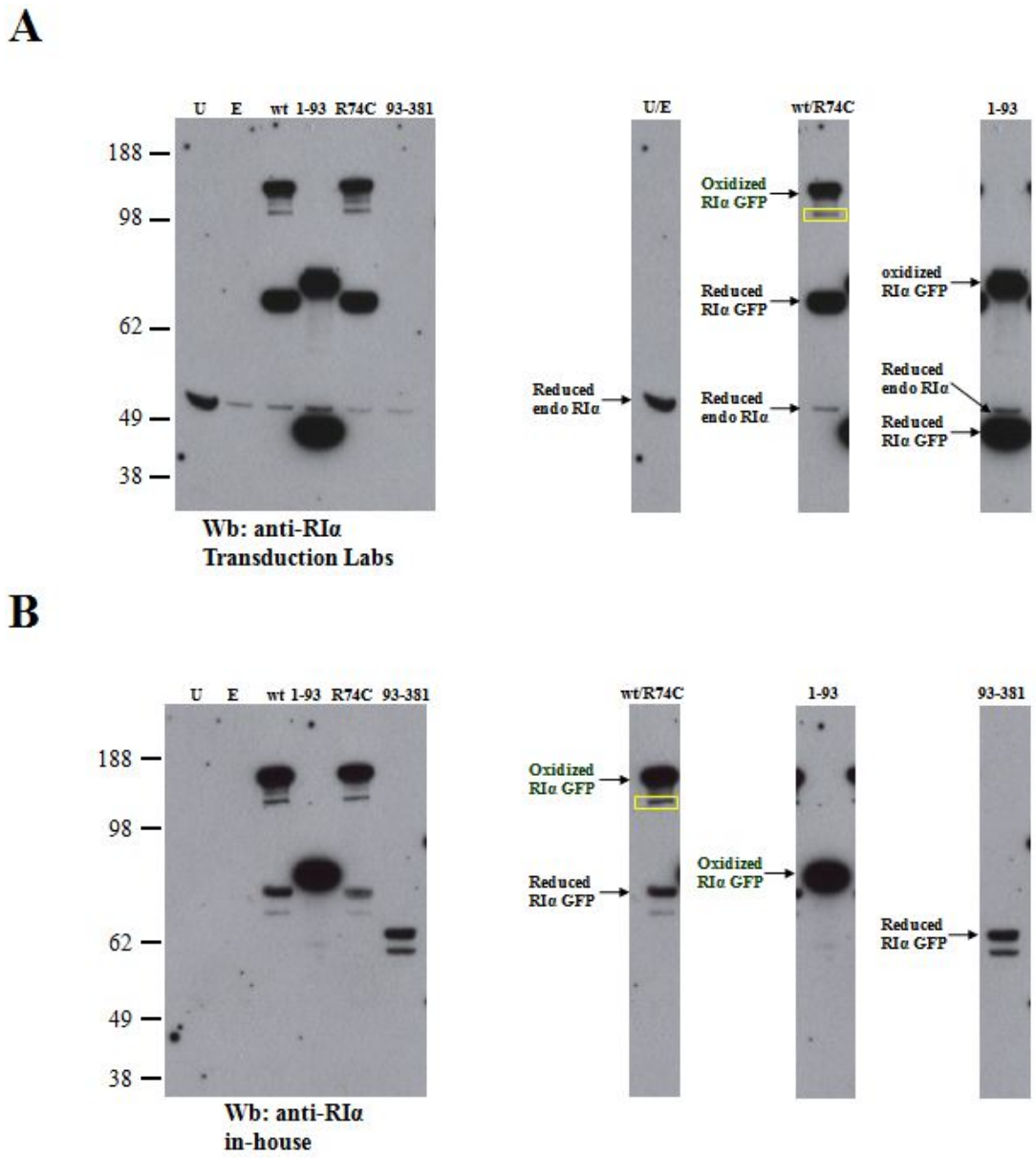

Figure 3.3: Dimerization of RIα GFP was not due to GFP.

GFP-tagged constructs, transiently transfected in HEK 293 cells, were analyzed under non-reducing conditions using two different antibodies. Untransfected cells are labeled as 'U', while cells transfected with empty GFP vector are labeled 'E'. Strips of each lane are labeled to the right of the full-size Western blot. Heterodimers of RIα GFP:endogenous RIα are indicated by the yellow squares. Since RIα(93-381) GFP, which does not have the dimerization domain, did not show an oxidized band in either gel, the oxidation of RIα dimers was due to the cysteines in RIα and not due to GFP. Commercially available antibody showed preferential recognition for the reduced form of RIα (A), when compared to the recognition by the in-house antibody (B).

Generation of stably expressed RIα cell lines. To determine how expression of RIα mutants influences the expression levels of endogenous RIα and to see whether these mutants bind to novel binding partners, RIα constructs with a TAP tag were engineered and transfected into HEK 293 cells to produce stable cell lines. The TAP system has two tags, a calmodulin binding peptide (CBP) and a streptavidin binding peptide (SBP), which are both at the N-terminus of RIα [Figure 3.4A]. HEK 293 cells stably expressing TAP-tag alone, TAP-tagged wild-type RIα, and TAP-tagged R74C were made. A Western blot of the cell lysates, probing for CBP, demonstrated which cell lines were stably transfected with TAP-tagged RIα [Figure 3.4B]. Cell line 3 was kept for wild-type, while cell lines 6, 7, and 8 were kept for R74C. One cell line stably expressing empty TAP-tag vector was also generated (data not shown). To confirm levels of expression, one line from each stable cell line was analyzed on a Western blot and probed with a mixture of the two RIα antibodies mentioned above [Figure 3.4C]. The samples, run under reducing conditions to keep all of the RIα in a reduced form, displayed similar levels of expression between TAP-tagged RIα and endogenous RIα. Next, we developed tools to purify RIα from these stably transfected cells and visualize the R subunit dimerization.

Stably expressed wild-type RIα form heterodimers with endogenous RIα. Diagonal electrophoresis provides a method to differentially separate and distinguish proteins that contain intramolecular or intermolecular disulfide bonds. In the first dimension, samples are run under non-reducing conditions on an SDS-PAGE gel. The samples

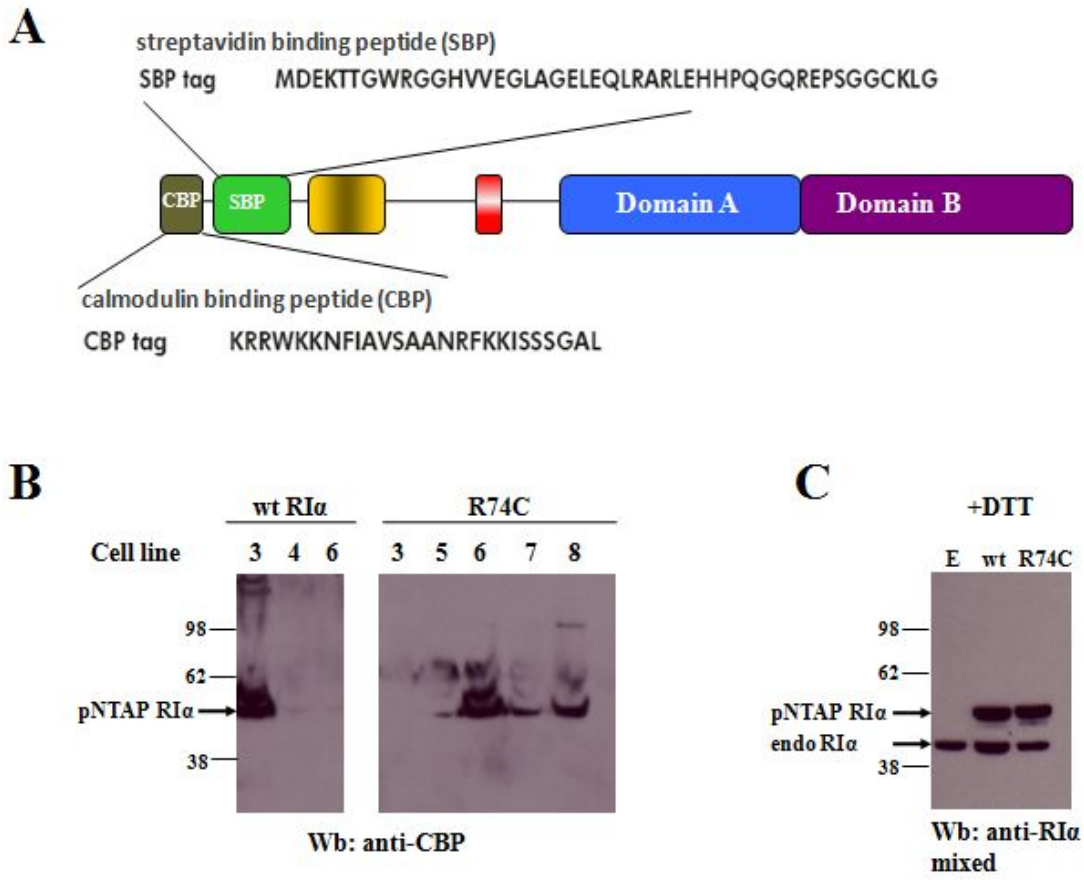

Figure 3.4: Generation of HEK 293 cells stably expressing TAP-tagged RIα.

(A) RIα constructs were cloned into TAP-tagged expression vectors. TAP-tag refers to tandem affinity purification tag. In this vector, the tags, a calmodulin binding peptide and a streptavidin binding peptide, were N-terminal to the protein and added about 8 kDa to the protein size. Stable cell lines were made with the TAP-tagged plasmids.

(B) A Western blot of cells transfected with TAP-tagged RIα constructs was used to check for stable transfections. The blot was probed with anti-calmodulin binding peptide (anti-CBP) to recognize the TAP-tagged constructs, indicated by the black arrow.

(C) One cell line from each stable cell (empty TAP vector, TAP-tagged wild-type RIα, and TAP-tagged R74C) was analyzed under reducing conditions with a mixture of the RIα antibodies (Transduction Laboratories and in-house) to compare expression levels of endogenous and TAP-tagged RIα. 'E' refers to the cells stably expressing empty TAP-tag vector.

are then run in a second dimension under reducing conditions. Bands that run off the diagonal indicate proteins that were disulfide-bonded [Figure 3.5A]. As proof of principle, the system was first tested with wild-type RIα that was purified from *E. coli* and was treated with 5 mM diamide [Figure 3.5B]. This purified RIα had both disulfide-bonded (oxidized) and non-disulfide bonded (reduced) populations under non-reducing conditions. Turning the lane 90° and running it under reducing conditions showed the composition of the protein population that was disulfide-bonded. Protein remaining on the diagonal indicated some of the sample remained oxidized under the experimental conditions.

To characterize the heterodimers of RIα, as well as search for its novel binding partners, we ran diagonal electrophoresis on the stable cell lysates [Figure 3.6]. A Western blot under non-reducing conditions revealed that most of the proteins existed as reduced proteins, most likely due to the reducing environment in mammalian cells. However, faint bands corresponding to the disulfide-bonded proteins could be detected. The Western blot from the second dimension, under reducing conditions, confirmed that the faint bands were disulfide-bonded proteins as the bands ran off the diagonal. We could identify a homodimer of TAP-tagged RIα, a heterodimer of TAP-tagged RIα:endogenous RIα, and a homodimer of endogenous RIα from the stable cells expressing TAP-tagged wild-type RIα, but the homodimer of endogenous RIα was not present in the stable cells expressing TAP-tagged R74C.

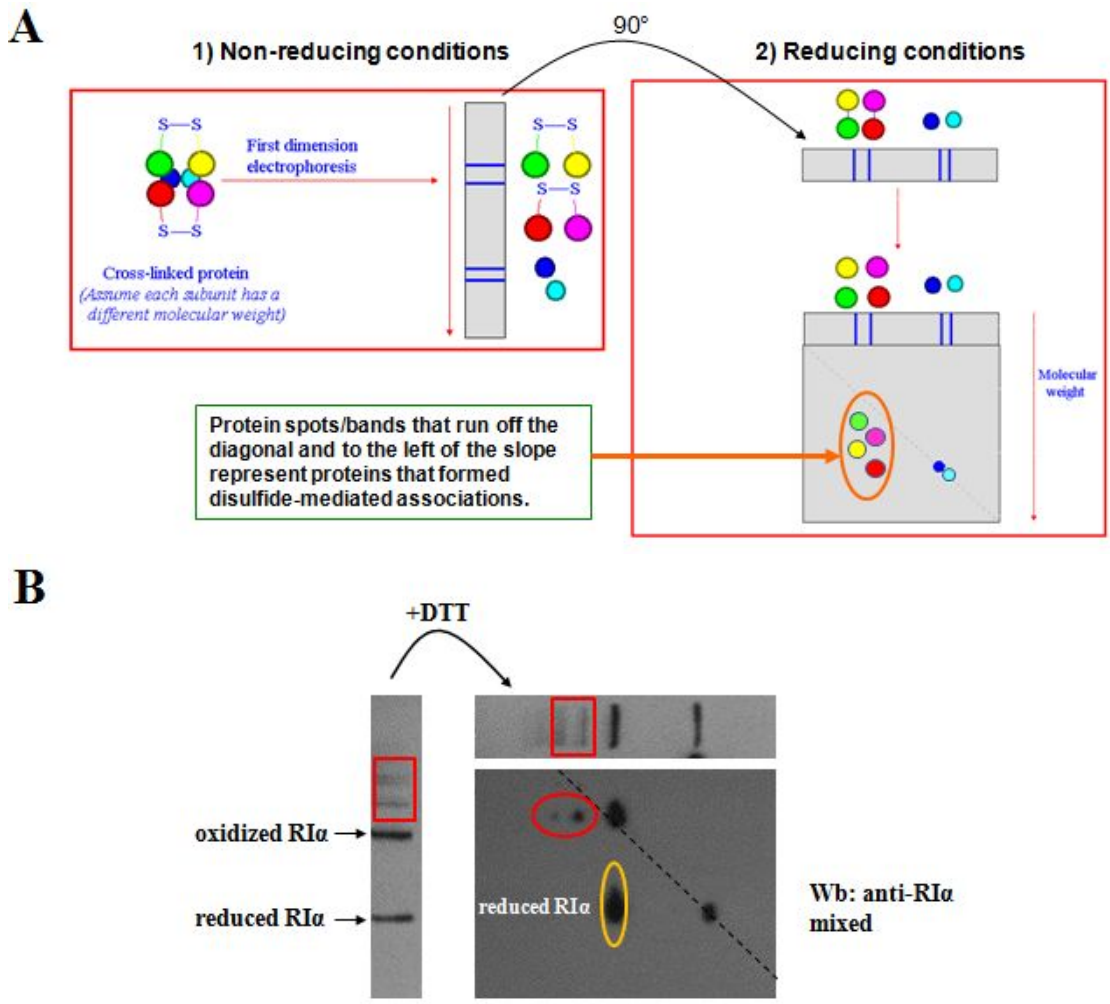

Figure 3.5: Diagonal electrophoresis can identify disulfide-bonded proteins.

(A) Diagonal electrophoresis provides a method to decipher what proteins are involved in a disulfide bond. In the first dimension, the samples are run under non-reducing conditions. Then, in the second dimension, the lane of interest is reduced and run horizontally in another gel. Under the reducing conditions, the proteins that were disulfide-bonded, circled in orange, will run off the diagonal. This figure is adapted from (http://www.food.rdg.ac.uk/online/fs460/lecture9/lecture9.htm).

(B) RIα purified from *E. coli* and treated with diamide (5 mM) was used as proof of principle for the diagonal electrophoresis method. Both an oxidized and reduced form of RIα is seen in the first dimension. In the second dimension, the oxidized protein is reduced to reveal RIα, circled in orange, as the proteins that were interacting in the bond. Faint upper molecular bands, circled in red, were seen above the oxidized protein, most likely due to aggregation of protein from incubation with diamide.

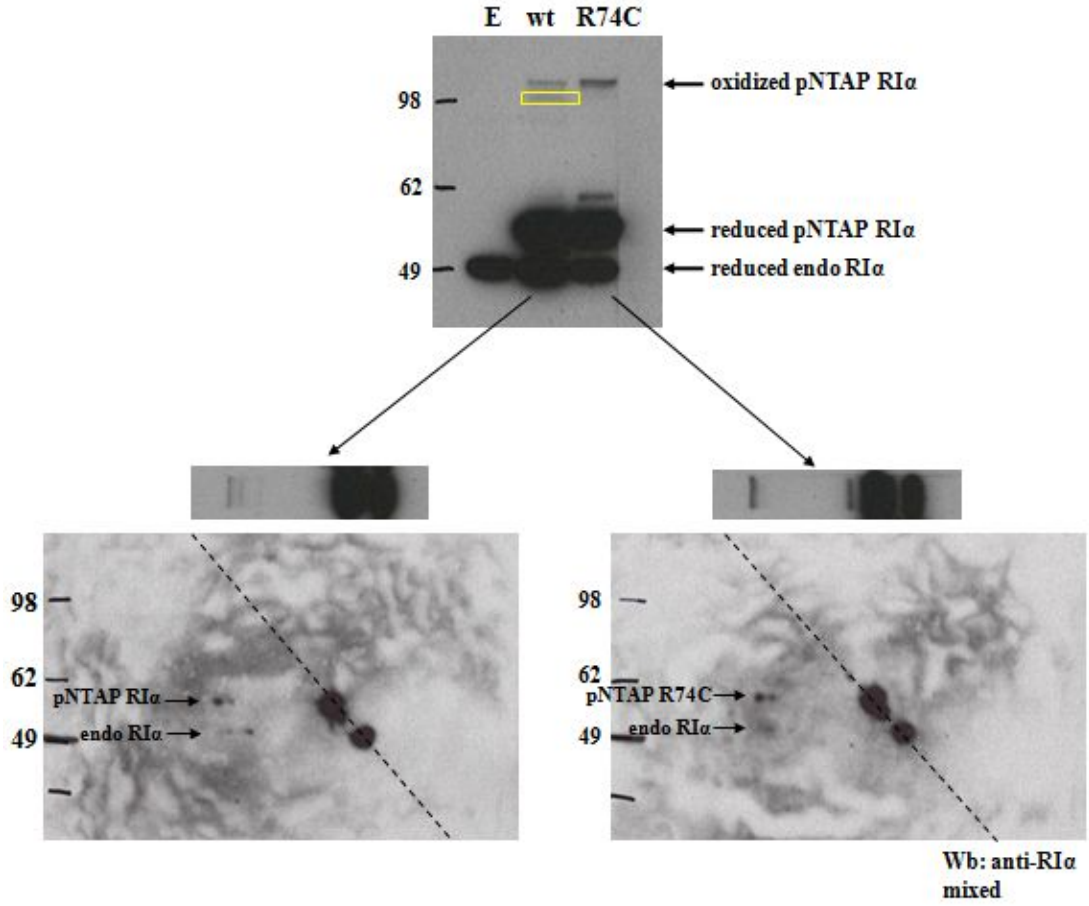

Figure 3.6: Diagonal electrophoresis on stable cell lysates showed the majority of RIα in the reduced state.

Stable cell lysates were analyzed using diagonal electrophoresis. Though the cell lines showed a majority of the TAP-tagged and endogenous RIα in the reduced state, faint bands corresponding to the disulfide-bonded dimer could be detected. In the second dimension, homodimers of TAP-tagged and endogenous RIα were seen. Additionally, heterodimers of TAP-tagged and endogenous RIα were present, also indicated by the yellow square in the first dimension. No heterodimers of RIα:RIβ were seen in this case.

Novel dimers formed in the presence of R74C. To enrich for the heterologous population, the TAP-tagged protein was purified using streptavidin resin [Figure 3.7]. When the TAP-tagged proteins were purified, all of the RIα proteins were now disulfide-bonded, indicating that in the absence of a reducing environment, the disulfide bond forms rapidly. A Western blot of purified TAP-tagged wild-type RIα revealed two protein populations: a homodimer of TAP-tagged protein and a heterodimer of TAP-tagged RIα with endogenous RIα. A Western blot of TAP-tagged proteins, purified from cells stably expressing R74C, revealed four protein populations: a dimer of TAP-tagged protein, a heterodimer of TAP-tagged with endogenous RIα as well as a novel dimer of TAP-tagged R74C and a novel heterodimer of TAP-tagged with endogenous RIα. These bands were analyzed by mass spectrometry and all were confirmed to be RIα. Therefore, we have found that novel disulfide bonds can form with the R74C mutation. Unfortunately, no other proteins that interacted with RIα through a disulfide bond were detected in these cells.

R74C reduced the levels of endogenous RIα homodimer. Hydrogen peroxide is a physiologically relevant oxidizing agent that can promote the formation of disulfide bonds. As discussed before, recent studies reported that disulfide bond formation correlated with the localization of RIα in cells [34]. Though the authors used tissue samples, we tested and confirmed the same results in rat cardiac myocytes in culture. A shift of RIα to the nuclear fraction was seen after treatment with hydrogen peroxide [Figure 3.8A]. Similarly, immunofluorescence microscopy showed that hydrogen

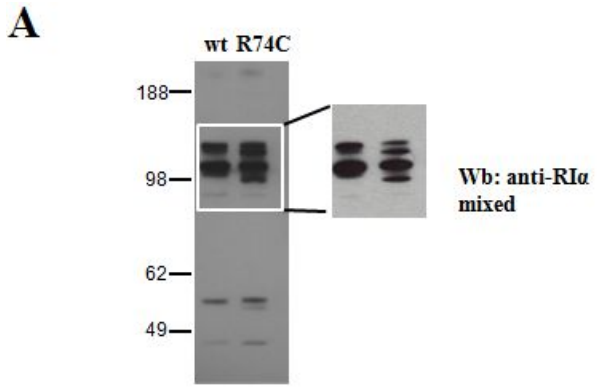

Figure 3.7: Purification of TAP-tagged RIα from stable HEK 293 cells under non-reducing conditions revealed novel dimers in the mutant.

(A) TAP-tagged RIα was purified from stable HEK 293 cells using streptavidin resin and run under non-reducing, denaturing conditions. The protein population was clarified by running the samples under reducing, denaturing conditions and analyzed by Western blot and silver stain in (B).

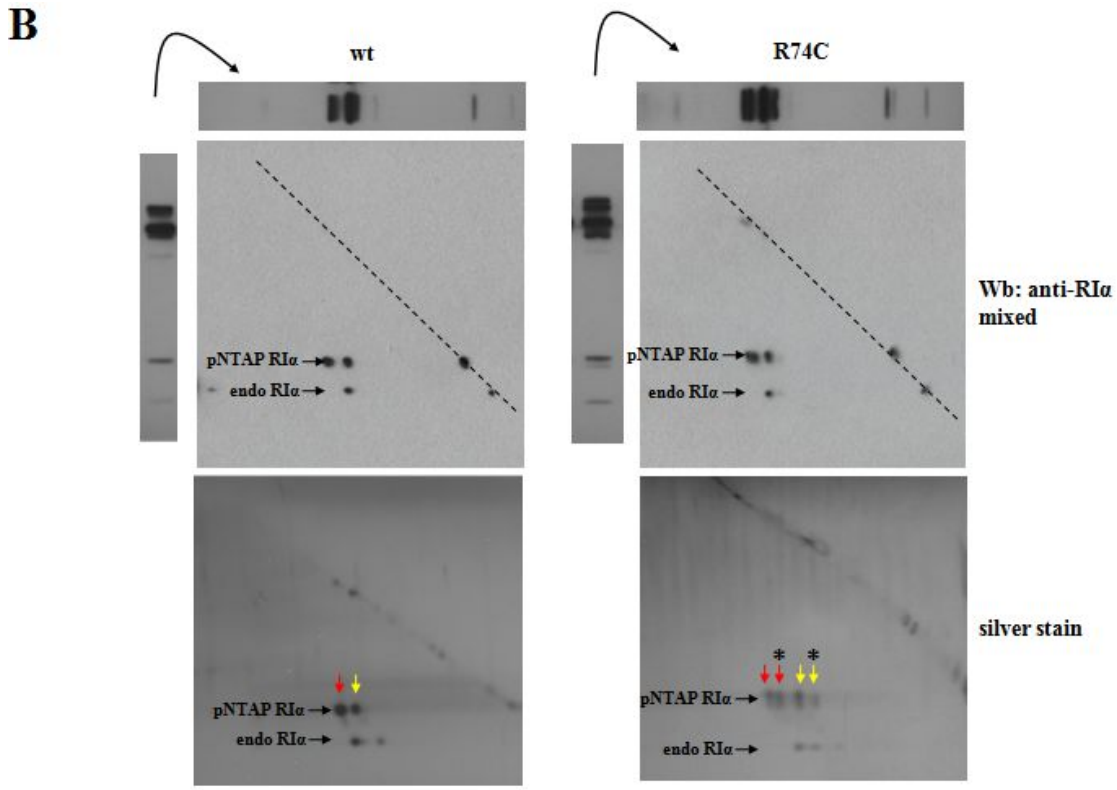

Figure 3.7: Purification of TAP-tagged RIα from stable HEK 293 cells under non-reducing conditions revealed novel dimers in the mutant, Continued.

(B) Purification of TAP-tagged wild-type RIα showed both a homodimer of TAP-tagged RIα (red arrows) and a heterodimer of TAP-tagged RIα:endogenous RIα (yellow arrows). Purification of TAP-tagged R74C showed a different environment. Not only was there a presence of the homodimer TAP-tagged RIα and heterodimer TAP-tagged RIα:endogenous RIα that ran at the same molecular weight as those seen from the cells stably expressing wild-type RIα, but two additional populations were present. These novel dimers are indicated by asterisks above their respective color coded arrow. These bands were analyzed by mass spectrometry and the proteins involved were all found to be RIα.

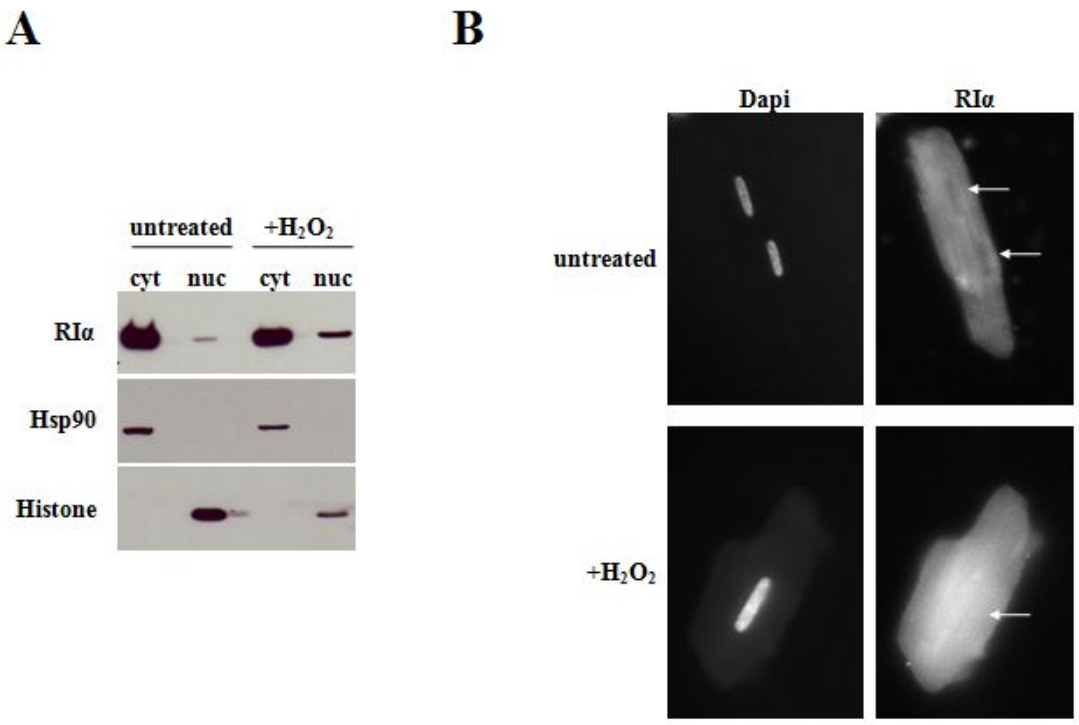

Figure 3.8: Hydrogen peroxide treatment of cardiac myocytes showed a translocation of RIα into the nucleus.

(A) A Western blot of the fractionation of cardiac myocytes treated with hydrogen peroxide showed a shift of RIα to the nucleus, compared to untreated cells. Controls for the compartments are shown – Hsp90 (cytosol) and histone (nucleus).

(B) Staining the treated and untreated cardiac myocyte cells showed additional evidence of the translocation of RIα into the nucleus.

peroxide led to the translocation of endogenous RIα into the nucleus [Figure 3.8B].

Stably transfected HEK 293 cells were also treated with hydrogen peroxide and the resulting R subunit dimers were examined. A Western blot was run on the cell lysates, TAP-tagged protein purified with streptavidin resin (eluted protein), and protein that did not bind to the resin (flow-through) [Figure 3.9]. The reduced form of RIα was not seen in either cell line, indicating that the hydrogen peroxide treatment promoted disulfide bond formations in these cells just as it did in cardiac myocytes.

Lysates from hydrogen peroxide-treated HEK 293 cells stably expressing wild-type RIα had two major protein populations: a heterodimer of TAP-tagged protein with endogenous RIα and a dimer of endogenous RIα. A small amount of TAP-tagged RIα homodimer was also seen. The amount of TAP-tagged RIα homodimer was higher after purification of TAP-tagged protein likely due to artificial oxidation during the purification. As expected, the endogenous RIα dimer was seen in the flow-through.

Lysates from HEK 293 cells stably expressing R74C also had two major bands, but in contrast, they were two heterodimers of TAP-tagged R74C with endogenous RIα. Again, the dimer of TAP-tagged R74C protein was not seen, while the dimer of endogenous RIα was observed in very low amounts. Similar to the purification of TAP-tagged RIα from stable cells of TAP-tagged wild-type RIα, homodimers of TAP-tagged R74C was seen only after purification. The two heterodimers were also among the purified proteins, while the endogenous RIα homodimer appeared only in the flow-through.

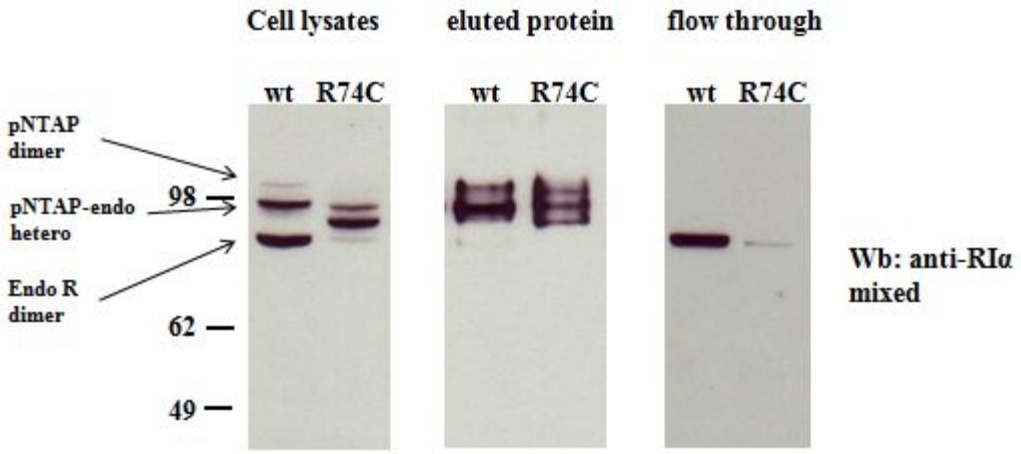

Figure 3.9: R74C altered the dimerization of wild-type RIα.

Cell lysates stably expressing TAP-tagged wild-type RIα and R74C were examined using a Western blot. Cells expressing TAP-tagged wild-type RIα showed three protein populations – homodimers of TAP-tagged and endogenous RIα as well as a heterodimer of TAP-tagged RIα:endogenous RIα. The amount of homodimer TAP-tagged RIα is significantly less than that of the other two protein populations. Cells stably expressing TAP-tagged R74C showed two heterodimers of TAP-tagged R74C:endogenous RIα. The homodimer of TAP-tagged R74C was not detected. The homodimer of endogenous RIα was detected, but in a significantly lower amount, compared to what was seen from the cells stably expressing TAP-tagged wild-type RIα.

3.4: Discussion

While most CNC patients have a haploinsufficiency of RIα due to the NMD-regulated degradation of one mutant *PRKAR1A* allele, a few patients have *PRKAR1A* mutations that escape NMD to create a heterozygous environment with one copy of the wild-type allele and one copy of the mutant allele. Thus, it was of particular interest to see how wild-type RIα is affected by the expression of a mutant RIα in a mammalian system. We expressed TAP-tagged RIα proteins and took advantage of the disulfide bond in the RIα D/D domain to "trap" RIα as a dimer so that RIα homodimers and heterodimers could be characterized from an SDS-PAGE gel.

By transfecting GFP-tagged RIα constructs into HeLa and HEK 293 cells [Figures 3.2, 3.3], we found that disulfide-bonded heterodimers formed. These GFP proteins showed some variation in their localization [Figure 3.1B]. Though the localization of RIα in cells is typically diffuse in the cytoplasm, wild-type RIα and R74C showed diffuse localization in the cytoplasm as well as a punctate pattern in HeLa cells. RIα(1-303) did not show this punctate pattern and was diffuse in the cytoplasm. RIα(1-246) was also diffuse in the cytoplasm and showed no puncta; however, it also localized strongly in the nucleus. Perhaps an undiscovered motif lies in the region from residues 246-303 or that region has a novel binding partner that retained RIα in the nucleus, but we did not pursue this further.

Heterodimers were also seen in HEK 293 cells stably expressing TAP-tagged RIα [Figures 3.6, 3.7, 3.9]. In the stable cells, most of the endogenous and TAP-

tagged RIα were reduced [Figure 3.6], but after purification from the streptavidin resin, they were oxidized and formed disulfide-bonded dimers.

To characterize these heterodimers, we employed diagonal electrophoresis [Figure 3.7]. From the stable cells expressing TAP-tagged wild-type RIα, a homodimer of TAP-tagged RIα and a heterodimer of TAP-tagged RIα:endogenous RIα were purified. The purification of TAP-tagged R74C revealed four protein populations. The same two populations formed by wild-type stables, plus another homodimer of TAP-tagged RIα R74C and another heterodimer of TAP-tagged R74C:endogenous RIα. Therefore, the extra cysteine from the R74C mutation could form additional disulfide bonds that caused the protein to migrate differently on a gel.

The RI subunits exist as dimers independently of any disulfide bonds. By lysing cells in the presence of N-ethylmaleimide (NEM) to block any free sulfhydryl groups and running an SDS-PAGE gel in the absence of DTT, one could tell how many of the dimers are actually disulfide-bonded. However, in our case, we could not use NEM on the TAP-tagged proteins because of the loss of recognition to streptavidin resin when a cysteine in the streptavidin binding peptide is blocked. Thus, oxidation during purification was unavoidable.

In *E. coli*, most of the RIα was disulfide-bonded [Figure 2.10B]. In mammalian cells, however, a significant amount was not disulfide-bonded, though this varied depending on cell type. HeLa cells, for example, did show some disulfide-bonded dimers of endogenous RIα, but most were reduced. Most of the RIα in adult

rat ventricular myocytes is also reduced, but upon treatment with hydrogen peroxide, the amount of disulfide-bonded dimer could be increased [34].

We saw the same effect after treating stable HEK 293 cells with hydrogen peroxide. Without treatment, most of the RIα in the stable HEK 293 cells existed in a reduced state [Figure 3.6]. However, after treatment with hydrogen peroxide, all of the RIα was disulfide-bonded [Figure 3.9], though the bands corresponding to TAP-tagged RIα homodimers were faint in the cells stably expressing wild-type RIα and not visible from the cells stably expressing R74C. In the stably transfected cells, the levels of expression of TAP-tagged RIα seemed close to that of endogenous RIα [Figure 3.4C]. We therefore would expect a 1:2:1 mixture of TAP-tagged dimer: TAP-tagged heterodimer: endogenous RIα dimer. Instead, in cells stably expressing TAP-tagged wild-type RIα, we saw a 1:1 mixture of TAP-tagged heterodimer and endogenous RIα homodimer [Figure 3.9]. The lack of TAP-tagged homodimer could be due to a steric hindrance from the N-terminal TAP tag since we saw that homodimers could easily form when the GFP-tag was at the C-terminus. Or the TAP-tagged homodimer could be missing because it was quickly degraded. More striking, however, was the low level of endogenous RIα homodimer in the cells stably expressing TAP-tagged R74C. This low level of endogenous RIα homodimer was in sharp contrast to the cells stably expressing TAP-tagged wild-type RIα. Different mechanisms for this observation are possible.

The low level of endogenous RIα homodimer may be due to the greater affinity of the TAP-tagged R74C for the endogenous RIα, preventing the

homodimerization of endogenous RIα. The observation that all the R74C protein was in a complex with endogenous RIα is similar to the result where a majority of RIβ formed heterodimers rather than homodimers in Reh cells [30]. However, it is more likely that a fast turnover of the RIα:R74C heterodimers took place. This fast turnover of the heterodimer would continually draw away the endogenous RIα to form new heterodimers, thus preventing the accumulation of endogenous RIα homodimer. The low level of endogenous RIα homodimer was not seen in cells stably expressing wild-type RIα.

We demonstrated that TAP-tagged RIα can form heterodimers with wild-type RIα, which can influence the levels of endogenous RIα homodimer. Therefore, any of the CNC-related mutants can also form heterodimers with wild-type RIα and thus delete the population of RIα homodimers. If CNC-related mutants, such as S9C, were defective in their AKAP binding, they could most certainly diminish the targeting of RIα. If they were less stable and were degraded more rapidly, as we would expect with mutant heterodimers, they could also deplete the endogenous RIα homodimer. Lastly, if they were defective in PKA activation, for example with A213D, a heterodimer could have a dominant negative effect. Since it has been suggested that RIα plays a role in cell cycle and cell growth [for references, see Chapter 1], the missing RIα homodimer could be detrimental to the cells' normal development, which later contributes to the Carney complex disease.

3.5: Acknowledgements

We would like to thank Frank Ma for useful advice on cloning RIα into the GFP vector. We would also like to thank Mira Sastri for help with cloning RIα into the pNTAP vector as well as guidance on generating stable cell lines. Thanks to Hemal Patel for the cardiac myocytes. This work was supported by the NIH/NCI Growth Regulation & Oncogenesis Training Grant and the UCSD Bioinformatics Program.

Chapter 3, in part, will be submitted for publication. Day, M.E., Koller, A., and Taylor, S.S. Analysis of disulfide bonds in PKA RIalpha dimers reveals the loss of wild-type RIalpha homodimers in the presence of Carney complex-associated mutant RIalpha. The dissertation author was the primary investigator and author of this work.

Chapter 4:

Proteomic analysis of the RIα interactome

4.1: Introduction

Historically, the R subunits were exclusively thought to be inhibitors of the PKA C-subunit. However, as more studies were done over the past several decades, it is becoming clear that the R subunits are multifunctional proteins with many different interactions. The interaction to C-subunit is through the pseudosubstrate inhibitor site while the interaction to AKAPs is through the D/D domain. Identifying the interacting partners for a protein of interest is essential for understanding the functionality of that protein and is one aspect of the growing field of proteomics. Several methods exist for determining protein-protein interactions. The traditional way is to use a yeast two-hybrid screen; however, with technological advancements, new methods include protein microarrays and immunoprecipitation followed by mass spectrometry, which make it possible to study proteins on a large-scale. By studying proteins on a large-scale, the complexities of protein-protein interactions are better understood which in turn lead to a more comprehensive understanding of mechanisms underlying disease. For this chapter, we developed affinity methods and mass spectrometry techniques to identify known and novel binding partners of RIα.

Literature searches for less canonical binding partners of RIα reveal at least 20 other proteins that putatively bind directly to RIα [Table 4.1]. Most of these binding partners were detected through the conventional yeast two-hybrid or immunoprecipitation methods and their mechanisms for binding were identified. GCP60 binds to sites at both the N- and C-terminus of RIα [personal communication, Dr. Donald Blumenthal], while binding of human X chromosome-encoded protein

Table 4.1: Known RIα binding partners.

Results from a literature search for binding partners to RIα are listed. Most of the sites of interaction are located in the D/D domain. Some sites were not indicated in the study and have been listed as 'not stated'. The experiments, species used, and references are listed.

RIα binding partners	**RIα binding site**	**Experimental validation**	**Source**	**Ref**
cAMP dependent protein kinase, catalytic, alpha	inhibitor site (IS)	Gel filtration	bovine heart	[79]
cAMP dependent protein kinase, type I beta, regulatory subunit	D/D domain	yeast 2 hybrid, WB of cells	human neoplastic B cell line	[30]
D-AKAP1/S-AKAP84/AKAP149	D/D domain	yeast 2 hybrid, surface plasma resonance	human	[40]
AKAP4/AKAP82/FSC1	most likely D/D domain	yeast 2 hybrid, in vitro binding	mouse testis	[80]
AKAP7 gamma	D/D domain	yeast 2 hybrid, co-IP	human (HEK 293 cells)	[81]
AKAP10/D-AKAP2	res 1-62	yeast 2 hybrid, co-IP	mouse testis	[39]
AKAP11/AKAP 220	D/D domain	IP	human testis	[82]
RFC40 (2nd subunit of replication factor c complex)	res 1-76	yeast 2 hybrid, colocalization in cells (IF)	human (MCF-10A cells)	[36]
ARFGEP2/BIG2 (ADP-ribosylation factor guanine nucleotide exchange factor 2)	res 1-59	yeast 2 hybrid	human liver cells	[83]
PRKX	RRXA	surface plasma resonance	monkey (COS cells)	[84]
myo7A (myosin 7A)	res 19-76	yeast 2 hybrid, co-IP	human (HEK 293 cells)	[85]
Grb2	SH3 binding domain	IP	human (MCF-10A cells)	[26]
EGFR	not stated	IP	human (MCF-10A cells)	[26]
α4 integrin	not D/D domain	IP	Jurkat cells, mouse embryonic fibroblasts	[86]
cyclin E1	RXL motifs	IP	human (MCF-7 & HEK 293 cells)	[87]

Table 4.1: Known RIα binding partners, Continued.

RIα binding partners	RIα binding site	Experimental validation	Source	Ref
cdk4	RXL motifs	IP	human (MCF-7 & HEK 293 cells)	[87]
cdk2	RXL motifs	IP	human (MCF-7 & HEK 293 cells)	[87]
GLUT4 (insulin-regulated glucose transporter)	not stated	IP/LC-MS/MS	rat skeletal muscle (L6 myoblasts)	[88]
Cox Vb (cytochrome c oxidase subunit Vb)	res 1-76	yeast 2 hybrid	CHO cells	[89]
AID (activation-induced cytidine deaminase)	not stated	pull-down	B cells	[90]
hypothetical protein MGC13057/LOC84281	not stated	yeast 2 hybrid	human	[91]
PYCARD (PYD and CARD domain containing)	not stated	yeast 2 hybrid	human	[91]
pleckstrin homology domain	not stated	yeast 2 hybrid	human	[91]
PAP7 (peripheral-type benzodiazepine receptor (PBR) associated protein)/ GCP60 (Golgi complex-associated protein of 60 kDa)	not stated N and C-terminus	yeast 2 hybrid (RIα was bait) peptide array	human lymphocyte personal communication, Dr. Don Blumenthal	[92]
MCRS1 (microspherule protein 1)	not stated	IP/LC-MS (MCRS1 was bait)	human (HEK 293 cells)	[93]
TUSC4 (tumor suppressor candidate 4)	not stated	IP/LC-MS (TUSC4 was bait)	human (HEK 293 cells)	[93]
UBE2M (ubiquitin-conjugating enzyme E2M)	not stated	IP/LC-MS (for both case, as bait or target)	human (HEK 293 cells)	[93]
ARK5 (AMPK-related protein kinase 5)	not stated	IP/LC-MS (ARK5 was bait)	human (HEK 293 cells)	[93]
PRPF40A (pre-mRNA processing factor 40 homolog A)	not stated	yeast 2 hybrid	human	[91]
RSK (ribosomal S6 kinase)	most likely linker region	pull-down	mouse (B82L cells)	[94]

kinase X (PRKX) to RIα is mediated by the C-subunit recognition site, specifically the pseudosubstrate inhibitor site [95].

The binding sites for the second subunit of Replication Factor C complex (RFC40) [36] and myosin 7A [85] were identified at the N-terminus of RIα. RFC40, a key component of DNA synthesis during S phase and DNA repair, was used as bait to screen a human placental cDNA library using the yeast two-hybrid method. From this screen, RIα was identified as a novel interacting partner. Using pull-down assays, these authors were able to map the interactions to the N-terminal 76 residues of RIα; furthermore, this interaction is independent of the C-subunit. On the other hand, α4 integrin, bound to the RIα:C-subunit (Type I holoenzyme) but not to free RIα [86]. Through immunoprecipitation with Cα antibodies, these authors identified a PKA-α4 integrin interaction in Jurkat T cells, though this interaction was not through the D/D domain of RIα, as evidenced by the lack of effect when using peptides to block the D/D domain. These studies identified a role for Type I holoenzyme in cell migration.

Another protein, ribosomal S6 kinase (RSK1), had the ability to bind to both the Type I holoenzyme and the free RI subunit [94]. These authors used immunoprecipitation with C-subunit antibodies to identify RI subunit, C-subunit, and RSK1 in a complex. By incubating purified RI subunit and RSK1 together, followed by pull down with cAMP resin, they found that RI subunit and RSK1 interacted directly, but this interaction did not alter RSK1 activity. Furthermore, by activating RSK1 with EGF in HeLa cells, followed by pull down with cAMP resin, they discovered that active RSK1 bound to the holoenzyme via the C-subunit while

inactive RSK1 preferentially bound to RI subunit. Localization of active RSK1 to the nucleus was changed in the presence of Ht31, a peptide that disrupts binding between RI and AKAPs, thus suggesting that an indirect interaction with AKAPs was important for the nuclear localization of RSK1. Without this nuclear localization, active RSK1 increased the phosphorylation of its cytosolic substrates, TSC-2 and BAD, both of which play a role in regulating cell growth.

While the aforementioned examples had the binding sites mapped out, the binding sites in RIα of other proteins are not known. Some proteins, such as pre-mRNA processing factor and formin binding protein 3, were predicted through bioinformatic techniques that build protein-protein interaction maps based on large-scale yeast-two hybrid screens. Others, such as microspherule protein and AMPK-related protein kinase, were identified through a large-scale study of protein-protein interactions in human cells using a mass spectrometry-based approach. Overall, the binding of RIα to different protein partners and the binding of those proteins to other proteins makes RIα the center of a complex network of interacting proteins that are potentially involved in several different pathways that result in different cellular functionalities, such as cell migration and cell growth [Figure 4.1].

Looking at these different pathways could provide evidence for the mechanism of RIα involvement in Carney complex. Therefore, we were interested in identifying not only known binding partners but novel ones as well. Since we identified novel disulfide bond formations with the R74C mutant [Chapter 3], we also wanted to

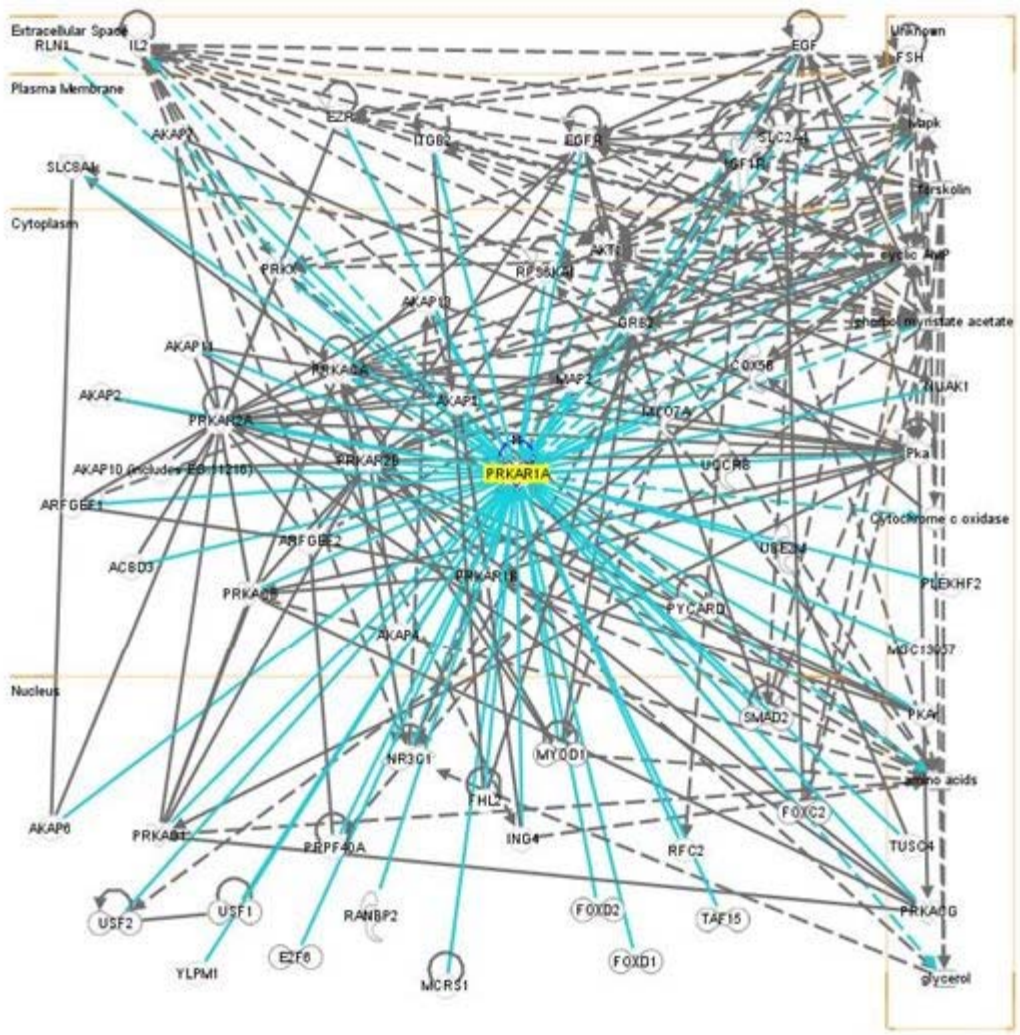

Figure 4.1: The complex network of RIα.

A network of *PRKAR1A* is graphically represented as the relationships between genes. Genes are represented as nodes, and the biological relationship between two nodes is represented as an edge (line). All edges are supported by at least one reference from the literature, from a textbook, or from canonical information stored in the Ingenuity Pathways Knowledge Base. Edges that show a relationship between *PRKAR1A* and another gene are highlighted in teal. Human, mouse, and rat orthologs of a gene are stored as separate objects in the Ingenuity Pathways Knowledge Base, but are represented as a single node in the network. The network was generated through the use of Ingenuity Pathways Analysis (Ingenuity® Systems, www.ingenuity.com).

determine whether the R74C mutant had novel binding partners. For this chapter, we used three different affinity methods followed by mass spectrometry to identify binding proteins [Figure 4.2]: (1) To identify proteins that bind to all four R isoforms and to characterize expression profiles for all of the isoforms, we used cAMP affinity chromatography. (2) To selectively identify proteins that bind either directly or indirectly to free RIα or to RIα holoenzyme, we used TAP-tagged RIα that has two tandem affinity tags, a calmodulin binding peptide and a streptavidin binding peptide. (3) To identify proteins that bind either directly or indirectly to RIα in the absence of the C-subunit, we eluted the TAP-tagged RIα from the streptavidin resin and then bound it to cAMP resin. From these methods, we found an AKAP that binds with high affinity to RIα as well as other potential binding partners.

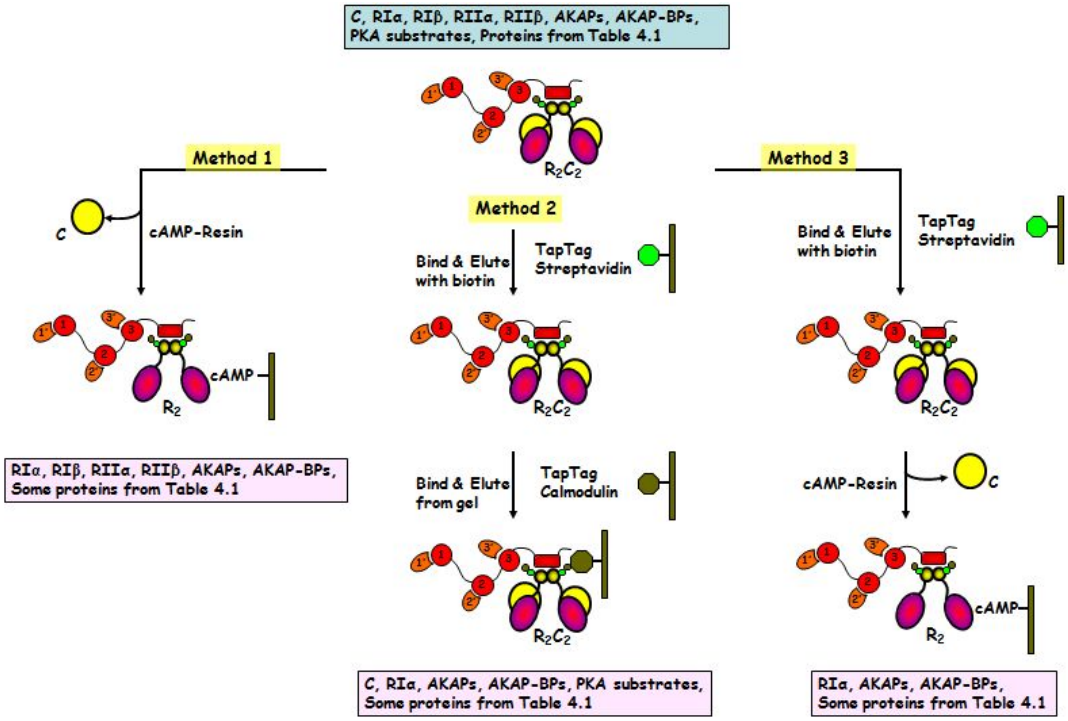

Figure 4.2: Affinity purification methods.

Three different methods were used to study the RIα interactome. From the whole cell lysates, we begin with the proteins highlighted in blue. The proteins we expect to isolate through the different methods are highlighted in pink.

4.2: Experimental Procedures

Antibodies. The following antibodies were used in this chapter: mouse monoclonal anti-Flag M2 (Sigma), mouse polyclonal anti-AKAP11 (Novus Biologicals), mouse monoclonal anti-actin (Abcam), and rabbit polyclonal anti-γ-catenin/plakoglobin (Cell signaling).

Cloning. Human RIα was subcloned into the HindIII-KpnI site of pcDNA3-FLAG (Invitrogen). Single site mutation, R74C, was introduced by QuikChange mutagenesis (Stratagene). All constructs were verified by sequencing.

Growth Curve. Relative cell growth was measured by counting number of cells on a 10 cm plate per day. Day 1 started with 10,000 cells and after about 7 days, the cells reached maximum capacity on the plates. Cells were removed from the plates by trypsinization and resuspended in DMEM (5 mL), diluted further in DMEM if necessary for ease of counting. The cell suspension (50 μL) was mixed with one drop (~10 μL) of Trypan Blue Stain 0.4% (Gibco) for 5 minutes at room temperature to stain dead cells. Viable cells were counted using a hemacytometer (Hausser Scientific), placed on the stage of an inverted microscope.

Pull-down experiments.

FLAG. HEK 293 cells were transiently transfected with FLAG plasmids at 60% confluency. After 24 hours, cells were harvested and lysed in the following buffer (50

mM Tris (pH 7.4), 150 mM NaCl, 1 mM EDTA, and 0.1% NP-40) and bound to anti-FlagM2 affinity resin (Sigma) for 1 hour at 4°C. Proteins which bound to the beads were eluted with low pH IgG elution buffer (Pierce). Eluted proteins were analyzed by a Western blot using the TBST solution, as described in Chapter 2. The antibodies were used at the following dilutions: anti-FLAG (1:5000 dilution), anti-AKAP11 (1:500 dilution), anti-actin (1:2000 dilution), and anti-γ-catenin/plakoglobin (1:1000 dilution).

TAP-tag and cAMP. Untransfected and stable HEK 293 cells were grown on Nunc dishes (15 cm) and harvested at 80% confluency in PBS. Cells were lysed in 50 mM Tris (pH 7.0), 150 mM NaCl, 1 mM EDTA and 1.0% NP-40 by three freeze-thaw cycles. Lysates were bound to either cAMP beads (Sigma) for 16-24 hours or streptavidin and calmodulin resin (Stratagene) for 2 hours. Lysates that were bound to streptavidin resin were washed with streptavidin binding buffer two times, followed by elution of proteins with streptavidin elution buffer, and then followed by either binding to calmodulin resin or cAMP resin. Lysates bound to cAMP resin were washed with low salt buffer (10 mM Hepes (pH 7.4), 1.5 mM $MgCl_2$, and 10 mM KCl) three times before proteomic analysis. Proteins were analyzed as described below.

Proteomics Analysis.

Proteins bound to cAMP resin. Proteins pulled down with cAMP beads were resuspended in 0.1 M ammonium bicarbonate. Reduction and alkylation of the sample was performed by adding DTT to a final concentration of 2 mM, incubating at room temperature for 30 minutes, and then adding iodoacetamide to a final concentration of 4 mM and incubating at room temperature for 30 minutes in the dark. Trypsin (0.5 µg) was added to the beads and incubated at 37°C overnight. The sample was acidified with formic acid (final concentration 5%) and then separated from the cAMP beads by microfuge centrifugation and dried in a speed vacuum. The dried peptides were resuspended in 10 µl of Buffer A (5% acetonitrile, 0.1% formic acid) and analyzed by automated microcapillary liquid chromatography-tandem mass spectrometry. Fused-silica capillaries (100 µm i.d.) were pulled using a P-2000 CO_2 laser puller (Sutter Instruments, Novato, CA) to a 5 µm i.d. tip and packed with 10 cm of 5 µm Magic C18 material (Agilent, Santa Clara, CA) using a pressure bomb. This column was then placed in-line with a Quaternary Agilent (Foster City, CA) 1100 series HPLC pump equipped with an 1100 series autosampler. The column was equilibrated in Buffer A, and the peptide mixture was loaded onto the column using the autosampler. The HPLC pump flowed at 100 µL/min, and the flow rate to the electrospray tip was reduced to ~ 200-300 nL/min by a split. The HPLC separation was provided by a gradient between Buffer A and Buffer B (90% acetonitrile, 0.1% formic acid). The HPLC gradient was held constant at 100% Buffer A for 5 minutes after peptide loading, followed by a 30 minute gradient from 5% Buffer B to 40%

Buffer B. The gradient was then switched from 40% to 80% Buffer B over 5 minutes and held constant for 3 minutes. Finally, the gradient was changed from 80% Buffer B to 100% Buffer A over 1 minute, and then held constant at 100% Buffer A for 15 additional minutes. The application of a 1.8 kV distal voltage electrosprayed the eluted peptides directly into the LTQ ion trap mass spectrometer equipped with a nanoLC electrospray ionization source (ThermoFinningan, San Jose, CA). Full masses (MS/MS) spectra were recorded on the peptides over a 400-2000 *m*/*z* range, followed by five tandem mass (MS/MS) events sequentially generated in a data-dependent manner on the first, second, third, fourth, and fifth most intense ions selected from the full MS spectrum (at 35% collision energy). Mass spectrometer scan functions and HPLC solvent gradients were controlled by the Xcalibur data system (ThermoFinningan, San Jose, CA).

Isolation of proteins bound to calmodulin resin. Proteins pulled down with calmodulin resin were run on a 4-12% Bis-Tris SDS-PAGE gel for 5 minutes. Gel bands were incubated with 20% acetonitrile in 0.1 M ammonium bicarbonate for 20 minutes and dehydrated with 100% acetonitrile. After drying, the gel pieces were resuspended in 1 mM DTT in 0.1 M ammonium bicarbonate and incubated for 30 minutes at room temperature. Next, iodoacetamide (2 mM) was added and samples were incubated for 30 minutes at room temperature. The supernatant was aspirated and gel pieces dehydrated with 100% acetonitrile. After drying, 250 ng of trypsin was added in 0.1 M ammonium bicarbonate and incubated overnight. After incubation, the

supernatant with the peptides were removed. The gel pieces were washed with 10% acetonitrile, 0.1% formic acid, and the washes combined with the supernatant. This solution was dried in a speed vacuum and the pellet was resuspended in 0.1% formic acid in 5% acetonitrile and loaded into the LTQ ion trap mass spectrometer, as described above.

Data analysis. MS/MS spectra were extracted from the RAW file with Readw.exe (http://sourceforge.net/project/showfiles.php?group_id=69281&package_id=68160). The resulting mzXML file contained all the data for all MS/MS spectra and was read by the subsequent analysis software. The MS/MS data was searched with Inspect [96] against a human IPI database with optional modifications: +16 on methionine, +57 on cysteine, +80 on threonine, serine, tyrosine. Only peptides with a p-value of 0.01 or less were analyzed further.

The data were stored on Excel spreadsheets and analyzed for number of spectra as a rough measure of abundance of proteins, labeled as "Number of hits" in Tables 4.2-4.7. The number of unique peptides was also counted to confirm confidence in the presence of proteins, labeled as "Unique peptides" in Tables 4.2-4.7. Only proteins with at least two unique peptides was considered true positive.

4.3: Results

Affinity purification methods. Since R subunits have two cAMP binding sites, cAMP resin can be used to purify R subunits that are released from its C-subunit partner. This method provides an excellent starting point for profiling the general PKA proteome in any cell line or tissue. In this study, we used HEK 293 cells.

To study the RIα interactome, we developed additional affinity methods to characterize RIα binding partners using HEK 293 cells that were stably expressing TAP-tagged RIα. Stable cell lines were created with TAP-tagged wild-type RIα and with TAP-tagged R74C mutant. First, to study the binding partners of all four R isoforms, cAMP resin was used. Although the TAP-tagged proteins caused an increase in levels of total RIα, this method still showed what proteins were binding under basal conditions. In addition to using the cAMP affinity method, we used the TAP-tag system, where RIα was purified with streptavidin and calmodulin resins. Furthermore, by using the TAP-tag system followed by cAMP, we disassociated the C-subunit and pulled out proteins that bound to the free TAP-tagged RIα [Figure 4.2]. A result was considered true positive if it had at least two unique peptides.

Characterization of the PKA proteome based on cAMP affinity. To identify proteins that bind to the free R subunits, the cell lysates were bound to cAMP resin. The cAMP resin was directly subjected to trypsin digestion instead of eluting the proteins from the beads because it proved difficult to elute RIα from cAMP resin. The digested peptides were then analyzed by mass spectrometry. We first characterized

untransfected HEK 293 cells by using cAMP resin to purify all the R subunits and their binding partners. The proteins identified from this purification are listed in Table 4.2. Three R isoforms were identified: RIα, RIIα, and RIIβ. Some peptides of RIα were phosphorylated on S83. Two AKAPs, D-AKAP1 and AKAP9, were also identified.

We next used cAMP to identify proteins from HEK 293 cells that were stably transfected with wild-type RIα. The proteins that were identified [Table 4.3] included three R subunit isoforms and three AKAPs: AKAP5, AKAP9, and AKAP11. In this case, the phosphorylation on S83 was not detected. Proteins that are highly abundant – myosin, tubulin, actin - were also easily detected. Tubulin may have been identified because of its indirect interaction with RIα since RIα can be localized to microtubules potentially through AKAP binding [53]. Myosin may be detected because of its binding to calmodulin. Since actin peptides were highly abundant, other proteins, such as drebrin, tropomyosin, and filamin, which bind to actin, were also identified.

Characterization of the RIα interactome using TAP-tagged RIα. To analyze proteins that specifically bind to RIα and RIα holoenzyme, we took advantage of the tandem affinity tags in TAP-tagged RIα. This method allowed the pull down of proteins binding to RIα holoenzyme as well as any disassociated RIα. In this case, we expected to find RIα, C-subunit, and any protein that binds to either RI subunit or specifically to the holoenzyme. Cell lysates were bound to streptavidin resin first,

Table 4.2: Proteins from untransfected HEK 293 cells bound to cAMP resin.

Method 1 was used to identify proteins that bind to all four R subunits in HEK 293 cells. The three isoforms of R subunits that were detected are highlighted in red, while the two AKAPs are highlighted in yellow. For all other protein groups, only those with greater than 5 unique peptides are shown.

Protein description	IPI	Number of hits	Unique peptides
cAMP-dependent protein kinase type I-alpha regulatory subunit	IPI00021831	64	19
cAMP-dependent protein kinase type II-alpha regulatory subunit	IPI00219774	104	31
cAMP-dependent protein kinase type II-beta regulatory subunit	IPI00554752	6	4
A-kinase anchor protein 9	IPI00019223	148	70
A-kinase anchor protein 1	IPI00022585	9	5
Tubulin	IPI00011654 IPI00387144 IPI00007752	55	33
Vimentin	IPI00418471	35	18
Glyceraldehyde-3-phosphate dehydrogenase	IPI00219018	40	15
Phosphodiesterase 4D interacting protein	IPI00337544	22	9
Actin	IPI00848058	16	8
Histone H2B – type 1-J	IPI00515061	14	9
Histone H2B	IPI00815755		
Histone H2A.J	IPI00220855	5	2
Heterogeneous nuclear ribonucleoprotein K	IPI00216049	7	6
Heterogeneous nuclear ribonucleoprotein H1	IPI00479191	5	3
Heterogeneous nuclear ribonucleoprotein L	IPI00027834	2	2
Heterogeneous nuclear ribonucleoprotein M	IPI00171903	3	2
Elongation factor 1-alpha 1	IPI00396485	17	5
Pyruvate kinase isozymes M1/M2	IPI00783061	15	5
Macrophage migration inhibitory factor	IPI00293276	9	5
60S ribosomal protein L13	IPI00465361	5	4
60S ribosomal protein L6	IPI00790342	5	3
60S ribosomal protein L24	IPI00793696	2	2
60S ribosomal protein L8	IPI00012772	3	2
T-complex protein 1 subunit beta	IPI00290770	4	4
T-complex protein 1 subunit theta	IPI00784090	4	3
T-complex protein 1 subunit zeta	IPI00027626	3	3
T-complex protein 1 subunit delta	IPI00302927	2	2

Table 4.3: Proteins from HEK 293 cells stably expressing TAP-tagged wild-type RIα bound to cAMP beads.

Method 1 was used to identify R subunit binding partners in HEK 293 cells overexpressing TAP-tagged wild-type RIα. The three isoforms of R subunit that were detected are highlighted in red. Three AKAPs that were detected are highlighted in yellow. For all other protein groups, only those with greater than 10 unique peptides are shown.

Description	IPI	Number of hits	Unique peptides
cAMP-dependent protein kinase type I-alpha regulatory subunit	IPI00021831	57	19
cAMP-dependent protein kinase type II-alpha regulatory subunit	IPI00219774	15	12
cAMP-dependent protein kinase type II-beta regulatory subunit	IPI00554752	9	6
A-kinase anchor protein 11	IPI00007411	9	8
A-kinase anchor protein 9	IPI00220628	5	4
A-kinase anchor protein 5	IPI00307794	2	2
Myosin-9	IPI00019502	586	240
Isoform 3 of Myosin-10	IPI00790503	171	98
Isoform 1 Of Myosin-8A	IPI00017030	37	24
Myosin-6	IPI00844172	25	20
Myosin -1C	IPI00743335	24	14
Isoform 2 of Myosin-14	IPI00607818	12	10
Isoform 2 of Myosin-1B	IPI00414980	16	11
Isoform 1 of Myosin-1D	IPI00329719	7	6
Isoform 1 of Myosin-5A	IPI00000807	2	2
Actin	IPI00848058 IPI00023006 IPI00021439	429	124
Drebrin	IPI00003406	50	27
Isoform 3 of Tropomyosin-1 alpha chain	IPI00216135	39	25
Isoform 1 of Tropomyosin-4 alpha chain	IPI00010779	13	10
Isoform 2 of Tropomyosin-3 alpha chain	IPI00218319	13	7
Isoform Beta of LIM domain and actin-binding protein 1	IPI00008918	38	23
Vimentin	IPI00418471	34	23
Isoform 1 of Myosin phosphatase Rho-interacting protein	IPI00305344	26	22

Table 4.3: Proteins from HEK 293 cells stably expressing TAP-tagged wild-type RIα bound to cAMP beads, Continued.

Description	IPI	Number of hits	Unique peptides
Tubulin	IPI00645452 IPI00387144	26	16
Glyceraldehyde-3-phosphate dehydrogenase	IPI00219018	29	15
Isoform 1 of Ankycorbin	IPI00759532	17	15
Myosin regulatory light chain	IPI00033494	52	14
Isoform Non-muscle of Myosin light polypeptide 6	IPI00335168	34	13
Myosin light polypeptide 6B	IPI00027255	4	3
Myosin light chain 3, skeletal muscle isoform	IPI00220332	12	2
Spectrin, alpha	IPI00744706	22	13
Spectrin, beta, non-erythrocytic 1 isoform 1 variant	IPI00794135	10	8
filamin A, alpha	IPI00302592	13	12
Poly [ADP-ribose] polymerase 1	IPI00449049	14	11
Elongation factor 1-alpha 1	IPI00847435	18	11
Elongation factor 2	IPI00186290	2	2
60S ribosomal protein L4	IPI00003918	17	9
60S ribosomal protein L27a	IPI00456758	5	3
60S ribosomal protein L13	IPI00465361	3	3
60S ribosomal protein L3	IPI00550021	4	3
60S ribosomal protein L19	IPI00025329	2	2
60S ribosomal protein L6	IPI00329389	2	2
60S ribosomal protein L35	IPI00412607	2	2
Casein kinase II	IPI00016613	7	7
Casein kinase II subunit beta	IPI00010865	2	2
Casein kinase II subunit alpha	IPI00020602	3	2
Isoform A2 of Heterogeneous nuclear ribonucleoproteins A2/B1	IPI00414696	8	7
Heterogeneous nuclear ribonucleoprotein U isoform a	IPI00644079	7	6
Isoform 3 of Heterogeneous nuclear ribonucleoprotein K	IPI00807545	5	3
Isoform 1 of Heterogeneous nuclear ribonucleoprotein M	IPI00171903	2	2
Isoform 1 of Heterogeneous nuclear ribonucleoprotein A3	IPI00419373	3	2
Similar to Heterogeneous nuclear ribonucleoprotein A1	IPI00738822	2	2
Heterogeneous nuclear ribonucleoprotein L isoform b	IPI00465225	2	2
Histone H2A type 1-J	IPI00552873	16	7
Histone H4	IPI00453473	11	6

Table 4.3: Proteins from HEK 293 cells stably expressing TAP-tagged wild-type RIα bound to cAMP beads, Continued.

Description	IPI	Number of hits	Unique peptides
Histone H2B type 1-J	IPI00515061	13	6
Histone H1.4	IPI00217467	4	3
Histone H1.2	IPI00217465	2	2
Histone H2A.X	IPI00219037	2	2
40S ribosomal protein S6	IPI00021840	7	4
40S ribosomal protein S8	IPI00216587	3	3
40S ribosomal protein S13	IPI00221089	5	3
40S ribosomal protein S14	IPI00026271	3	2

proteins eluted, then bound to calmodulin resin. As with the cAMP resin, proteins were not eluted from the calmodulin resin since the InterPlay Mammalian TAP System manual (Stratagene) indicated the difficulty of disassociating TAP-tagged protein from these beads. Instead, we ran the protein-bound calmodulin resin on an SDS-PAGE gel for a very short time to remove the calmodulin that was attached to the beads. The gel pieces were digested and analyzed by mass spectrometry to identify proteins [Tables 4.4, 4.5]. Peptides corresponding to RIα, Cα subunit, and AKAP11 were found. Two interacting proteins of interest were heterogeneous nuclear ribonucleoprotein U, which is involved in pre-mRNA processing and histone H2A, which form nucleosomes and are a basic component of chromatin.

We also pulled out binding partners unique to the R74C mutant that were not seen with wild-type RIα [Table 4.5]. One interesting isoform that was detected with TAP-tagged R74C, but not with TAP-tagged wild-type RIα, was RIβ. Another interesting protein that was detected was plakoglobin. We also identified binding partners that were overlapping with the ones from wild-type RIα holoenzyme. AKAP11 was again detected in high abundance. Phosphorylation at S83 in peptides of wild-type RIα or R74C was detected in both stable cell lines.

Purification of TAP-tagged RIα homodimers and heterodimers. To purify R subunit disassociated from the C-subunit, we used streptavidin resin followed by cAMP resin. Proteins that bind directly to wild-type RIα are shown in Table 4.6. Both isoforms of RI (α and β) were seen as well as AKAP11. The detection of RIβ indicated that a

Table 4.4: Proteins bound to wild-type RIα holoenzyme.

Method 2 was used to identify proteins binding directly or indirectly to TAP-tagged wild-type RIα. RIα was detected (highlighted in red) as well as C-subunit (highlighted in purple). AKAP11 was the only AKAP identified. Proteins of interest are highlighted in gray.

Protein description	IPI	Number of hits	Unique peptides
cAMP-dependent protein kinase type I-alpha regulatory subunit	IPI00021831	434	29
cAMP-dependent protein kinase, alpha-catalytic subunit	IPI00217960 IPI00396630	8	5
A-kinase anchor protein 11	IPI00007411	13	9
Myosin-9	IPI00019502	29	19
Actin	IPI00021439 IPI00848058	20	14
Tubulin	IPI00387144 IPI00011654	9	5
Histone H2A type 3	IPI00031562	5	2
Isoform 1 of Myosin-1B	IPI00376344	3	2
Isoform short of heterogeneous nuclear ribonucleoprotein U	IPI00479217	3	2

Table 4.5: Proteins bound to R74C holoenzyme.

Method 2 was used to identify proteins binding directly or indirectly to TAP-tagged R74C. This purification identified RIβ, which was not detected in the Method 2 purification of TAP-tagged wild-type RIα. Other proteins not found from the Method 2 purification of wild-type RIα are highlighted in turquoise with plakoglobin, a protein of interest, highlighted in gray.

Protein description	IPI	Number of hits	Unique peptides
Common with wt stable			
cAMP-dependent protein kinase type I-alpha regulatory subunit	IPI00021831	433	33
cAMP-dependent protein kinase, alpha-catalytic subunit	IPI00396630 IPI00217960	10	7
A-kinase anchor protein 11	IPI00007411	22	12
Actin	IPI00021440 IPI00848058 IPI00021439	162	48
Myosin-9	IPI00019502	68	31
Isoform 1 of Myosin-1B	IPI00376344	9	5
Tubulin	IPI00011654 IPI00387144	10	5
Histone H2A type 3	IPI00031562	2	2
Unique to R74C			
cAMP-dependent protein kinase type I-beta regulatory subunit	IPI00787996	2	2
Heat shock 70 kDa protein isoforms	IPI00003865 IPI00795040	8	6
Junction plakoglobin	IPI00554711	4	3
Isoform 3 of Myosin-10	IPI00790503	8	6
Myosin regulatory light chain	IPI00604523 IPI00033494	14	7
Myosin-6	IPI00008455 IPI00844172	7	6
Isoform 1 of spectrin alpha chain, brain	IPI00478292	3	3
Isoform Non-muscle of Myosin light polypeptide 6	IPI00335168	2	2
Histone H4	IPI00453473	4	2
Myosin light chain 6	IPI00795576	5	2
Ubiquitin C	IPI00798127	3	2

Table 4.6: Proteins bound to wt RIα (>3 unique peptides).

Method 3 was used to detect proteins binding directly to TAP-tagged wild-type RIα. Both RI isoforms were detected (highlighted in red). AKAP11 was again detected.

Protein description	IPI	Number of hits	Unique peptides
cAMP-dependent protein kinase type I-alpha regulatory subunit	IPI00021831	721	63
cAMP-dependent protein kinase type I-beta regulatory subunit	IPI00787996	21	14
A-kinase anchor protein 11	IPI00007411	113	59
Myosin-9	IPI00019502	98	81
Actin	IPI00021439 IPI00023006	65	45
Acetyl-CoA carboxylase 1	IPI00011569	17	17
Isoform 2 of Acetyl-CoA carboxylase 1	IPI00847501	8	8
Methylcrotonoyl-CoA carboxylase subunit alpha, mitochondrial precursor	IPI00024580	9	7
Drebrin 1	IPI00794221	7	6
Heat shock 70kDa protein 8 isoform 2 variant (Fragment)	IPI00795040	6	6
Myosin-1B	IPI00795618	6	6
HSPA5 protein	IPI00003362	7	4
EF-hand domain-containing protein 2	IPI00060181	6	4
Tropomyosin 3 isoform 5	IPI00477649	4	4
ACTA2 protein (Fragment)	IPI00816229	5	3
Stomatin-like protein 2	IPI00334190	4	3
40S ribosomal protein S3	IPI00011253	3	3
Isoform 1 of Myosin-1D	IPI00329719	3	3
Heterogeneous nuclear ribonucleoprotein L isoform b	IPI00465225	3	3

heterodimer of TAP-tagged RIα:RIβ was formed. Heterogeneous nuclear ribonucleoprotein L was detected. Again, peptides from myosin and actin were detected in high abundance. Table 4.7 lists the proteins that were common with those found from cell stably expressing wild-type RIα and those that were unique to the cells stably expressing R74C. Again, RIβ and AKAP11 were detected. In both purifications, some peptides of wild-type RIα and R74C had a phosphorylation at S83, but the phosphorylation was not constitutive.

Confirmation of AKAP11 binding to RIα. AKAPs typically bind tightly to RII isoforms, but some are dual-specific. However, we would not expect to find these dual-specific AKAPs through our methods because of their lower affinity due to a faster off-rate. Therefore, it was surprising that AKAP11 peptides were detected in high abundance in all of the purifications of RIα. Hence, we may have found an AKAP that binds tightly to RIα. The peptides of AKAP11 were not only abundant but also covered almost the entire AKAP11 sequence [Figure 4.3].

To independently confirm some of the binding partners, we made FLAG-tagged constructs of RIα, with FLAG expressed at the C-terminus of RIα. HEK 293 cells were transiently transfected with these FLAG-tagged RIα constructs. One construct, R211K, is defective in cAMP binding. Purification of these constructs was performed using FLAG resin and samples were analyzed by Western blot using antibodies for AKAP11, plakoglobin, and actin [Figure 4.4]. All three proteins

Table 4.7: Proteins bound to R74C (>3 unique peptides).

Method 3 was used to identify proteins binding directly to the TAP-tagged R74C mutant. Similar to the Method 3 purification of wild-type RIα, both RI isoforms were detected as well as AKAP11. Proteins that were uniquely identified from this purification are highlighted in turquoise.

Protein description	IPI	Number of hits	Unique peptides
Common with wt stables			
cAMP-dependent protein kinase type I-alpha regulatory subunit	IPI00021831	545	62
cAMP-dependent protein kinase type I-beta regulatory subunit	IPI00787996	22	13
A-kinase anchor protein 11	IPI00007411	132	64
Myosin-9	IPI00019502	141	111
Actin	IPI00021439 IPI00023006	60	40
Acetyl-CoA carboxylase 1	IPI00011569	15	15
Isoform 2 of Acetyl-CoA carboxylase 1	IPI00847501	8	8
Tropomyosin 3 isoform 5	IPI00477649	7	7
Heat shock 70 kDa protein 8 isoform 2 variant (Fragment)	IPI00795040	12	7
Drebrin 1	IPI00794221	7	6
Methylcrotonoyl-CoA carboxylase subunit alpha, mitochondrial precursor	IPI00024580	4	4
Stomatin-like protein 2	IPI00334190	5	4
Isoform 1 of Myosin-1D	IPI00329719	3	3
Myosin-1B	IPI00795618	3	3
Unique to R74C stables			
Isoform 1 of Myosin phosphatase Rho-interacting protein	IPI00305344	4	4
Poly [ADP-ribose] polymerase 1	IPI00449049	4	4
Isoform 1 of Cellular tumor antigen p53	IPI00025087	3	3
Isoform 2 of Myosin-14	IPI00607818	3	3

Figure 4.3: Human AKAP11 sequence with peptide coverage highlighted.

The AKAP11 sequence is shown with the peptides from mass spectrometry analysis highlighted. The color key for number of queries is listed as follows: Red (>5), Yellow (5), Green (4), Turquoise (3), Gray (2), Purple (1). Some peptides were overlapping and had different number of queries. Peptides are underlined to show their start and end.

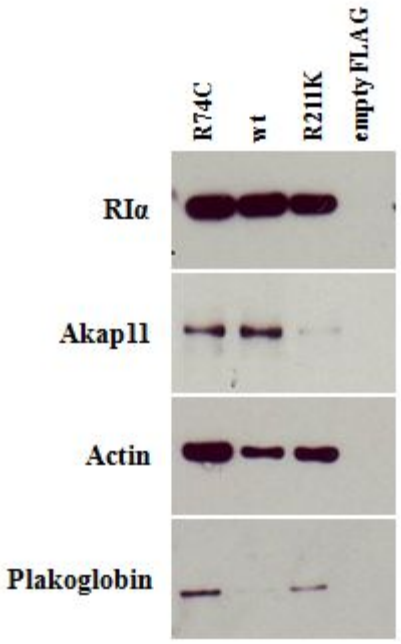

Figure 4.4: AKAP11 binds with high affinity to RIα.

HEK 293 cells were transiently transfected with FLAG-tagged RIα constructs. Pull-down experiments were employed using FLAG beads and showed binding of RIα to AKAP11, actin, and plakoglobin. No binding of these proteins to empty FLAG vector was detected.

bound to FLAG-tagged RIα, but not to empty FLAG vector. Corroborating the results from mass spectrometry analysis, plakoglobin was pulled out with R74C, but not with wild-type RIα. Since plakoglobin was not detected from the control pull-down experiment, we may have found a novel binding partner to R74C. PARP was also tested but showed binding even with empty FLAG (data not shown). p53, another potential novel partner that was identified from the cells stably expressing R74C, was not tested.

4.4: Discussion

Recent work from a number of different research groups suggests that RIα subunit is a multifunctional protein, not just an inhibitor of the PKA C-subunit. One way to understand protein function is through the mapping of its protein interaction partners. Here, we used several different affinity purification methods followed by mass spectrometry to study the RIα interactome. We isolated the R subunits from untransfected HEK 293 cells using cAMP resin. Then, we used three different methods to isolate RIα from stable cell lysates expressing a TAP-tagged version of RIα: Method 1) cAMP resin was used to profile the R subunit interactome, Method 2) Streptavidin resin followed by calmodulin resin was used to identify RIα-associated and holoenyzme-associated proteins, and Method 3) Streptavidin resin followed by cAMP resin was used to identify RIα-associated proteins. Though there was a high background from these different affinity methods, we focus here on the most relevant proteins for PKA interactions. These proteins are summarized in Table 4.8.

Our methods worked to pull out anticipated PKA proteins. RIα was detected in all of the purification methods, while RII subunits were identified only when using cAMP resin alone. As expected, C-subunit, specifically the Cα isoform, was identified only when purifying RIα without adding cAMP resin. The detection of RIβ from Method 3 was indicative of a heterodimer formation with TAP-tagged RIα. Furthermore, RIβ was detected with R74C holoenzyme but not with wild-type RIα holoenzyme.

Table 4.8: Summary of PKA-associated proteins detected from different purification methods.

The PKA subunits, AKAPs, and novel and abundant proteins from the different purification methods are listed.

Cells	**Untrans 293 cells**	**wt stables**			**R74C**	**stables**
Purification method	**Method 1 cAMP resin**	**Method 1 cAMP resin**	**Method 2 strept/CaM resin**	**Method 3 strept/ cAMP resin**	**Method 2 strept/CaM resin**	**Method 3 strept/ cAMP resin**
PKA subunits	RIα RIIα RIIβ	RIα RIIα RIIβ	RIα C-subunit	RIα RIβ	RIα RIβ C-subunit	RIα RIβ
AKAPs	AKAP1 AKAP9	AKAP11 AKAP9 AKAP5	AKAP11	AKAP11	AKAP11	AKAP11
Potential novel partners	hnRNP Histone H2A.J H2B	hnRNP Histone H1.2 H1.4 H2A type 1-J H2A.X H2B type 1-J H4 PARP	hnRNP Histone H2A type 3	hnRNP	Histone H2A type 3 H4 Plakoglobin	PARP p53
Abundant proteins	Vimentin Tubulin Actin	Vimentin Tubulin Actin Myosin	Tubulin Actin Myosin	Actin Myosin	Tubulin Actin Myosin	Actin Myosin

Using cAMP resin alone identified the most AKAPs. This result was not surprising since most of the AKAPs identified thus far have stronger association with RII isoforms than with RI isoforms. From the untransfected cells, AKAP1 and AKAP9 were detected, while in the stably transfected cells, AKAP5, AKAP9, and AKAP11 were identified. AKAP9 was most likely identified due to its binding to the RII subunits [97] and thus we did not see it with TAP-tagged RIα. AKAP9 encompasses a family of alternatively spliced AKAPs whose splice forms include AKAP350, AKAP450, CG-NAP, and yotiao [98] and it was identified as an RII AKAP through a yeast two-hybrid screen [99], RII overlay [100], and indirect immunofluorescence [99]. AKAP5 is a 79 kDa protein that has been shown to bind with high affinity to both RIIα and RIIβ. AKAP5 can also target to beta2-adrenergic receptor, which is a substrate for PKA [101]. AKAP1/D-AKAP1 is a dual-specific AKAP, but was not detected in the stable cells, probably because of its weaker affinity to RIα compared to RII. However, to our surprise, one AKAP, AKAP11, was consistently identified in the different purification methods from the stable cells.

Other than the AKAPs, the list of proteins identified using cAMP resin was quite extensive and more informative after comparing it to the lists from the other purification methods so that proteins directly binding with RIα could be identified. Most of them were putative PKA substrates [102]. Some of the proteins that are known to be RIα binding partners [Table 4.1] were detected from this study, though others, such as PRKX, myosin 7A, and RSK were not detected. This could be due to the cell lines used or the pull-down conditions. Another reason could be that an intact

peptide seen in the first MS analysis did not fragment so the peptide was not seen in the MS/MS and the protein could not be identified.

Two proteins were consistently detected which implied the interactions of RIα in the nucleus: heterogeneous nuclear ribonucleoprotein (hnRNP) and histone. hnRNP binds to actin in HeLa cells [102, 103] and a mutation in hnRNP can cause embryonic lethality in mice [104]. Furthermore, it is involved in formation and processing of mRNA. hnRNP was not detected in the pull downs from the R74C stables, implying that this mutation could have affected binding of RIα to this protein. Histones, specifically, H1, H2A, H2B, and H3, are substrates of PKA [105-108], and have been shown to activate PKA by binding to RIα [109]. Interestingly, histone H2A was not detected from our pull downs of RIα that were disassociated from C-subunit, indicating that in HEK 293 cells, it binds to RI holoenzyme, but not free RIα.

Some other proteins were also consistently detected. Vimentin, the most widely expressed intermediate filament protein, was identified only when using cAMP resin alone, leading us to deduce that vimentin binds to RII subunits. Tubulin, on the other hand, was identified from all methods except Method 3, indicating it can bind to RI holoenzyme, but not free RI. This result leads us to believe that it may be RI holoenzyme and not free R that is localizing to microtubules, consistent with the work from Imaizumi-Scherrer *et al.* [53]. Actin, an abundant cytoskeletal protein, was identified from all methods, suggesting it binds to RI subunits whether in complex with or disassociated from C-subunit.

To confirm some potential binding partners, we purified FLAG-tagged RIα from transiently transfected HEK 293 cells [Figure 4.4]. Three proteins were tested: AKAP11, plakoglobin, and actin. AKAP11, plakoglobin, and actin were pulled down with the purified FLAG-tagged RIα construct but not with the empty FLAG vector, thus confirming our mass spectrometry results. Plakoglobin has not been reported as an RIα binding partner before, so we may have found a novel binding partner to mutant RIα. Plakoglobin/γ-catenin is an 82 kDa protein that is a component of desmosomes, a cell structure specialized for cell-to-cell adhesion. They likely influence the arrangement and function of both the cytoskeleton and the cells within the tissue. A deficiency of plakoglobin in mice was associated with severe cardiac defects [110]. Therefore, if this binding is confirmed, we suspect that the binding of R74C to plakoglobin could contribute to plakoglobin deficiency, which could result in cardiac defects similar to those seen in Carney complex patients.

On the other hand, the binding of AKAP11 to RIα has been reported in human testis lysates [82], although it was not quantified. Since the authors were able to co-immunoprecipitate RIα with AKAP11 antisera from human testis homogenates, they deduced that AKAP11 can bind to RIα. To our knowledge, the binding of AKAP11 to RIα has not been reported in any other cell line. AKAP11, first discovered as an anchoring protein a little over ten years ago [111], is a 220 kDa protein that has been reported to bind to both RIα and RIIα [82]. AKAP11 targeting is not completely clear, but in rats, it potentially targets to peroxisomes because of the final three amino acids

–CRL [111]. However, human AKAP11 protein does not contain these final amino acids, and its targeting and function have not been established.

Most AKAPs are known to bind to the RII isoforms to bring them to various organelles or membranes, but ones with dual specificity have 25-100-fold greater affinity for the RII isoforms [40, 41]. Furthermore, the off-rate of AKAPs with RIα is typically fast so that gel overlays do not work. Here, we find the binding of AKAP11 to RIα even with our most stringent washes during purification. Thus, we believe AKAP11 may be the first dual-specific AKAP that displays high binding affinity to RIα.

Three putative R binding sites exist in human AKAP11 [82], located at residues 611-623, 1539-1556, and 1650-1663. Because of its high sequence conservation with other RII AKAP binding sites, coupled with the analysis of a deletion mutant of rat AKAP11 [111], the site at residues 1650-1663 was deduced to be the RII binding site in human AKAP11. Computer analysis of the entire AKAP11 sequence, using the common motif for RII binding domains, identified two other putative R binding sites. It is possible that one of these two sites is more specific for RIα than RII subunits. To look into the RI specificity of these two putative sites, a multiple sequence alignment was performed on the RI binding sites from various AKAPs that are known to bind RI subunits [Figure 4.5A]. Previously, residues in the A-Kinase Binding (AKB) domain of D-AKAP2 that were important for binding specificity to either RIα or RIIα were identified using a peptide substitution array [41]. Eight residues in the AKB showed decreased tolerance for substitution, but three of

A

D-AKAP2	L	A	W	K	I	A	K	M	I	V	S	D	V	M
Can substitute	I,W,Y	G			F,L, M,W ,Y	I,V			-	F,M			A,I,L	A,G,H,N,P,Q,R,S,T,V,W, Y
Enhanced RIα binding	F	-			-	-			-	I,L,W			-	F,I,L
Disrupted RIα binding	A,C,K	F,H,I,K,L,M ,N,V,W,Y			-	-			-				-	-

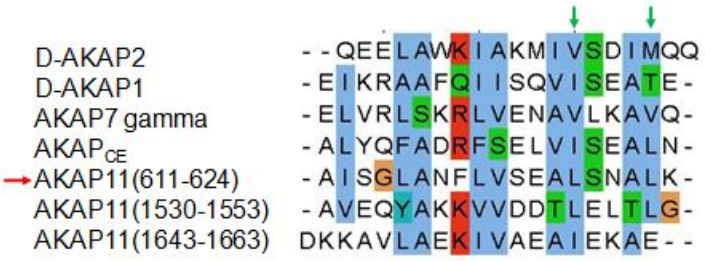

B

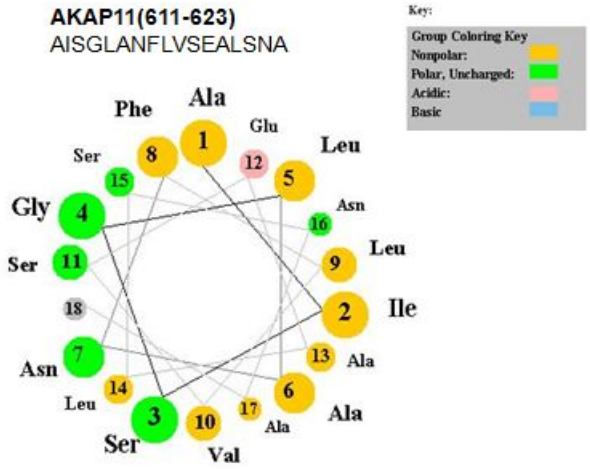

Figure 4.5: Three potential R binding sites exist in AKAP11.

(A) Effects on RIα binding with residue substitutions in D-AKAP2(AKB) are summarized in the table based on a peptide substitution array [41]. Red letters indicate a decreased tolerance for substitution and positions were used to analyze the alignment of putative AKAP11 R binding sites with known RI binding sites. In the alignment, from MUSCLE [16], green arrows indicate positions where substitutions in AKAP11(611-624) and AKAP11(1530-1553) would enhance RIα binding. The red arrow points to the sequence that seemed most likely to bind to RIα.

(B) The alpha helical wheel of AKAP11(611-623) predicts an amphipathic helix (http://cti.itc.virginia.edu/~cmg/Demo/wheel/wheelApp.html).

them could be substituted with other specific residues to enhance RIα binding. Two substitutions that lead to enhanced RIα were found in AKAP11(611-624) and AKAP11(1530-1553) but only the alpha helical wheel of AKAP11(611-623) revealed an amphipathic helix [Figure 4.5B]. Furthermore, a peptide array of AKAP11(1530-1553) did not show binding to RIα [personal communication, Dr. William McLaughlin]. Therefore, we believe the binding of RIα may be through residues 611-623 of AKAP11.

Similar to RIα, the regulation of AKAP11 expression levels is important. Based on Northern blots, AKAP11 showed low level expression in most tissues but high expression in human heart, testis, and brain [82]. The mRNA expression level is also high in HEK 293 cells [112]. An increased expression of AKAP11 has been implicated in oral cancer [113], and knockout of AKAP11 leads to embryonic lethality in mice [personal communication, Dr. John Scott]. Prior to these observations, its involvement in cell cycle regulation had already been suggested. AKAP11 binds to type I protein phosphatase (PP1), which was postulated as a way to optimally position PP1 and PKA to reversibly modulate the phosphorylation state of substrates [114]. It was later found that the binding of RII subunit with AKAP11 to PP1 enhances the inhibition of PP1 [115]. PP1 is a negative regulator of cell cycle progression because it dephosphorylates retinoblastoma 1 (Rb) [116]. In its dephosphorylated state, Rb binds to and sequesters E2F, thus repressing the transcription of genes required for DNA synthesis and cell cycle progression. When Rb is phosphorylated, it releases E2F so that transcription is now turned on and there is proliferation of cells.

Our preliminary data showed faster cell growth when wild-type RIα was overexpressed [Figure 4.6A]. In addition, several unique peptides corresponding to PP1 were detected from the purification of TAP-tagged wild-type RIα using streptavidin followed by cAMP resin. Thus, we hypothesize that the binding of RIα to AKAP11 could also enhance the inhibition of PP1, similarly to RII subunit, and this inhibition could contribute to the increased cell proliferation we observed in the cells stably expressing wild-type RIα [Figure 4.6B]. The overexpression of RIα has also been implicated with proliferation in breast cancer [62]. Therefore, our finding of its tight interaction with AKAP11 could explain another mechanism by which the overexpression of RIα leads to cancer.

4.5: Acknowledgements

We would like to Nuno Bandeira and Sam Payne for technical support in using Inspect and Vineet Bafna for fruitful discussions regarding the analysis of mass spectrometry data. We would also like to thank William McLaughlin for useful discussions regarding analysis of the R subunit binding motifs in AKAPs. Thanks to Sventja von Daake for assistance in making the figure on affinity methods. This work was supported by the NIH/NCI Growth Regulation & Oncogenesis Training Grant.

Chapter 4, in part, will be submitted for publication. Day, M.E., Koller, A., Sastri, M., and Taylor, S.S. AKAP220 is a dual A-kinase anchoring protein with high affinity for the RIalpha subunit of PKA. The dissertation author was the primary investigator and author of this work.

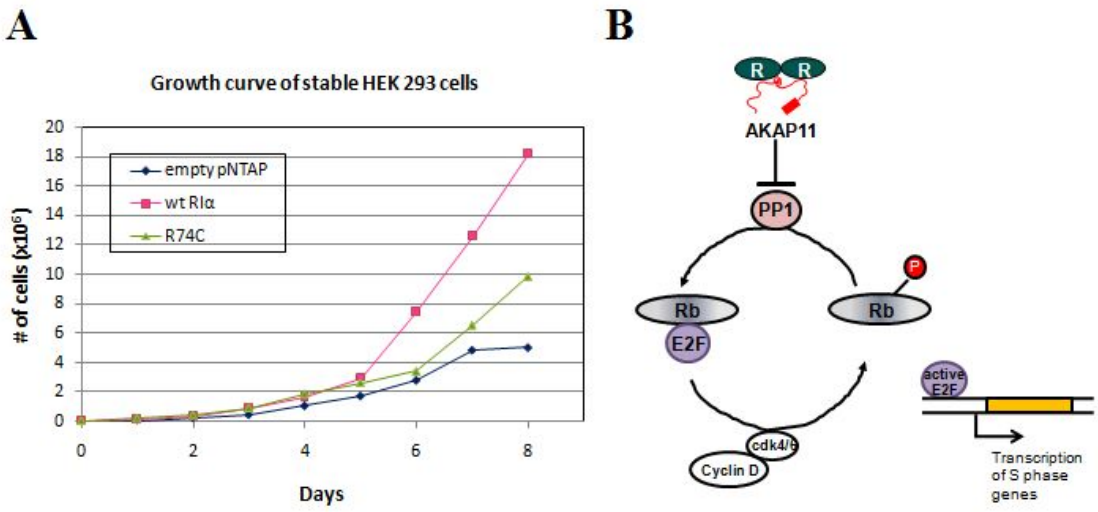

Figure 4.6: Overexpression of wild-type RIα leads to increased cell proliferation.

(A) The growth rate of cells stably expressing TAP-tagged wild-type RIα was compared to cells stably expressing empty pNTAP vector and TAP-tagged R74C. The growth rate of cells overexpressing RIα was faster than the growth rate of cells with endogenous levels of RIα and cells overexpressing R74C.

(B) A model for how overexpression of RIα may lead to uncontrolled cell growth. RIα binding to AKAP11 may enhance the inhibition of PP1 which leads to hyperphosphorylation of Rb protein. The phosphorylation of Rb protein releases E2F, a transcription factor that is involved in cell cycle regulation and DNA synthesis in mammalian cells.

Chapter 5:

Targeting of free RIα to membranous organelles

5.1: Introduction

Although in most cells, RIα is generally diffuse throughout the cytoplasm, some instances show distinct subcellular localization. The localization of RIα at the neuromuscular junction of mouse skeletal muscle was demonstrated using immunohistochemistry [117]. RIα is also associated with microtubules throughout the cell cycle [53]. RIα is sequestered along the fibrous sheath of mammalian spermatozoa [80] and associated with the unconventional myosin VIIA in sensory cells in the ear and retina [85]. Furthermore, upon stimulation of human T cells with anti-CD3, RIα, but not RIIα, redistributed from the cytoplasm to the area of the cell where the T cell receptor-CD3 complex was capped [118]. Most recently, the localization of RIα to late endosomes and autophagosomes was reported [58]. These authors also suggested an interaction between mammalian target of rapamycin (mTOR) and RIα. An inactivation of mTOR results in autophagy, and they observed fewer numbers of autophagosomes with the knockout of RIα thus implying an interaction between mTOR and RIα that inactivated mTOR.

With diverse localizations come different functionalities. RIα is the only isoform that cannot be compensated for by the other isoforms. In general, the R isoforms act as inhibitors to the catalytic subunit thus regulating its activity. However, one study provided evidence of RIα acting in a catalytic subunit-independent manner [89]. RIα interacted with cytochrome *c* oxidase subunit Vb (Cox Vb) of the mitochondrial electron transport chain to decrease its oxidase activity when bound. Upon cAMP stimulation, RIα disassociated from Cox Vb, leading to an increase in

oxidase activity. The effects of RIα on cytochrome *c* may have significant implications on the mechanism of cAMP-induced apoptosis in eukaryotic cells.

In this chapter, we investigated the puncta that were initially observed with the overexpression of GFP-tagged RIα in HeLa cells [Chapter 3]. We showed that these puncta were RI-specific and were not observed with one CNC-related mutant, RIα(1-303). The localization of these puncta was dependent on the N-terminus of RIα, including the D/D domain. Mutating the cAMP binding site also blocked puncta formation. Fractionation studies confirmed the localization of endogenous and overexpressed RIα to membranous compartments, although recruitment of RIα to these compartments was abolished when RIα was co-expressed with C-subunit. The puncta could be reversibly formed with forskolin/IBMX treatment and were independent of PKA C-subunit activity. Using correlated light and electron microscopy, we demonstrated that RIα localized to multivesicular bodies, which are involved in sorting endocytosed proteins to different destinations. Through these various experiments, we discovered a potentially novel mechanism for targeting of RIα.

5.2: Experimental Procedures

Antibodies and reagents. The antibodies used for Western blot analyses in this chapter were purchased commercially: PKAc (Transduction Laboratories), Hsp90 (Transduction Laboratories), Prohibitin (Abcam), Histone (Cell Signaling), LC3 (Cell signaling), p70 S6 kinase (Cell Signaling), phospho-p70 S6 kinase (Cell Signaling), Vimentin (Abcam) and Tubulin (Sigma). The following antibodies were used for staining organelle markers: PMP70 for peroxisomes (Sigma), SKL for peroxisomes (kindly provided by Dr. S. Subramani, University of California, San Diego), AIF for mitochrondria (Cell Signaling), LC3 for autophagosomes (Cell Signaling), and EEA1 for early endosomes (Cell Signaling). The following reagents were used to stain other organelles: ERTracker for endoplasmic reticulum (Molecular Probes) and LysoTracker for lysosomes (Molecular Probes).

Cloning and expression of RIα and other proteins. GFP constructs from Chapter 3 were used. Single site mutations were made in the full length sequence, as described in Chapter 2. R isoforms cloned into A-Kinase Activity Reporter (AKAR) vectors were made by Dr. F. Ma, University of California, San Diego. PKAc tagged with mCherry and PKI tagged with CFP were kindly provided by Dr. R. Tsien, University of California, San Diego, while D-AKAP2 constructs tagged with mCherry were made by Dr. C. Eggers, University of California, San Diego.

Cell lines and culture conditions. HeLa cells were obtained from the American Type Culture Collection. Mouse embryonic fibroblasts (MEFs) were immortalized by transformation with pBRSV encoding the SV40 virus (kindly provided by Dr. G.S. McKnight, University of Washington, Seattle, Washington and Dr. M. Ginsberg, UC San Diego). Cells were maintained, as described in Chapter 3. Transfections were carried out with Fugene 6 (Roche) one day prior to imaging.

Fractionation. *Prkar1a*+/+ MEFs were grown on 15 cm Nunc dishes to about 80% confluency. RIα knockout MEFs (*Prkar1a-/-* MEFs) were transfected using Lipofectamine 2000 (Invitrogen) and grown to about 80% confluency. One set was left untreated, while the other set was treated with 20 μM forskolin (Sigma) simultaneous with 200 μM IBMX (Sigma) for 1 hour. Cells were harvested in 2 mL cold PBS and fractionated with the Qproteome Cell Fractionation kit (Qiagen). Western blots were run on samples using equal volume loads, as described in Chapter 2. All primary antibodies were used at a dilution of 1:1000 except for Hsp90 (1:2000 dilution) and Prohibitin (1:100 dilution).

Colocalization of RIα by immunofluorescence microscopy. For immunofluorescence, HeLa cells and MEFs were grown overnight in poly-d-lysine coated glass bottom dishes (MatTek), transfected with GFP-tagged RIα for 18-24 hours, and fixed with 4% paraformaldehyde (Electron Microscopy Sciences) for 15 minutes at room temperature. In general, cells were then permeabilized in 0.2%

Triton X-100 (Sigma) for 5 minutes at room temperature and blocked in 2% BSA (Sigma) followed by sequential incubations in primary and secondary antibodies. Staining in primary antibodies was done overnight at 4°C, while staining with secondary antibodies was for 1 hour at room temperature. Primary antibodies were used at a dilution of 1:100 in 2% BSA, except for anti-SKL (1:1000 dilution). Donkey anti-rabbit Cy5 (Jackson ImmunoResearch) was used as secondary antibody at a dilution of 1:100. Cells were washed with 1X Dulbecco's PBS (Mediatech) 5 times for 5 minutes each at room temperature before and after each antibody incubation. The method for staining LC3 was slightly altered from that described above. The cells were permeabilized in 0.05% Triton X-100 and blocked in 3% BSA. To stain for ER and lysosomes, cells were incubated with probes diluted in pre-warmed DMEM (ERTracker, final concentration 500 nM; LysoTracker, final concentration 50 nM) for 1 hour at 37°C before fixation. Epifluorescent and confocal images were acquired at room temperature on Zeiss Axiovert 200M using 40x 1.3 oil objective and Olympus FluoView 1000, respectively. Confocal images were maximum intensity projection stacks (z= 30-40 slices; z step = 0.3 μm).

Endosomal pathway.

Degradative pathway. HeLa cells, transfected with GFP plasmids, were serum starved in DMEM supplemented with 0.5% BSA for 6 hours. Texas Red-labeled epidermal growth factor (EGF) (Molecular Probes) diluted in cold DMEM to a final concentration of 1 μg/mL was added to the cells. Unbound EGF was removed by

washing in cold PBS. Pre-warmed DMEM was added to the cells and different time points were taken by fixing cells in 4% paraformaldehyde for 15 minutes at room temperature.

Recycling pathway. HeLa cells, transfected with GFP plasmids, were serum starved in DMEM supplemented with 0.5% BSA for 2 hours. AlexaFluor 568 Transferrin receptor (Invitrogen) was added to the cells at a final concentration of 50 μg/mL for 1 hour at 37°C. Cells were washed once with cold PBS, once with cold stripping buffer (500 mM NaCl, 0.5% Acetic acid, pH 3.0) for 45 seconds, and two more times with cold PBS. Cells were fixed with paraformaldehyde, as described above.

Measurement of autophagy levels. Autophagy was induced in cells by amino acid and glucose starvation using Earle's balanced salt solution (Invitrogen) for 4 hours at 37°C. Two lysosomal inhibitors, pepstatin A (Calbiochem, 1 μM) and EST (Calbiochem, 10 μM), were used to prevent the degradation of LC3-II. To measure the association between RIα and autophagy, cell pictures were uploaded into ImageJ [119] and normalized to the same threshold of LC3 intensity. Only cells showing at least 10 LC3 dots were considered as cells undergoing autophagy. Statistical analysis was performed using Fisher's exact probability test, where p-values less than 0.05 is considered statistically significant. To measure protein expression levels at basal level, Western blots were run on samples using equal volume loads, as described in Chapter 2. All primary antibodies were used at a dilution of 1:1000.

Live cell imaging. *Prkar1a-/-* MEFs were grown overnight on poly-d-lysine coated glass bottom dishes (MatTek) and co-transfected with GFP-tagged RIα and mCherry-tagged C-subunit [Figures 5.2A, 5.13] or co-transfected with GFP-tagged RIα, mCherry-tagged C-subunit, and CFP-tagged PKI [Figure 5.2B]. 18 hours post-transfection, DMEM growth media was replaced with Opti-MEM (Invitrogen). cAMP levels were elevated by addition of 20 μM forskolin (Sigma) and 200 μM IBMX (Sigma) simultaneous at 37°C. PKA activity was inhibited by addition of 10 μM H89 (Upstate). For the movies in Figure 5.2, cells were placed on a heated stage (37°C) and images were acquired live at 1.75 minute intervals for 45 minutes on an Olympus FluoView1000 microscope using an oil immersion 63X objective, N.A. 1.42. For the movie in Figure 5.13, images were acquired live at 2.3 minute intervals for 3 hours. For the movies in Figures 5.2A and 5.13, excitation was with 488-nm and 568-nm laser. For the movie in Figure 5.2B, excitation was with 405-nm, 488-nm, and 568-nm laser. Sequential 0.3 μm confocal sections (25-30 slices) were acquired and stacked using ImageJ.

EM staining. *Prkar1a-/-* MEFs were grown on poly-d-lysine coated glass bottom grid dishes (MatTek). After 18 hours of transfection (using Fugene 6), cells were fixed in 2% paraformaldehyde and 2.5% glutaraldehyde in 0.10 M cacodylate buffer (pH 7.4) solution for 5 minutes at room temperature, and then moved to ice for a duration of 30 minutes for optimal cell ultrastructural preservation. The cells were washed 5 times in ice-cold 0.1 M sodium cacodylate buffer (pH 7.4) and 3 mM calcium chloride, each

taking two minutes, in order to remove excess aldehydes. 1K by 1K images of cells were recorded using a Bio-Rad MRC-1024 confocal system on a Zeiss Axiovert 35M microscope using 488-nm and 568-nm laser excitation and a 40x water objective lens (confocal stacks of z = 37, z step = 0.36 μm). A transmitted image was taken with either 10x or 20x objective lens to determine the grid location. The cultured cells were post-fixed in ice-cold 1% osmium tetroxide with 0.8% potassium ferrocyanide and 3 mM calcium chloride for 30 minutes, washed five times in double-distilled water for 2 minutes each to stop the osmium tetroxide reaction, and *en block* stained in ice-cold 2% uranyl acetate for overnight to help increase membrane contrast. Afterwards, the cultured cells were dehydrated in an ethanol series for three minutes each starting with 20, 50, 70, and 90% on ice and ending with four changes of 100% ethanol at room temperature. The dehydrated cells were infiltrated in a 1:1 ratio of absolute ethanol to Durcupan ACM epoxy resin (Electron Microscopy Sciences) for 30 minutes and then with three changes of Durcupan ACM epoxy resin for one hour each. Finally, a fourth Durcupan ACM epoxy resin change was done and immediately the MatTek disk was placed in a vacuum oven at 60°C to be polymerized for 48-72 hours. After polymerization, the coverslip was removed from the MatTek dish and plastic blocks were sawed out and glued onto dummy blocks. 80 nm ultrathin serial sections were prepared using an ultramicrotome (Reichert-Jung Ultra-cut E) with a diamond knife (Diatome) and the sections were supported onto 200 mesh copper grids. The 80 nm sections were post-stained in Sato lead for 1 minute and the stained sections were imaged using a JEM-1200EX II electron microscope at 80 kV.

5.3: Results

RIα localization in cultured cells. Though RIα localization is predominantly cytoplasmic, a faint punctate pattern was observed when GFP-tagged RIα was expressed in HeLa cells [Chapter 3, Figure 3.1B and Figure 5.1A, left]. To characterize the localization of RIα GFP without the presence of wild-type RIα, RIα knockout mouse embryonic fibroblasts (*Prkar1a-/-* MEFs) were also transiently transfected [Figure 5.1A, right]. In both cells lines, RIα GFP formed a punctate pattern. We then characterized these puncta.

Importance of Free RIα versus Holoenzyme. To determine whether RIα holoenzyme as well as free RIα localized to puncta, wild-type RIα was co-expressed with C-subunit (from here on, referred to as PKAc). When both RIα and PKAc were overexpressed in *Prkar1a-/-* MEFs, RIα localization was diffuse in the cytoplasm [Figure 5.1B, left]. These results suggested that the binding of PKAc to RIα prevented its localization to puncta. To test whether the holoenzyme complex could be disassociated, cells were treated with forskolin/IBMX. Forskolin activates adenylyl cyclase and increases the intracellular levels of cAMP, while isobutylmethylxanthine (IBMX) is a non-specific inhibitor of phosphodiesterases that prevents the breakdown of cAMP. Figure 5.1B (right) shows that the forskolin/IBMX treatment released RIα from the holoenzyme complex and the punctate pattern reappeared.

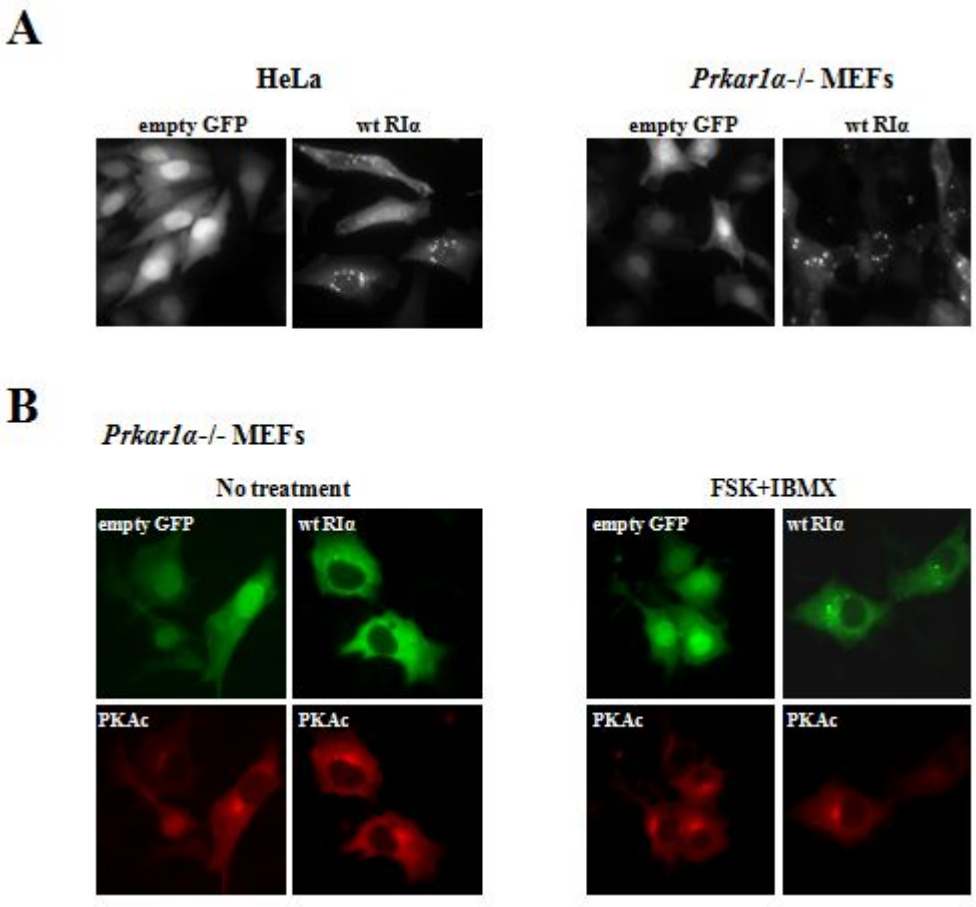

Figure 5.1: Expression of wild-type RIα in mammalian cells revealed a punctate pattern.

(A) Transient transfection of GFP-tagged RIα in HeLa cells (left) and *Prkar1a-/-* MEFs (right) revealed a punctate pattern.

(B) Co-expression of GFP-tagged RIα with mCherry-tagged PKAc showed a diffuse pattern (left), which upon disassociation (right), revealed the punctate pattern.

Live cell imaging demonstrates the puncta formation is reversible. In order to follow the formation of the puncta, live cell imaging was done with *Prkar1a-/-* MEFs, transiently transfected with RIα GFP and PKAc mCherry [Figure 5.2A]. After 18 hours of transfection, cells were equilibrated in Opti-MEM for 1 hour and imaged at 37°C on a confocal microscope. Before treatment (baseline), both RIα and PKAc showed a diffuse pattern. Within about two minutes of treating cells with 20 μM forskolin and 200 μM IBMX, RIα showed a punctate pattern. This phenotype was reversible, since washing away the drugs caused the diffuse pattern to reappear within approximately 4 minutes. When the cells were again treated with forskolin/IBMX, the punctate pattern reappeared. This phenotype was again reversible when the drugs were washed away with Opti-MEM.

Punctate pattern is independent of PKA activity. To determine whether localization of RIα to puncta required active PKAc, cells were treated with an inhibitor of PKA, an ATP analog, H89, for 10 minutes before treatment with forskolin/IBMX. However, these cells showed the same effect as cells treated with forskolin/IBMX alone (Figure 5.2A, last panel). Another inhibitor of PKAc is the heat-stable protein kinase inhibitor (PKI). To further confirm that the punctate pattern is independent of PKAc activity, PKI was used. Cells were transfected with RIα GFP, PKAc mCherry, and PKI CFP simultaneously [Figure 5.2B]. The cells showed a diffuse pattern at the start, and upon treatment with forskolin/IBMX, RIα showed a punctate pattern. However, the punctate pattern was not reversible when the drugs were removed. In the presence of

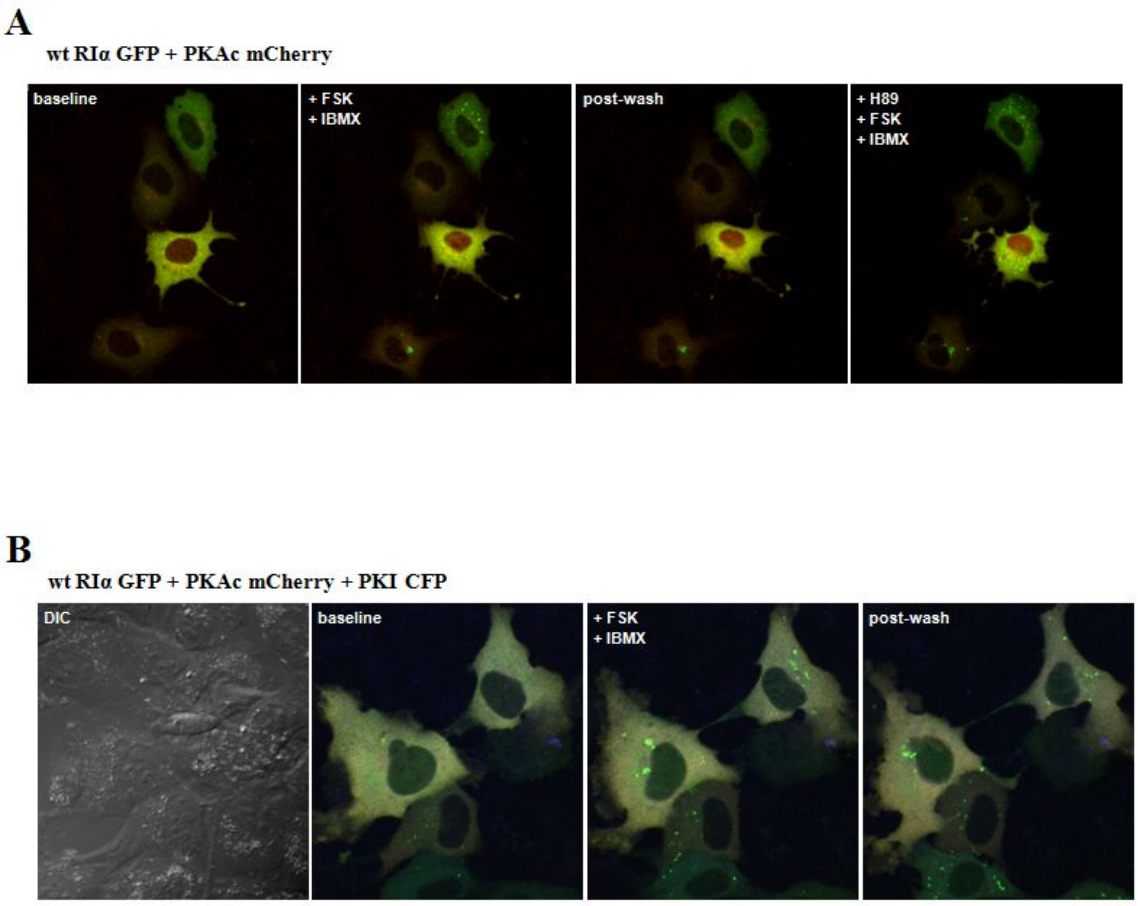

Figure 5.2: Representative pictures from live cell imaging.

Live cell imaging movies were made of *Prkar1a-/-* MEFs transiently transfected with either GFP-tagged RIα and mCherry-tagged PKAc (A) or GFP-tagged RIα, mCherry-tagged PKAc, and CFP-tagged PKI (B). A few frames were taken before and after the addition of forskolin/IBMX. Representative pictures from each step are shown.

(A) The puncta disappeared with the removal of the treatments. The puncta reappeared with the re-addition of forskolin/IBMX. H89 was added prior to the last addition of forskolin/IBMX to confirm the punctate pattern was independent of PKAc activity.

(B) Similar to the movie from (A), the green puncta did not appear until after the addition of forskolin/IBMX. However, the puncta did not disappear after the removal of treatment. This difference was most likely the result of an inability of RIα to compete with PKI for binding to PKAc.

cAMP, PKI binds with high affinity to PKAc, so the irreversibility of the puncta indicated a tighter binding of PKI than RIα to PKAc so that once PKAc was bound to PKI, RIα could not outcompete PKI for binding to PKAc and RIα remained in its free form.

Punctate pattern is RI-specific. We next explored the different R subunit isoforms to see if formation of puncta was unique to RIα. Constructs of the four R subunit isoforms tagged with both YFP and CFP (AKAR vector) were expressed in *Prkar1a-/-* MEFs [Figure 5.3A], but only the excitation of YFP was used. The overexpression of RI isoforms showed a punctate pattern, while overexpression of the RII isoforms showed a diffuse pattern. Therefore, the punctate pattern was an RI isoform-specific phenotype.

We then investigated various RIα mutants to determine where the sites or domains responsible for puncta formation were located [Figure 5.3B]. Single site mutations were introduced into the GFP-tagged RIα construct. We tested whether the disulfide bonds formed by the N-terminal cysteines, C18 and C39, were required for the puncta by individually mutating the residues to alanine and expressing them in *Prkar1a-/-* MEFs. Since both cysteine mutants still showed a punctate pattern, we concluded that the phenotype is independent of the disulfide bond. Mutating the constitutive phosphorylation site, S83, to alanine had no effect. We then mutated the alanine in the IS site to a serine to mimic the behavior of RII isoforms; however, the phenotype was again unchanged. Lastly, we mutated two prolines in the putative

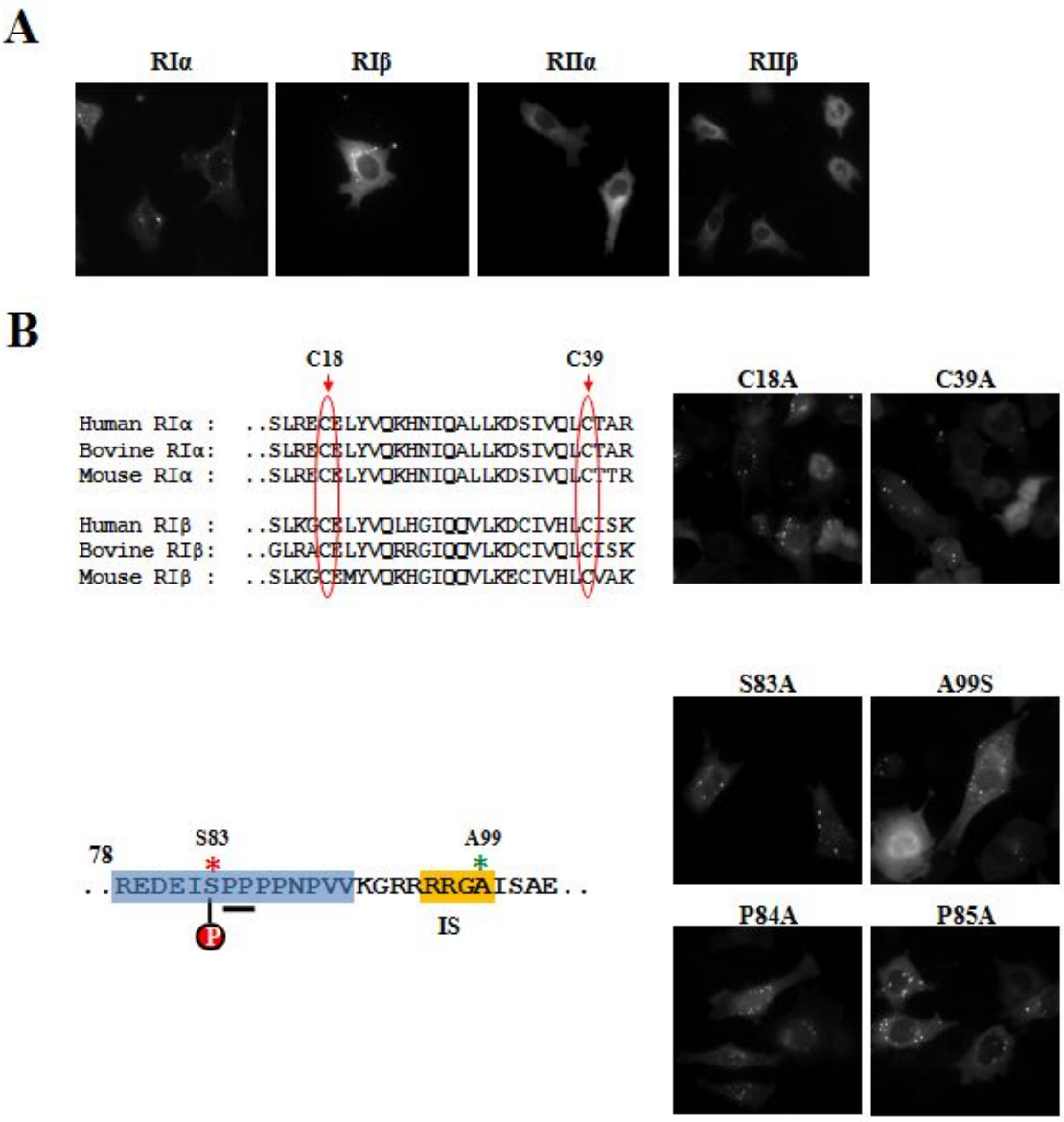

Figure 5.3: Some RI-specific residues did not contribute to punctate pattern.

(A) R subunit isoforms were expressed in *Prkar1a-/-* MEFs and revealed that the punctate pattern was RI-isoform specific.

(B) Expression of mutations in the D/D domain and in the linker region of RIα in *Prkar1a-/-* MEFs did not change the punctate phenotype. The N-terminal cysteines are circled in red. The PEST sequence (residues 78-91) is highlighted in blue while the IS site is highlighted in yellow. S83 and A99 are indicated by a red and yellow asterisk, respectively. P84 and P85 are indicated by an underline.

PEST sequence, P84 and P85, to alanine, which were predicted to remove the PEST sequence (https://emb1.bcc.univie.ac.at/toolbox/pestfind/pestfind-analysis-webtool.htm). With these mutations, the punctate pattern was still observed.

Differential punctate pattern from CNC-related mutants. We were also interested in looking at the localization of the two CNC-related mutants, which were biochemically characterized in Chapter 2. GFP-tagged R74C and RIα(1-303) were transiently transfected in addition to GFP-tagged R211K, which was used as a control since it has a mutation in the PBC that is defective in cAMP binding [Figure 5.4A]. We observed a punctate pattern from the overexpression of GFP-tagged R74C in both transiently transfected HeLa cells and *Prkar1a-/-* MEFs. However, when we expressed the R211K mutant or the truncated protein, RIα(1-303), neither formed puncta.

Since co-expression of PKAc with wild-type RIα abolished the punctate pattern [Figure 5.1B, left], co-expressions of PKAc with these other mutants were done as well [Figure 5.4B]. A diffuse pattern in R74C was seen while there was no change in the diffuse pattern that had previously been seen from the single expressions of R211K and RIα(1-303). However, R211K seemed to show strong colocalization with PKAc at the Golgi apparatus, seen by the increased localization next to one side of the nucleus. After adding forskolin/IBMX, the punctate pattern in R74C appeared; however, R211K and RIα(1-303) still showed a diffuse pattern.

To directly activate the holoenzyme complex, transfected cells were also incubated with increasing concentrations of a cell-permeable cAMP analog that is

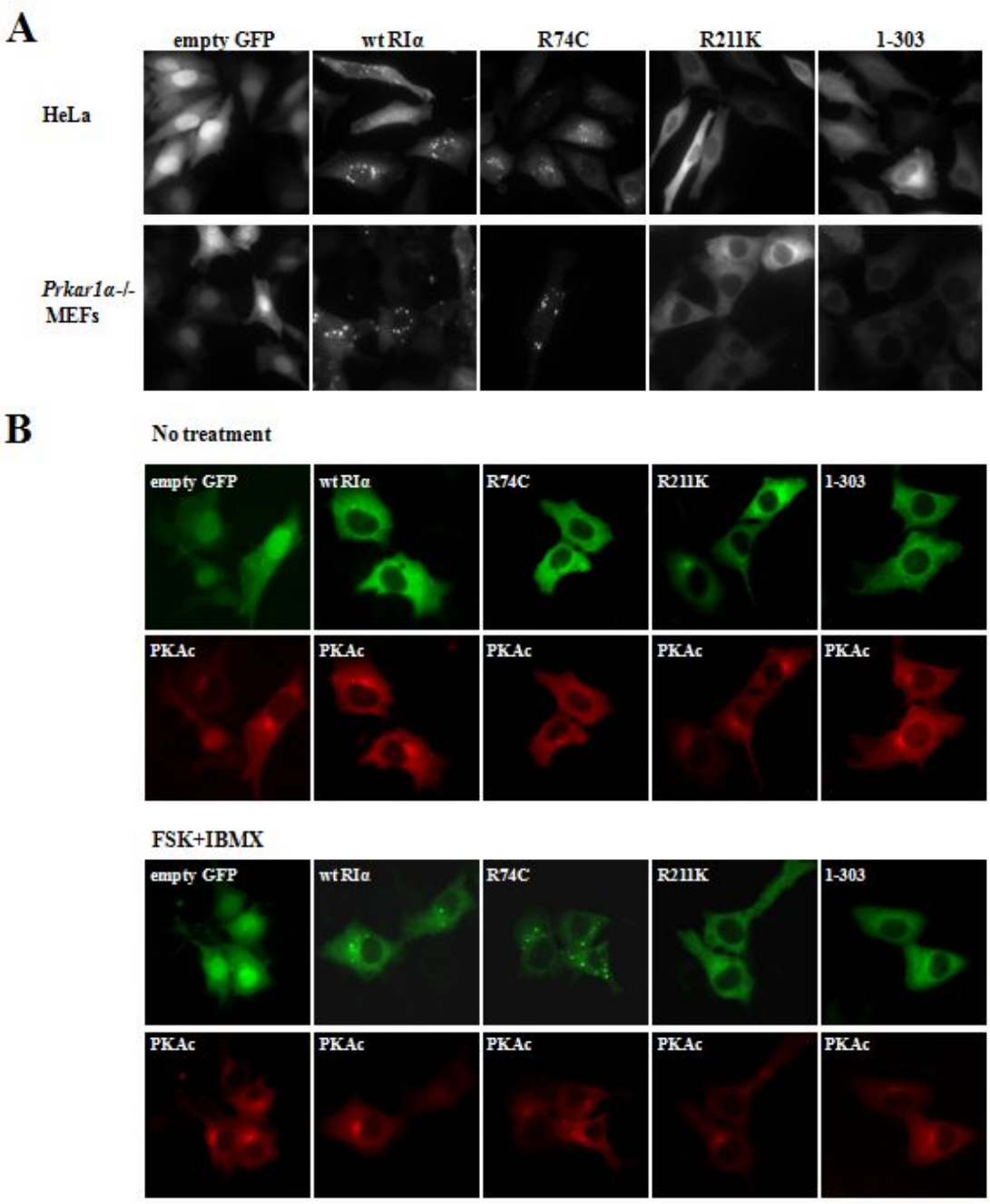

Figure 5.4: Free RIα relocalized to form a punctate pattern.

(A) Transient transfections of GFP-tagged R74C showed a punctate pattern similar to GFP-tagged wild-type RIα, while R211K and RIα(1-303) were diffuse.

(B) Co-expression of R74C with PKAc showed a diffuse pattern, which changed to the punctate pattern with the addition of forskolin/IBMX.

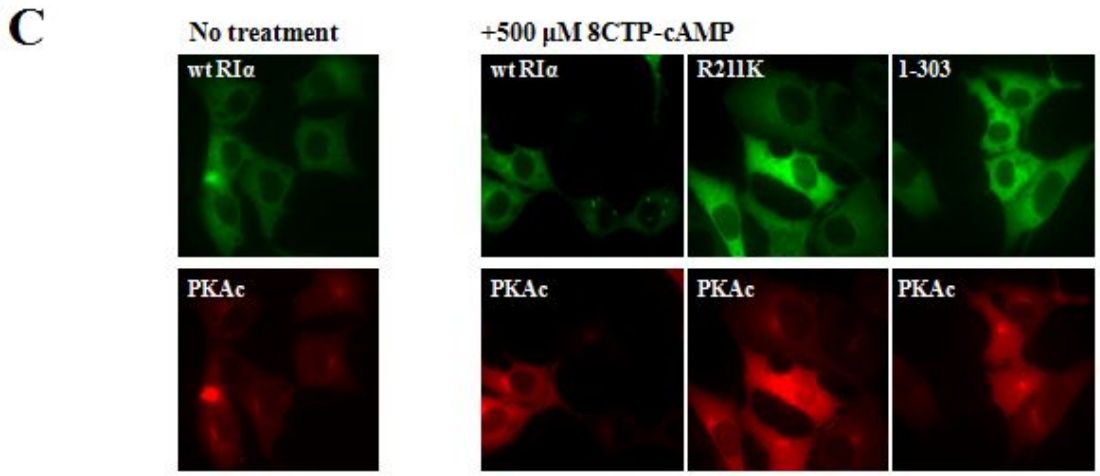

Figure 5.4: Free RIα relocalized to form a punctate pattern, Continued.

(C) Direct activation of PKAc with 500 µM 8CPT-cAMP was not enough to release R211K or RIα(1-303) from the holoenzyme complex.

resistant to phosphodiesterase activity, 8-(4-chlorophenylthio)-cAMP, (8CPT-cAMP) for 30-60 minutes (data not shown). Cells overexpressing wild-type RIα started to form puncta with 100 μM 8CTP-cAMP and had bright puncta with 500 μM 8CTP-cAMP. However, even with 500 μM 8CPT-cAMP, the diffuse pattern of RIα(1-303) and R211K remained unchanged [Figure 5.4C]. The R211K:PKAc complex requires a 20-fold higher concentration of cAMP than the wild-type RIα:PKAc complex for activation [120]. In Chapter 2, we saw that the RIα(1-303):PKAc complex was also less sensitive, by about 4-fold, to cAMP. From these results, we confirmed that it was free RIα that localized to puncta and binding to PKAc disrupted this localization. The RIα(1-303) and R211K mutants were presumably not released from the holoenzyme.

Localization to puncta may be through AKAP targeting. To show which regions of RIα were responsible for formation of the puncta, GFP-tagged RIα(1-93) and RIα(93-381) were expressed [Figure 5.5A]. The RIα(1-93) construct includes the D/D domain but excludes the IS site, while the RIα(93-381) construct includes the IS site and the two tandem cAMP domains. A faint punctate pattern was seen from RIα(1-93), but no puncta were seen from RIα(93-381). Thus, the N-terminal part of RIα is necessary for the punctate pattern.

AKAPs, which bind to the N-terminal D/D domain, help localize the R subunits in cells and a few AKAPs have been found to bind to RIα (for references, see Chapter 4). Several single site mutations in RIα are known to reduce binding to D-AKAP1 [32]. Two mutations in the D/D domain that are important for AKAP

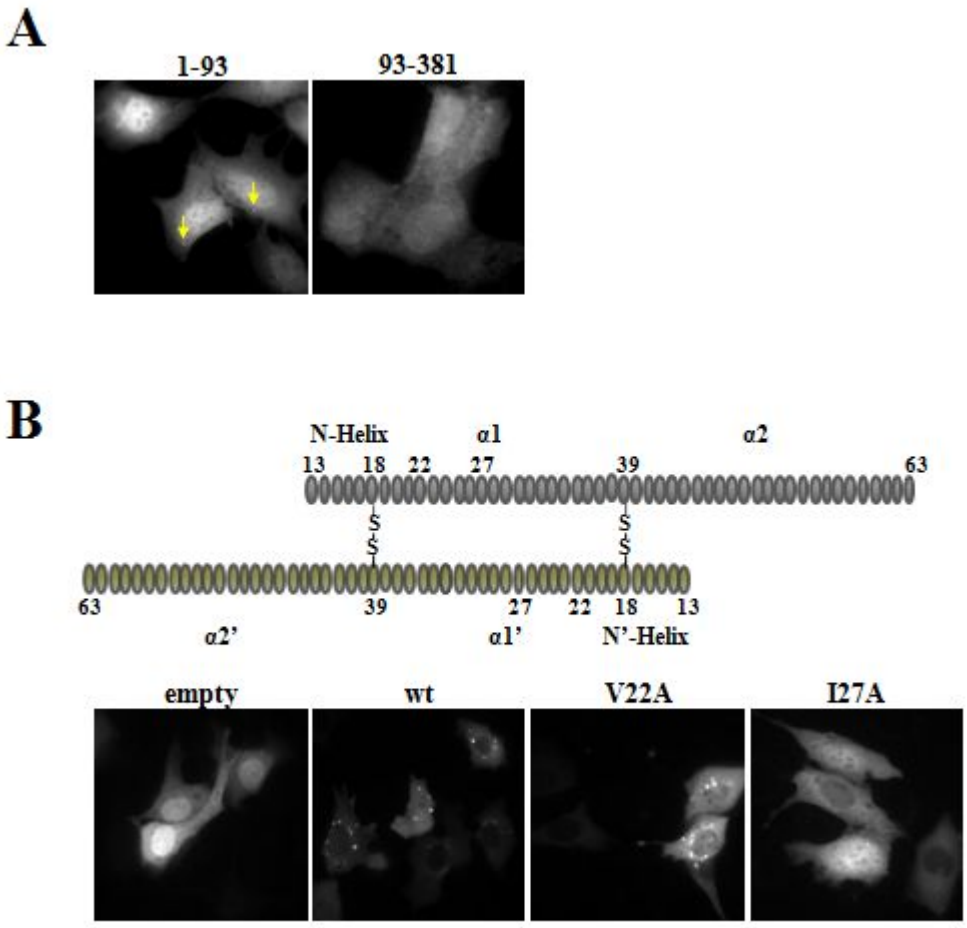

Figure 5.5: Localization to puncta is likely due to the binding of an AKAP.

(A) Expression of RIα(1-93), but not RIα(93-381), in *Prkar1a-/-* MEFs showed a faint punctate pattern. The high background expression of this truncated protein in the cytoplasm made it difficult to see the puncta clearly (two are indicated by yellow arrows).

(B) One mutation that has been reported to disrupt D-AKAP1 binding, I27A, showed a clear change in localization, compared to wild-type RIα when expressed in *Prkar1a-/-* MEFs.

C

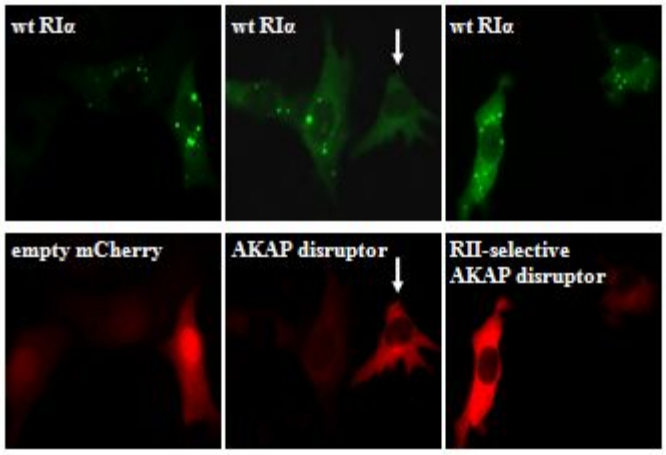

Figure 5.5: Localization to puncta is likely due to the binding of an AKAP, Continued.

(C) Overexpression of the A-Kinase Binding (AKB) domain from D-AKAP2 (AKAP disruptor) abolished the puncta when expressed at high levels, indicated by white arrows, whereas overexpression of an RII-specific AKAP did not.

binding, V22 (located in the N-Helix) and I27 (located in the α1 Helix), were each mutated in the full length sequence to alanine. Although the punctate pattern was still seen with the V22A mutation and appeared to be brighter than those seen from wild-type RIα [Figure 5.5B], this corroborates well with data that showed RIα with N-Helix deleted could still bind to D-AKAP1 [32]. In contrast, the punctate pattern disappeared with the I27A mutation [Figure 5.5B]. Furthermore, with the I27A mutation, nuclear localization was observed. This result provided evidence that the localization of RIα to the puncta was through AKAP binding. Also, AKAP binding could have prevented RIα from going into the nucleus. A putative nuclear localization signal in RIα that is required for localization of its binding partner, Replication Factor C complex (RFC40), has been reported [35].

To test this theory of AKAP involvement further, GFP-tagged RIα was co-expressed with mCherry-tagged D-AKAP2 constructs in *Prkar1a-/-* MEFs [Figure 5.5C]. Co-expressing wild-type RIα with an AKAP disruptor (the last forty residues of D-AKAP2 that contain the PKA binding motif), caused the punctate pattern of RIα to become diffuse. The truncated D-AKAP2 expresses at higher levels and should act to disrupt interactions between PKA and other AKAPs. As a control, an RII-selective AKAP disruptor (mCherry-tagged RII-selective D-AKAP2) was co-expressed with RIα and the puncta remained. Taken together, these results also supported the notion that an AKAP may be involved in localizing RIα to the puncta.

Fractionation of MEFs reveals a migration of free RIα to membrane. To determine whether the puncta corresponded to membranous organelles or aggregates of protein, fractionation studies were done [Figure 5.6]. *Prkar1a*+/+ MEFs were used to look at migration of endogenous RIα. At basal levels of cAMP, the majority of RIα was in the cytosolic fraction. However, upon 60 minutes of forskolin/IBMX treatment, RIα showed a significant shift to the membrane fraction (mem) [Figure 5.6, left panel]. Meanwhile, no change in PKAc levels was observed. Markers for each fraction were used to show equal loads of samples. The same experiment was done in *Prkar1a-/-* MEFs overexpressing both GFP-tagged RIα with mCherry-tagged PKAc [Figure 5.6, right panel]. Likewise, an increase of RIα levels in the membrane fraction was observed after forskolin/IBMX treatment with no change in PKAc levels. These results confirmed the migration of the free RIα to membranes.

Involvement of RIα in autophagy. Since it was previously reported that RIα colocalized with autophagosomes, these were the first organelles we stained [58]. However, in contrast to their report, we found no colocalization with autophagosomes, as stained by light chain 3 (LC3), which localizes to autophagosomal membranes. In fact, cells that showed wild-type RIα puncta had lower levels of autophagy compared to cells without wild-type RIα puncta [Figure 5.7A]. However, an inverse correlation of RIα was apparent when using the Fishers exact test to assess the statistical significance of association between GFP puncta and autophagy (table in Figure 5.7A). Total numbers of cells were counted as well as number of cells expressing RIα GFP

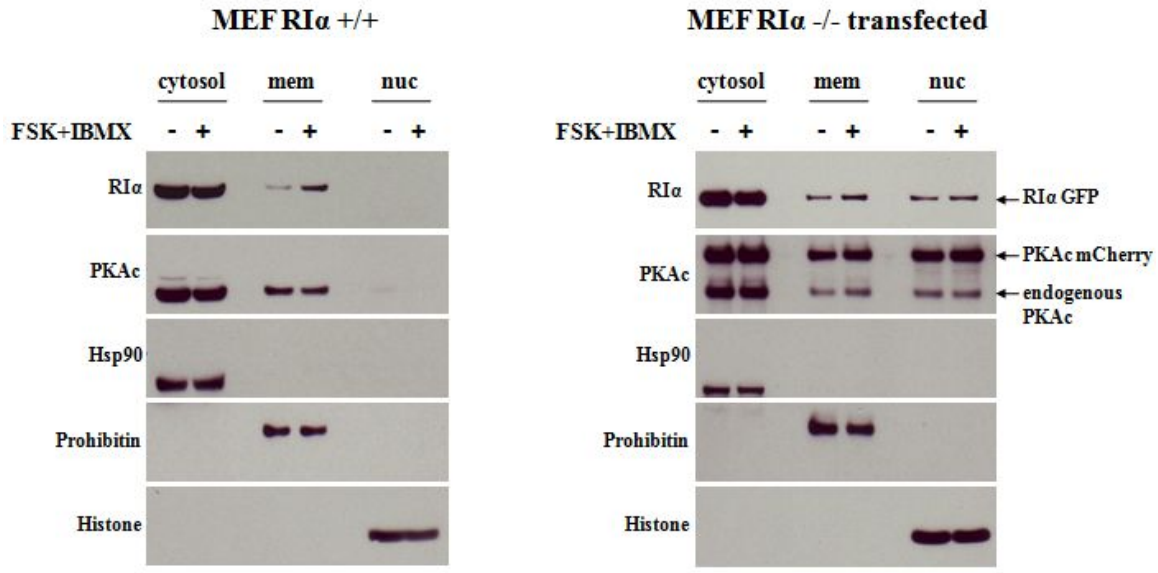

Figure 5.6: Fractionation of MEFs showed that free RIα is localizing to membranes.

Prkar1a+/+ MEFs were treated with forskolin/IBMX and fractionated to observe the localization of RIα. A shift of RIα to the membrane fraction (mem) was seen when *Prkar1a*+/+ MEFs were treated with forskolin/IBMX (left panel). This shift to the membrane fraction indicated that free RIα was localizing to a membranous compartment. To confirm that the puncta seen from live cell imaging were also localizing to a membranous compartment, *Prkar1a*-/- MEFs were transiently transfected with GFP-tagged RIα and mCherry-tagged PKAc, treated with forskolin/IBMX, and fractionated (right panel). Again with the treatment, a shift of free RIα to the membrane fraction was observed.

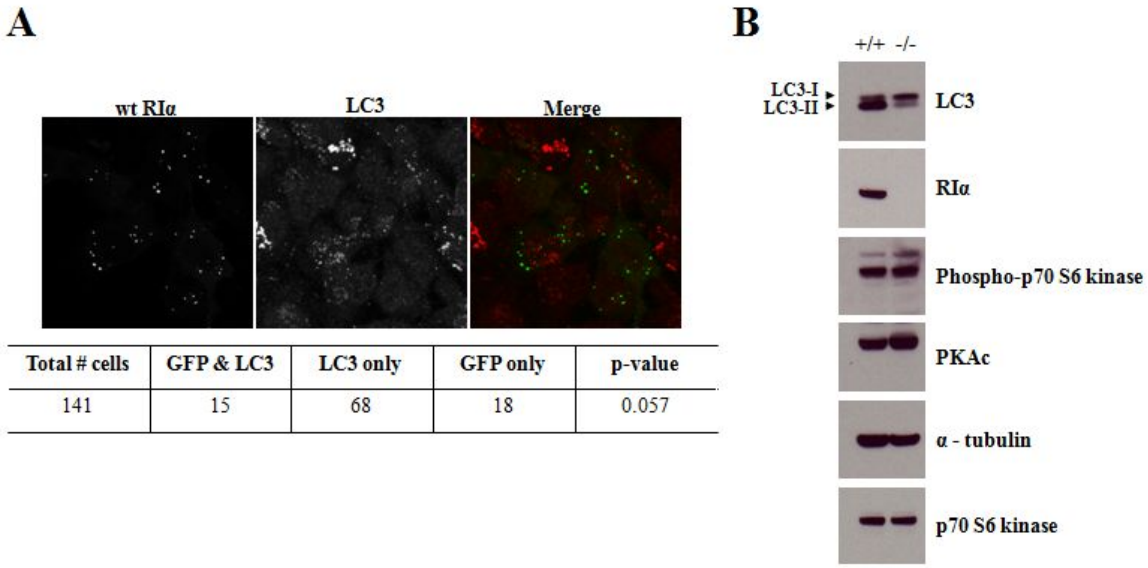

Total # cells	GFP & LC3	LC3 only	GFP only	p-value
141	15	68	18	0.057

Figure 5.7: RIα affects levels of autophagy.

(A) Staining for autophagosomes using LC3 showed no colocalization with RIα, contradictory to results from Mavrakis *et al.* [58]. Instead, cells seemed to show fewer autophagosomes in cells expressing RIα puncta. This inverse relationship was statistically quantified using Fishers exact test.

(B) The basal level of autophagy seen in *Prkar1a*+/+ MEF cells was not seen in the *Prkar1a*-/- MEFs, implying a relationship between RIα and autophagy. No change in the levels of phosphorylation of p70 S6 kinase (phospho-p70 S6 kinase) was detected.

puncta with or without LC3 puncta or with LC3 puncta alone. The p-value was calculated using the hypergeometric distribution which assumes under the null hypothesis that the expressions of RIα and LC3 puncta are independent events in each cell. We defined a p-value cutoff at 0.05 as significant, independent events. Thus, with a p-value close to 0.05, the expressions of wild-type RIα with LC3 puncta were not independent events; instead, there was an inverse correlation where overexpression of RIα levels led to fewer LC3-positive puncta.

Another way to detect autophagy is through the analysis of LC3 conversion (LC3-I to LC3-II) on a Western blot since the amount of LC3-II is directly correlated with the number of autophagosomes. To further substantiate the involvement of RIα in autophagy, a Western blot of cell lysates under basal conditions showed a lower level of LC3 conversion in the *Prkar1a-/-* MEFs than the *Prkar1a*+/+ MEFs (Figure 5.7B). We also checked the levels of phosphorylated p70 S6 kinase and found no change in levels of phosphorylation between the two MEFs. This data is also in contrast to what was reported in the abovementioned paper, where they suggested that the decrease in autophagy in *Prkar1a-/-* MEFs compared to *Prkar1a*+/+ MEFs was due to the activation of mTOR [58]. p70 S6 kinase is directly phosphorylated by active mTOR so if mTOR activity was increased in the *Prkar1a-/-* MEFs, we would have expected to see an increase in the levels of phosphorylated p70 S6 kinase. Therefore, whether RIα levels were decreased or increased, a change in levels of autophagy was seen, which corroborates published reports of RIα involvement in cell growth regulation (for references, see Chapter 1).

Colocalization studies of RIα. To determine to what other possible membranous organelle the free R subunit was localizing, commercially available antibodies were used to stain various organelles in HeLa cells and *Prkar1a-/-* MEFs [Figure 5.8]. HeLa cells were transiently transfected with GFP-tagged RIα and stained for early endosomes (EEA1). No overlap was detected, though the puncta were similar in size to EEA1. They were also very close, almost touching, but not overlapping. *Prkar1a-/-* cells transfected with RIα were also stained for lysosomes, endoplasmic reticulum, and mitochondria, but no colocalization was observed with these organelles.

Since the puncta were in such close proximity to EEA1, we looked for colocalization along the endosomal pathway [Figure 5.9]. The recycling pathway was marked using Rhodamine-transferrin. No overlap with the recycling pathway was detected. A search for RIα puncta localizing to an organelle along the degradative pathway was performed using Texas Red-labeled epidermal growth factor (EGF). Cells were fixed at different time points after the uptake of EGF to follow the different stages of the endosomal pathway. A great amount of overlap between Texas Red EGF and EEA1 at 10 minutes indicated that EGF was localized to the early endosomes at 10 minutes. No overlap between RIα and EGF/EEA1 was seen, although close proximity was consistently observed.

On the other hand, when staining for peroxisomes using two different antibodies, we found partial overlap with GFP-tagged RIα in both HeLa cells and *Prkar1a-/-* MEFs [Figure 5.10]. One antibody, anti-PMP70, recognizes peroxisomal

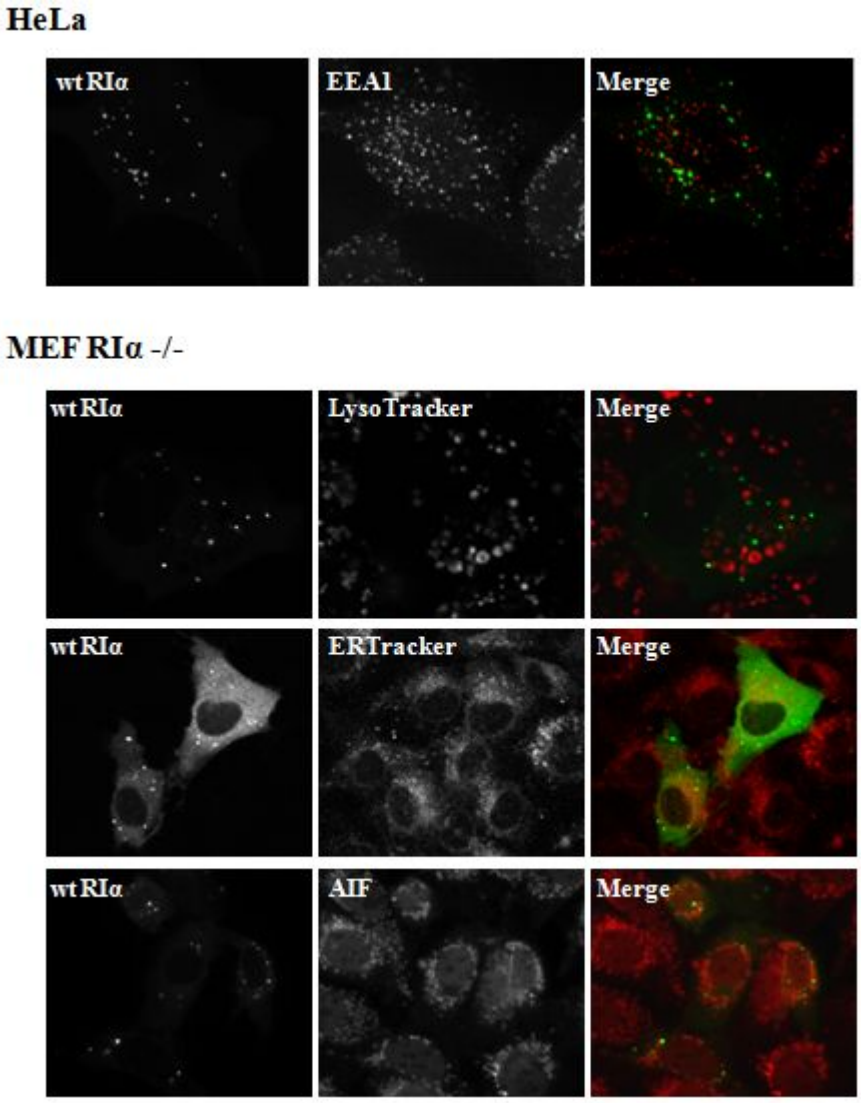

Figure 5.8: Immunofluorescence was used to detect localization to membranous organelles.

A search for the membranous organelle to which the RIα was localizing was performed using indirect immunofluorescence. HeLa cells were transiently transfected with GFP-tagged RIα and stained for early endosomes (EEA1). *Prkar1a-/-* MEFs were transiently transfected with GFP-tagged RIα and stained for lysosomes (LysoTracker), endoplasmic reticulum (ERTracker), and mitochondria (AIF). No overlap was seen with any of these markers.

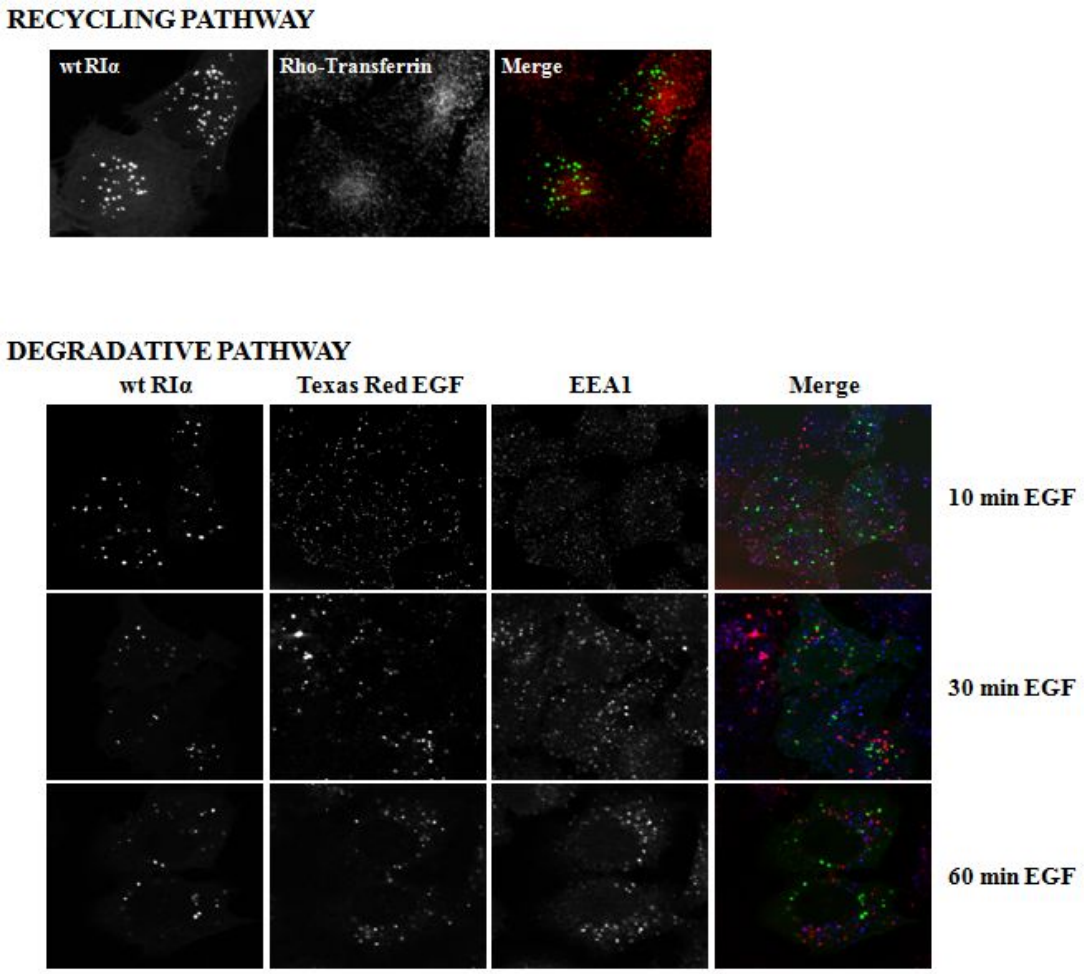

Figure 5.9: No colocalization with markers along the endosomal pathway.

Rhodamine-transferrin was used to follow the recycling pathway while Texas Red EGF was used to follow the degradative pathway. HeLa cells, transiently transfected with RIα, were fixed at different time points after the uptake, to follow the different stages of the endosomal pathway. Cells were stained for EEA1 to indicate the stage of the pathway. At 30 minutes, EGF was past the early endosomes. No overlap was seen along the endosomal pathway.

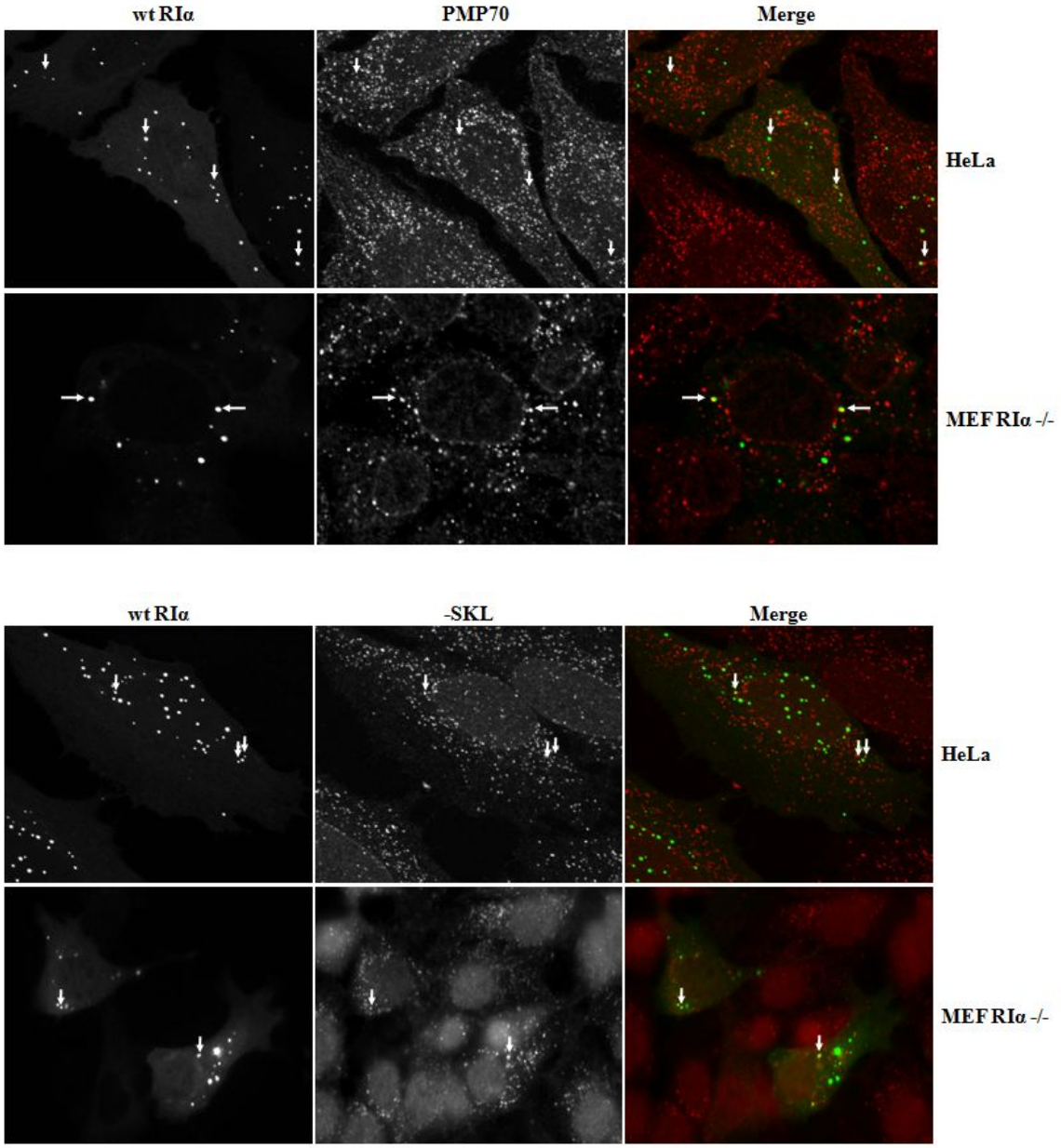

Figure 5.10: A subset of RIα GFP puncta showed partial overlap with peroxisomes.

Two different peroxisomal antibodies, anit-PMP70 and anti-SKL, showed a partial overlap with transfected RIα. This overlap, indicated by white arrows, was seen in both HeLa cells and *Prkar1a-/-* MEFs.

membrane protein 70, which is an abundant integral membrane protein of the peroxisome. The other antibody, anti-SKL, recognizes all proteins that have the –SKL sequence, a peroxisomal targeting sequence, at their C-terminus.

Electron microscopy studies reveal localization to multivesicular bodies. To confirm the identity of the membranous structures to which RIα was localizing, we did an ultrastructural analysis of the *Prkar1a-/-* MEFs transiently expressing GFP-tagged RIα alone or co-expressing GFP-tagged RIα and mCherry-tagged PKAc using correlated light and electron microscopy [Figure 5.11, top and middle row]. A post-stain with lead was done prior to imaging to enhance the visualization of cell membranes. Antibody staining was not necessary because GFP from the transfected protein produced enough electron-dense products to be viewed at the electron microscopy level. In both cases, we observed a localization of RIα GFP to a membranous organelle that resembled multivesicular bodies. As a control, we also looked at untransfected *Prkar1a-/-* MEFs treated with forskolin/IBMX [Figure 5.11, bottom row]. No electron dense product was observed in the multivesicular bodies from these cells, further verifying that the dark electron-dense product seen in previous pictures did correlate with RIα GFP.

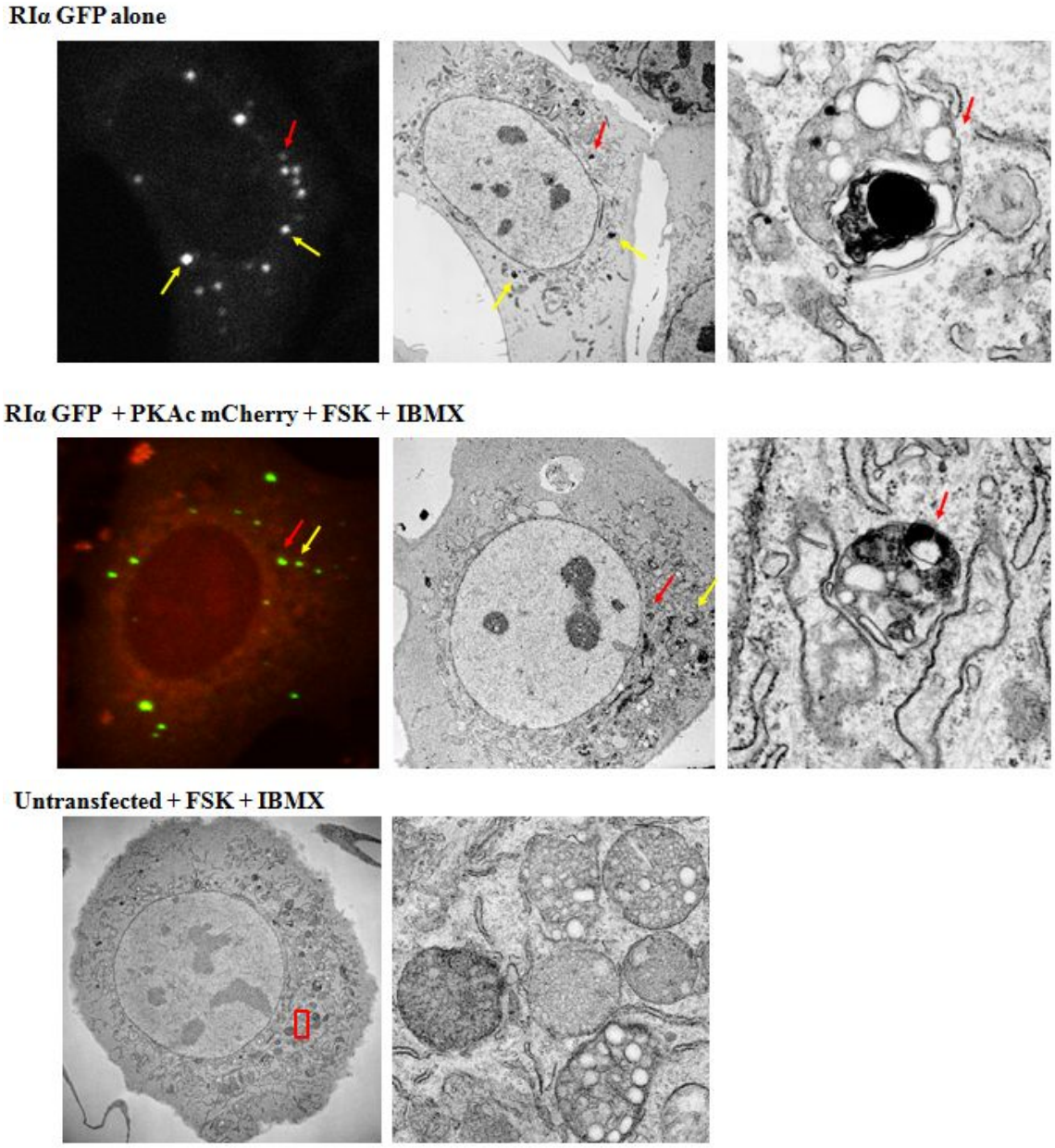

Figure 5.11: Localization of RIα to multivesicular bodies was seen by ultrastructural analysis.

Light and electron microscopy pictures were correlated to look for localization of GFP-tagged RIα. The red arrow is pointing to a multivesicular body that correlates with RIα GFP. RIα is the dark black area within the multivesicular body. As a control, untransfected *Prkar1a-/-* MEFs were treated with forskolin/IBMX and imaged using electron microscopy. An enlarged image of multivesicular bodies in the red square is shown. No dark staining inside these multivesicular bodies was observed.

5.4: Discussion

In this chapter, we characterized the significance of the punctate pattern that was observed in HeLa cells transiently transfected with GFP-tagged RIα [Chapter 3]. The overexpression of RIα in RIα knockout mouse embryonic fibroblasts (*Prkar1a-/-* MEFs) still resulted in the same punctate phenotype. Through the expression of the different R subunit isoforms, we showed the puncta were RI-specific. Disruption of the punctate pattern did not occur through single site mutations within the RIα sequence. Instead, it seemed to depend on both an AKAP binding as well as a disassociation from C-subunit. By controlling its interactions with the C-subunit through forskolin/IBMX, the localization was reversible; moreover, the localization did not depend on C-subunit activity. These puncta localized to membranous organelles, seen from the partial overlap with peroxisomes at the light microscopy level and multivesicular bodies at the electron microscopy level.

When staining for peroxisomes, we found a subset of RIα puncta that had partial overlap [Figure 5.10]. From Chapter 4, we saw that AKAP11 was bound to RIα in both stably and transiently transfected HEK 293 cells. AKAP11 has been suspected to localize to peroxisomes [111]. Thus, AKAP11 is potentially responsible for the localization of RIα to these puncta.

However, the localization of RIα was a dynamic process that made it difficult to define its location temporally; therefore, we used ultrastructural analysis to determine the membranous organelle. We found that at the electron microscopy level, GFP-tagged RIα showed dark staining in organelles that resembled multivesicular

bodies [Figure 5.11]. However, the process by which RIα reached the multivesicular bodies has yet to be determined.

Multivesicular bodies are a part of the endosomal pathway that sort endocytosed proteins to different destinations in the cell. Multivesicular bodies can only be definitively identified at the ultrastructural level [121]. The transition from an early/sorting endosome to a multivesicular body is a gradual process and the boundaries are not clearly defined. Cargo destined for degradation will concentrate on intralumenal vesicles that accumulate to give rise to multivesicular bodies [122]. One way to target proteins to multivesicular bodies is through ubiquitination [121]. The PEST sequence is one signal that is recognized by the ubiquitin machinery and RIα has a potential PEST sequence in its linker region [Figure 1.4]. This PEST sequence has been correlated with the ubiquitination of RIα upon cAMP binding in *Aplysia* neurons [27]. Thus, it seemed likely that the PEST sequence might be responsible for the localization of GFP-tagged RIα to multivesicular bodies. Both R211K and RIα(1-303) bind tightly to PKAc so that disassociation does not occur and the PEST sequence does not get revealed. However, in this case, the PEST sequence does not seem to be responsible for targeting to multivesicular bodies. When mutations were made within the PEST sequence so that it was no longer present, the punctate pattern was still observed [Figure 5.3B]. Furthermore, HEK 293 cells overexpressing wild-type RIα did not show ubiquitination (data not shown).

Another possibility is that an AKAP is responsible for targeting the free RIα to multivesicular bodies since a diffuse pattern was observed with the I27A mutation

[Figure 5.5B]. Because we saw a partial overlap of RIα with peroxisomes, a third possibility is that AKAP11 is targeting RIα to peroxisomes, which then merge with multivesicular bodies. In plant cells, a novel organelle, peroxisomal multivesicular bodies, has been found [123]. Perhaps a similar organelle exists in mammalian cells as well.

Another way for free RIα to reach multivesicular bodies could be through the model shown in Figure 5.12. An AKAP could target RIα to peroxisomes, which then could be degraded by autophagy through its sequestration in autophagosomes. An example of the degradation of peroxisomes through the autophagic pathway has been reported [124]. These matured autophagosomes could then fuse with multivesicular bodies to form another organelle, amphisomes, which eventually fuse with lysosomes. Filimonenko *et al.* reported that functional multivesicular bodies were required for autophagic degradation [125]. By electron microscopy, an amphisome looks very similar to a multivesicular body, so perhaps what we observed in our electron microscopy pictures were actually amphisomes. Alternatively, an AKAP could target RIα directly to multivesicular bodies which then fuse with the matured autophagosome to form amphisomes.

Our electron microscopy results showing RIα GFP inside a membranous compartment seemed inconsistent with the reversibility of the RIα puncta during live cell imaging. To address this question, cells were followed over a longer period of time [Figure 5.13]. From this movie, we observed a few puncta that still remained

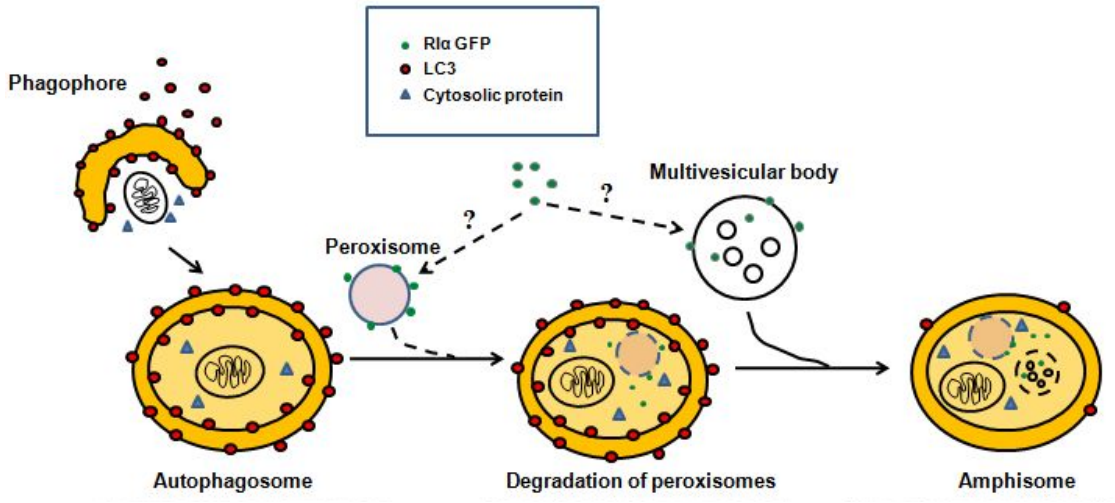

Figure 5.12: A model of targeting to multivesicular bodies.

A model for the merging of peroxisomes and multivesicular bodies is depicted based on results from previous studies [124, 125]. Peroxisomes can be degraded by autophagy by first being isolated by the autophagosomal membranous layers. These autophagosomes can then fuse with multivesicular bodies to form amphisomes. These amphisomes contain both endocytic and autophagic cargo. Representative EM pictures of each step can be obtained from http://cellimages.ascb.org/, where the EM picture of an amphisome looks very similar to one of a multivesicular body.

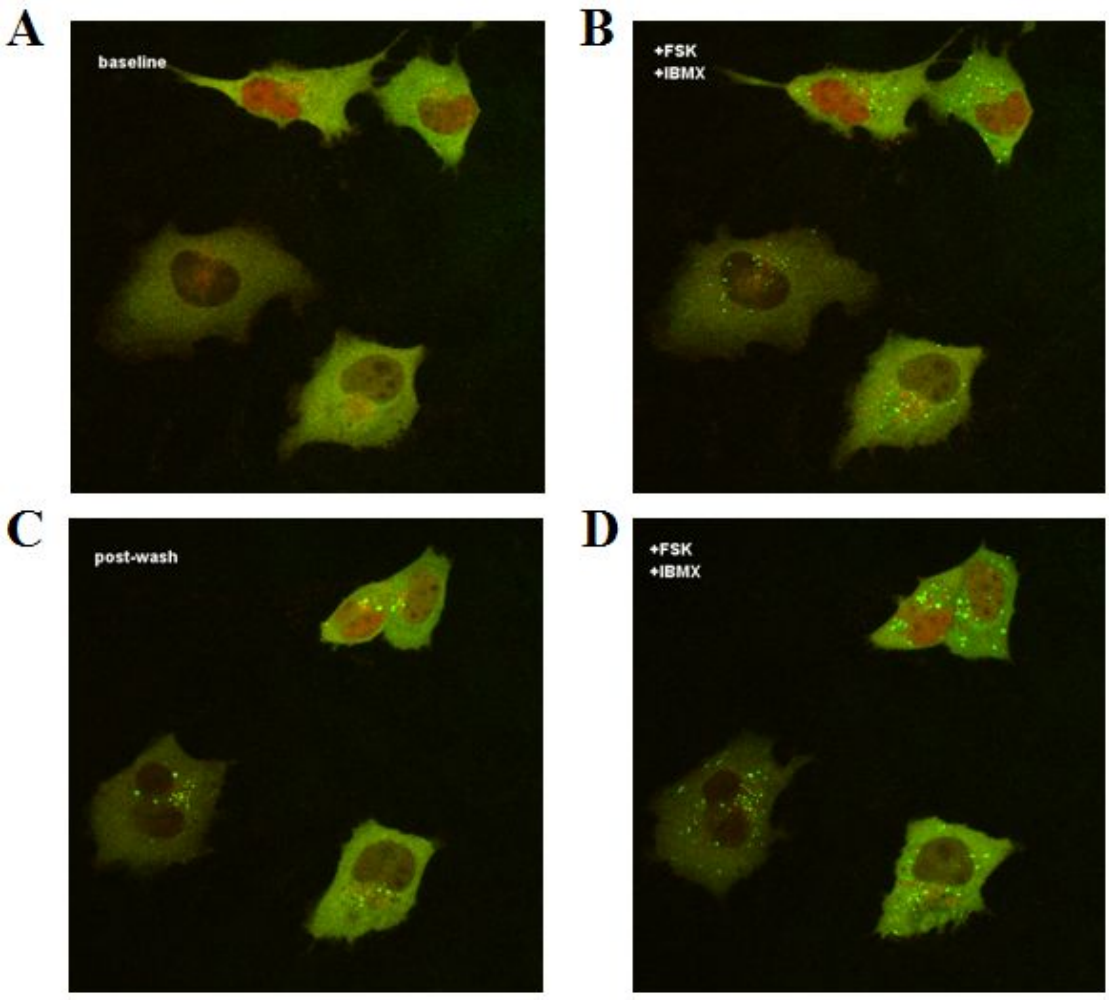

Figure 5.13: Representative pictures from a longer live cell movie.

(A) Co-expression of GFP-tagged RIα and mCherry-tagged PKAc showed a diffuse pattern in *Prkar1a-/-* MEFs.

(B) Similar to the results from Figure 5.2, puncta appeared in the cells after two minutes of treatment with forskolin/IBMX. The forskolin/IBMX treatment was left on the cells for approximately 1.5 hours.

(C) Most of the puncta disappeared within two minutes of treatment removal. However, a few puncta were still observed 45 minutes after the wash.

(D) More puncta reappeared within five minutes of a second round of forskolin/IBMX treatment.

even after washing away the forskolin/IBMX. These puncta could represent RIα molecules that have been engulfed by multivesicular bodies/amphisomes and so were unable to re-enter the cytosolic pool. Perhaps the reason we did not see an overlap of endogenous LC3 with RIα was because RIα and LC3 associate with autophagosomes at different times during the maturation of autophagosomes.

This targeting of RIα could be a method by which cells degrade free RIα to maintain a certain balance with the catalytic subunit. If formation of puncta was a sign of degradation of RIα, then cells may have difficulty degrading R211K and RIα(1-303), which are unable to target to multivesicular bodies. Therefore, it is possible that expression of RIα(1-303) in Carney complex patients could lead to the disease in part because of the inability to properly degrade the protein.

5.5: Acknowledgements

We would like to thank G. Stanley McKnight and James Lim (M. Ginsberg lab) for providing the RIα knockout mouse embryonic fibroblast cells. We would like to thank Brent Martin (R. Tsien lab) for providing mCherry-tagged C-subunit and CFP-tagged PKI, Frank Ma (S. Taylor lab) for AKAR R subunits constructs, Chris Eggers (S. Taylor lab) for mCherry-tagged AKAP constructs, and Suresh Subramani for anti-SKL antibody. We also thank Chris Eggers for help with the colocalization experiment along the endosomal pathway as well as useful discussions regarding the model for targeting. We would also like to thank Juniper Pennypacker for making some of the single site mutations. We appreciate the guidance on analysis of autophagy from Hilde Abrahamsen and Kun-Liang Guan. We express appreciation to many people at the National Center for Microscopy and Imaging Research (NCMIR) at UCSD for technical assistance and/or use of equipment: Fan Chang, Tom Deerinck, Mark Ellisman, Hiro Hakozaki, andYing Jones. We also thank Frank Ma for assistance in the initial stages of the EM analysis. This work was supported by the NIH/NCI Growth Regulation & Oncogenesis Training Grant (M.E.D.) and NIH DK54441 (S.S.T).

Chapter 5, in part, will be submitted for publication. Day, M.E., Gaietta, G., Mackey, M., Perkins, G., and Taylor, S.S. Novel targeting of the RIalpha subunit of PKA, disassociated from C-subunit, is mediated by protein kinase anchoring proteins. The dissertation author was the primary investigator and author of this work.

Chapter 6:

Concluding remarks and future directions

The research presented here provides several directions for future studies of RIα. Though four isoforms of R subunits exist, we chose to study RIα because the importance of maintaining its expression level in cells seems higher than that of the other isoforms. Knockout of RIα leads to embryonic lethality in mice, while overexpression of RIα is seen with breast cancer and underexpression of RIα causes Carney complex (CNC). Using two CNC-associated mutants, R74C and RIα(1-303), we discovered several major findings for the functionality and targeting of RIα.

Summary of results with the R74C mutant. The introduction of the extra cysteine, R74C, changed the disulfide bond formations in RIα [Chapter 2]. Two antiparallel disulfide bonds form between the cysteines in the dimerization/docking (D/D) domain of wild-type RIα. Though the presence of these disulfide bonds are not required for the constitutive formation of RIα dimers, the disulfide bonds form quite readily and have been correlated with a change in localization of RIα in adult rat ventricular myocytes [34]. When the extra cysteine, R74C, was introduced into bacterially expressed RIα, we found that it did not form a disulfide bond with either of the N-terminal cysteines; instead, the extra cysteine formed a disulfide bond with itself within a dimer and also between two dimers, forming a tetramer.

In mammalian cells, we also found an effect with the R74C mutant [Chapter 3]. By treating cells stably expressing TAP-tagged wild-type RIα or TAP-tagged R74C with hydrogen peroxide, all of the RIα subunits were oxidized. These oxidized proteins contained disulfide bonds so that dimers were maintained on a denaturing gel

and we could analyze the formation of homodimers and heterodimers. We found a surprising result. Endogenous RIα homodimers were present with the stable expression of TAP-tagged wild-type RIα; however, endogenous RIα homodimers were not seen with the stable expression of TAP-tagged R74C. This depletion implied that in the presence of mutant RIα, endogenous RIα homodimers could not form.

Summary of results with RIα(1-303). The expression of RIα(1-303) also showed an effect in both bacterial [Chapter 2] and in mammalian cells [Chapter 5]. Holoenzyme of RIα(1-303) showed a four-fold increase in PKA activation compared to wild-type RIα holoenzyme *in vitro*. RIα(1-303) showed a different localization from wild-type RIα when expressed in mammalian cells. GFP-tagged wild-type RIα was diffuse in the cytoplasm and localized to puncta. We found that this puncta was dependent on both disassociation from C-subunit and binding to an A-kinase anchoring protein (AKAP). Because we saw a tight binding of RIα to AKAP11 when studying the RIα interactome in Chapter 4, we suspect that AKAP11 may be the AKAP that is involved in this targeting. The puncta were associated with targeting of RIα to either peroxisomes or multivesicular bodies. Since these puncta were not observed with the expression of GFP-tagged RIα(1-303), this result implied that there may be a mis-targeting of some CNC-associated mutants in mammalian cells.

Potential loss of RIα homodimers through the formation of heterodimers. One main question that arose during our studies is how Carney complex can result from two

different mechanisms: whether there is a haploinsufficiency of RIα or an expression of mutant RIα. Carney complex patients showed a 50% decrease in total levels of wild-type RIα when mutant RIα mRNA was degraded through nonsense-mediated mRNA decay (NMD) [71]. Most of the CNC-associated RIα mutations fall into this category. A few RIα mutations, however, escape NMD regulation and express a mutant protein. For example, in patients where R74C was expressed, the total levels of RIα were unchanged [71], although there was not a discrimination between the wild-type and mutant RIα. Furthermore, the total level of RIα expression is not reflective of the amount of homodimers versus heterodimers. If possible, one should check if homodimers or heterodimers form, as was done with our analysis of cells stably expressing R74C. If this method were used on tissue samples from Carney complex patients, we believe that the amount of endogenous RIα homodimers would be significantly reduced compared to that found in normal patients. This decrease in amount of endogenous RIα homodimers could be similar or worse than the 50% reduction in protein expression levels from the haploinsufficiency of RIα.

Extension of studies from this dissertation. Another question we tried to address was whether novel proteins bind to the mutant homodimer or heterodimer. We found that plakoglobin, a component of desmosomes, bound to R74C but not to wild-type RIα. This novel interaction is an interesting one to pursue further.

The study of the RIα interactome may also be expanded to identify binding partners under specific conditions. The stable cells could be treated with hydrogen

peroxide to see whether novel binding partners bind under oxidizing conditions. We could also elute AKAPs with high affinity AKAP peptides specific for RI following the elution of all AKAPs with cAMP resin. Three examples of these strategies are depicted in Figure 6.1. Through these methods, RI-specific AKAPs may be identified. One AKAP has been identified in *Caenorhabditis elegans* (*C. elegans*) that has high affinity for its one regulatory subunit, that is homologous to RI subunits, but not RII subunits [126]. Thus, there may be other AKAPs that are RI-specific that have yet to be discovered.

RIα and the cell cycle. While we examined the effects of oxidation on RIα disulfide bond formation, we did not explore other conditions. For example, it could prove useful to use these affinity/mass spectrometry methods to study the modification states and binding partners of RIα throughout the cell cycle. Strong evidence showed the involvement of RIα in cell cycle progression and cell growth [54, 55]. Our initial studies also showed an involvement of RIα in cell cycle. When we tested whether expression of the CNC-associated RIα mutants affected cell cycle progression, we found that RIα(1-303) had an effect. Both HEK 293 and HeLa cells were transiently transfected with GFP-tagged constructs and arrested at the G2/M phase by treatment with nocodazole, a tubulin-depolymerizing agent. Flow cytometry data showed that while the HEK 293 cells that were transfected with empty GFP, wild-type RIα, and R74C arrested at the G2/M phase, the cells transfected with RIα(1-303) arrested at the G1/S phase [Figure 6.2A]. The cell cycle analysis was not as clear in the HeLa cells

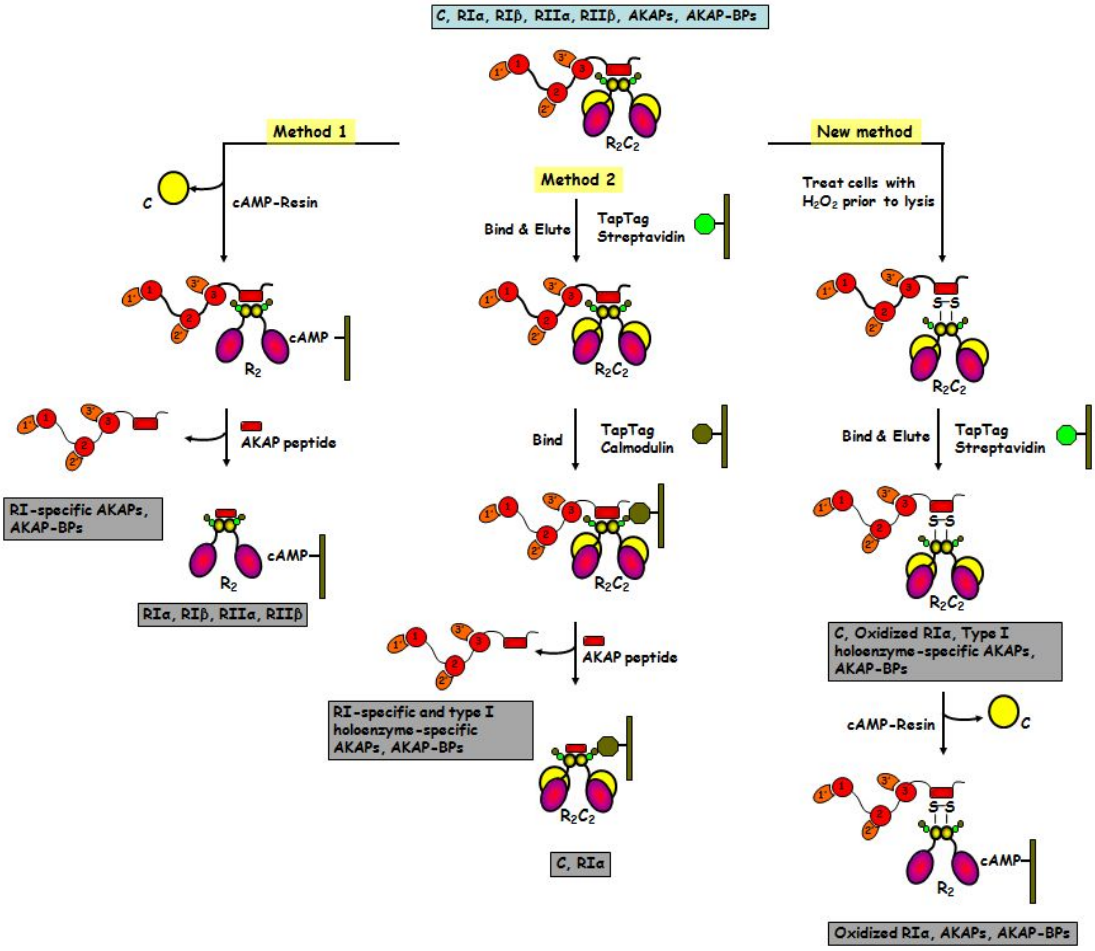

Figure 6.1: Expanded affinity purification methods.

Two of the different affinity methods used to study the RIα interactome from Chapter 4 may be expanded. Additionally, the stable cells may be treated with hydrogen peroxide prior to purification to detect binding partners under oxidizing conditions. The proteins we expect to isolate are highlighted in gray.

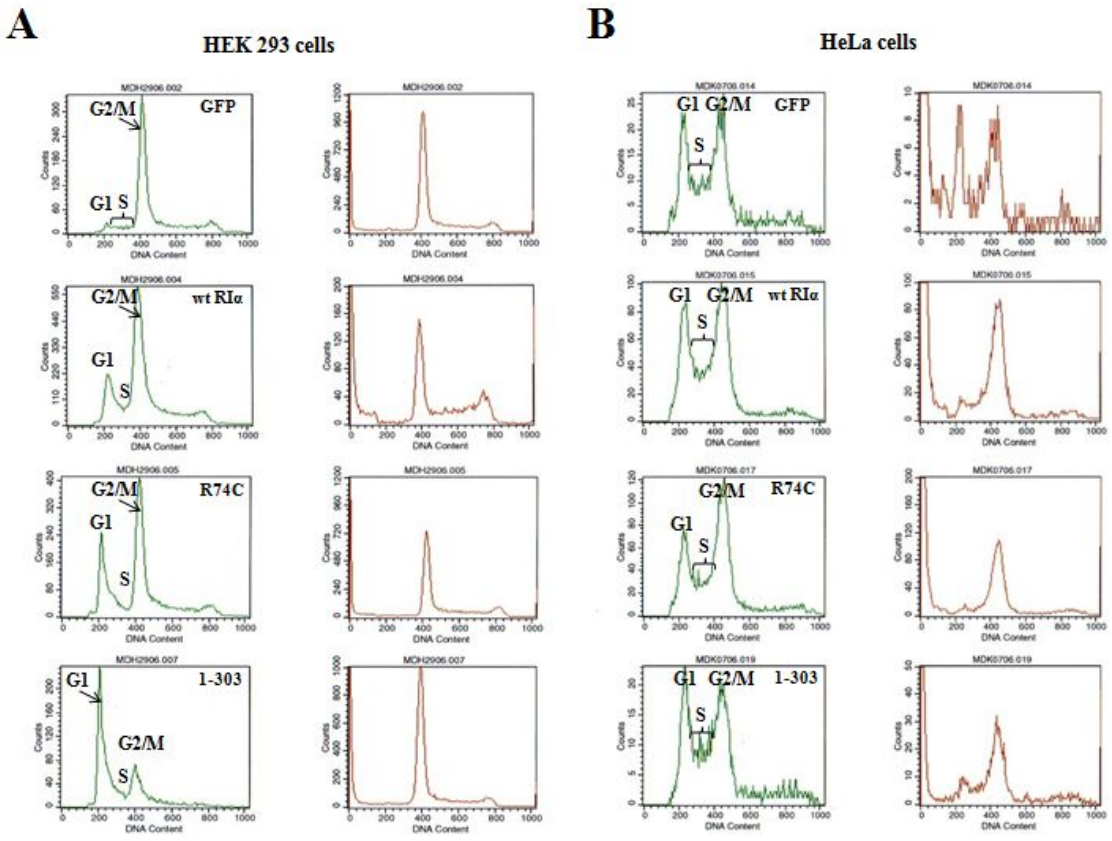

Figure 6.2: Wild-type RIα and R74C showed similar cell cycle progression, while RIα(1-303) showed a change in cell cycle progression.

Both HEK 293 and HeLa cells were transiently transfected with GFP-tagged constructs and treated with nocodazole. The cells were analyzed for stage of cell cycle using flow cytometry. The stage of cell cycle is shown in the left column for each construct, as indicated. The graphs in the right column show that all the cells analyzed were expressing the GFP protein.

(A) HEK 293 cells expressing empty GFP, wild-type RIα, and R74C arrested at G2/M, indicated by the higher peak at DNA content of 400. On the other hand, with transfection of RIα(1-303), more cells arrested at G1/S, indicated by the higher peak at DNA content of 200.

(B) A higher number of HeLa cells expressing empty GFP, wild-type RIα, and R74C arrested at G2/M than at G1/S. Transfection with RIα(1-303) arrested cells equally at both G1/S and G2/M. Greater accumulation in the S phase was seen from the transfection of HeLa cells in all cases.

because of a greater accumulation in the S phase [Figure 6.2B]. However, the cells transfected with empty GFP, wild-type RIα, and R74C showed more cells at the G2/M phase than the G1/S phase. On the other hand, the cells transfected with RIα(1-303) showed equal numbers at both the G1/S and G2/M phases. Therefore, after synchronizing the cells at specific stages, the phosphorylation state of RIα and its binding partners could be compared with those of RIα(1-303).

CNC-associated mutations for future studies. At the time of the studies in this dissertation, only four mutations that escape NMD regulation were known. Since then, many more have been uncovered. Three of the mutations will provide a good start for future studies using the methods described in this dissertation: S9C, A213D, and RIα(Δ61-116) [Figure 6.3]. S9C would result in a mutation close to the cysteines in the D/D domain. Though R74C did not interfere with the N-terminal disulfide bonds, S9C could interfere with the N-terminal cysteines and a change in the disulfide bonds could affect the translocation of RIα under oxidizing conditions. A213D results in a mutation in the phosphate binding cassette (PBC) of cAMP binding domain A (CBD A). A mutation of another residue, R211K, in the PBC of CBD A has already shown a defect in cAMP binding [120]. A similar result is expected with A213D. The expression of this mutant could show a mis-targeting in mammalian cells, similar to what was seen with RIα(1-303). RIα(Δ61-116), which deletes the linker region, would be defective in PKA recognition so that C-subunit would not bind. This mutant, as well as RIα(1-303), could be tested to see if RIα homodimers are lost in

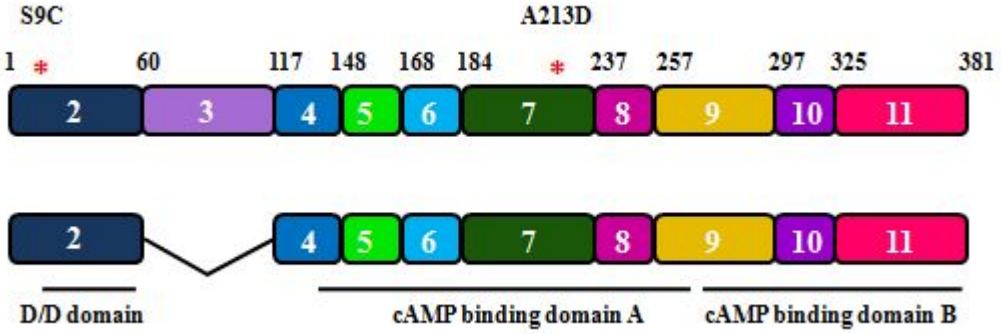

Figure 6.3: CNC-associated mutations for future studies.

Three mutations that would be a good start for future studies are illustrated. S9C is a mutation near the D/D domain, while A213D is a mutation in the phosphate binding cassette of cAMP binding domain A. The other mutation, RIα(Δ61-116), results in a deletion of the linker region.

Carney complex patients, as discussed above. These mutants may be also used to answer the following questions:

Is there a dominant negative effect with heterodimers? One direction that these mutants could be investigated is the characterization of the heterodimers. We showed that heterodimers exist in mammalian cells [Chapter 3]. The effect of these mutant heterodimers could affect PKA activation, translocation, or targeting through a dominant negative effect where one mutant RIα dimerized to wild-type RIα is enough to remove the normal functionality of the RIα dimer. Similar to the search for a change in amount of endogenous RIα homodimers, the effect of introducing these other CNC-associated mutants in the presence of wild-type RIα may also be done. We predict the amount of endogenous RIα homodimers would also be depleted and the presence of only the heterodimers may have a dominant negative effect.

Is there a faster turnover with heterodimers? A plausible mechanism for the depletion of endogenous RIα in the presence of mutant RIα may be due to a faster turnover of mutant heterodimers. A faster turnover of RI subunits versus RII subunits has already been reported [127]. This faster turnover was postulated to be related to the quicker response of RI subunits than RII subunits to increasing cAMP levels, combined with the accelerated degradation of R subunits when disassociated from C-subunit. It is possible that with the R74C mutant as well as with S9C or RIα(Δ61-116), there is an even faster turnover of the mutant homodimer or mutant heterodimer

as the mutants would be less stable. This faster turnover would result in mutant RIα continually drawing away the endogenous RIα to form new heterodimers, thus impeding the formation of endogenous RIα homodimers. Though not tested in this dissertation, one way to analyze the turnover rate could be to measure the rate of degradation using a pulse-chase assay. Assuming that under steady-state conditions, the rate of synthesis and rate of degradation are in equilibrium, either one will be directly correlated with the turnover rate.

Is there a change or disruption in binding partners to CNC-associated mutants? Though not too many novel binding partners were detected with the R74C mutant, many more could be found with the aforementioned CNC-associated mutants in future studies. For example, a heterodimer of wild-type RIα:S9C could change the docking surface in the D/D domain and alter AKAP binding. Perhaps with this mutant, AKAP11 would not be detected through the affinity methods.

Final thoughts. These different paths of future research are not trivial. Though many of the methods have been developed in this dissertation, others may require more optimization in addition to the use of new technologies. However, with continued dedication from other scientists as well as new information from the studies of these CNC-associated mutant RIα subunits, the functionality of RIα with regards to Carney complex may be elucidated.

References

1. Rall, T.W. and Sutherland, E.W., *Formation of a cyclic adenine ribonucleotide by tissue particles.* J Biol Chem, 1958. **232**(2): p. 1065-76.

2. Walsh, D.A., Perkins, J.P., and Krebs, E.G., *An adenosine 3',5'-monophosphate-dependant protein kinase from rabbit skeletal muscle.* J Biol Chem, 1968. **243**(13): p. 3763-5.

3. Gill, G.N. and Garren, L.D., *Role of the receptor in the mechanism of action of adenosine 3':5'-cyclic monophosphate.* Proc Natl Acad Sci U S A, 1971. **68**(4): p. 786-90.

4. Olsen, S.R. and Uhler, M.D., *Inhibition of protein kinase-A by overexpression of the cloned human protein kinase inhibitor.* Mol Endocrinol, 1991. **5**(9): p. 1246-56.

5. Wen, W., Meinkoth, J.L., Tsien, R.Y., and Taylor, S.S., *Identification of a signal for rapid export of proteins from the nucleus.* Cell, 1995. **82**(3): p. 463-73.

6. Reimann, E.M., Walsh, D.A., and Krebs, E.G., *Purification and properties of rabbit skeletal muscle adenosine 3',5'-monophosphate-dependent protein kinases.* J Biol Chem, 1971. **246**(7): p. 1986-95.

7. Lee, D.C., Carmichael, D.F., Krebs, E.G., and McKnight, G.S., *Isolation of a cDNA clone for the type I regulatory subunit of bovine cAMP-dependent protein kinase.* Proc Natl Acad Sci U S A, 1983. **80**(12): p. 3608-12.

8. Clegg, C.H., Cadd, G.G., and McKnight, G.S., *Genetic characterization of a brain-specific form of the type I regulatory subunit of cAMP-dependent protein kinase.* Proc Natl Acad Sci U S A, 1988. **85**(11): p. 3703-7.

9. Scott, J.D., Glaccum, M.B., Zoller, M.J., Uhler, M.D., Helfman, D.M., McKnight, G.S., and Krebs, E.G., *The molecular cloning of a type II regulatory subunit of the cAMP-dependent protein kinase from rat skeletal muscle and mouse brain.* Proc Natl Acad Sci U S A, 1987. **84**(15): p. 5192-6.

10. Jahnsen, T., Hedin, L., Kidd, V.J., Beattie, W.G., Lohmann, S.M., Walter, U., Durica, J., Schulz, T.Z., Schiltz, E., Browner, M., and et al., *Molecular cloning, cDNA structure, and regulation of the regulatory subunit of type II cAMP-dependent protein kinase from rat ovarian granulosa cells.* J Biol Chem, 1986. **261**(26): p. 12352-61.

11. Banky, P., Roy, M., Newlon, M.G., Morikis, D., Haste, N.M., Taylor, S.S., and Jennings, P.A., *Related protein-protein interaction modules present drastically different surface topographies despite a conserved helical platform.* J Mol Biol, 2003. **330**(5): p. 1117-29.

12. Su, Y., Dostmann, W.R., Herberg, F.W., Durick, K., Xuong, N.H., Ten Eyck, L., Taylor, S.S., and Varughese, K.I., *Regulatory subunit of protein kinase A: structure of deletion mutant with cAMP binding domains.* Science, 1995. **269**(5225): p. 807-13.

13. Altschul, S.F., Madden, T.L., Schaffer, A.A., Zhang, J., Zhang, Z., Miller, W., and Lipman, D.J., *Gapped BLAST and PSI-BLAST: a new generation of protein database search programs.* Nucleic Acids Res, 1997. **25**(17): p. 3389-402.

14. Notredame, C., Higgins, D.G., and Heringa, J., *T-Coffee: A novel method for fast and accurate multiple sequence alignment.* J Mol Biol, 2000. **302**(1): p. 205-17.

15. Thompson, J.D., Gibson, T.J., Plewniak, F., Jeanmougin, F., and Higgins, D.G., *The CLUSTAL_X windows interface: flexible strategies for multiple sequence alignment aided by quality analysis tools.* Nucleic Acids Res, 1997. **25**(24): p. 4876-82.

16. Edgar, R.C., *MUSCLE: a multiple sequence alignment method with reduced time and space complexity.* BMC Bioinformatics, 2004. **5**: p. 113.

17. Letunic, I. and Bork, P., *Interactive Tree Of Life (iTOL): an online tool for phylogenetic tree display and annotation.* Bioinformatics, 2007. **23**(1): p. 127-8.

18. Faux, M.C. and Scott, J.D., *More on target with protein phosphorylation: conferring specificity by location.* Trends Biochem Sci, 1996. **21**(8): p. 312-5.

19. Kuettel, M.R., Squinto, S.P., Kwast-Welfeld, J., Schwoch, G., Schweppe, J.S., and Jungmann, R.A., *Localization of nuclear subunits of cyclic AMP-dependent protein kinase by the immunocolloidal gold method.* J Cell Biol, 1985. **101**(3): p. 965-75.

20. Doskeland, S.O., Maronde, E., and Gjertsen, B.T., *The genetic subtypes of cAMP-dependent protein kinase--functionally different or redundant?* Biochim Biophys Acta, 1993. **1178**(3): p. 249-58.

21. Kim, C., Cheng, C.Y., Saldanha, S.A., and Taylor, S.S., *PKA-I holoenzyme structure reveals a mechanism for cAMP-dependent activation.* Cell, 2007. **130**(6): p. 1032-43.

22. Zawadzki, K.M. and Taylor, S.S., *cAMP-dependent protein kinase regulatory subunit type IIbeta: active site mutations define an isoform-specific network for allosteric signaling by cAMP.* J Biol Chem, 2004. **279**(8): p. 7029-36.

23. Herberg, F.W. and Taylor, S.S., *Physiological inhibitors of the catalytic subunit of cAMP-dependent protein kinase: effect of MgATP on protein-protein interactions.* Biochemistry, 1993. **32**(50): p. 14015-22.

24. Zimmermann, B., Schweinsberg, S., Drewianka, S., and Herberg, F.W., *Effect of metal ions on high-affinity binding of pseudosubstrate inhibitors to PKA.* Biochem J, 2008. **413**(1): p. 93-101.

25. Hofmann, F., Beavo, J.A., Bechtel, P.J., and Krebs, E.G., *Comparison of adenosine 3':5'-monophosphate-dependent protein kinases from rabbit skeletal and bovine heart muscle.* J Biol Chem, 1975. **250**(19): p. 7795-801.

26. Tortora, G., Damiano, V., Bianco, C., Baldassarre, G., Bianco, A.R., Lanfrancone, L., Pelicci, P.G., and Ciardiello, F., *The RIalpha subunit of protein kinase A (PKA) binds to Grb2 and allows PKA interaction with the activated EGF-receptor.* Oncogene, 1997. **14**(8): p. 923-8.

27. Hegde, A.N., Goldberg, A.L., and Schwartz, J.H., *Regulatory subunits of cAMP-dependent protein kinases are degraded after conjugation to ubiquitin: a molecular mechanism underlying long-term synaptic plasticity.* Proc Natl Acad Sci U S A, 1993. **90**(16): p. 7436-40.

28. Geahlen, R.L. and Krebs, E.G., *Studies on the phosphorylation of the type I cAMP-dependent protein kinase.* J Biol Chem, 1980. **255**(19): p. 9375-9.

29. Boeshans, K.M., Resing, K.A., Hunt, J.B., Ahn, N.G., and Shabb, J.B., *Structural characterization of the membrane-associated regulatory subunit of type I cAMP-dependent protein kinase by mass spectrometry: identification of Ser81 as the in vivo phosphorylation site of RIalpha.* Protein Sci, 1999. **8**(7): p. 1515-22.

30. Tasken, K., Skalhegg, B.S., Solberg, R., Andersson, K.B., Taylor, S.S., Lea, T., Blomhoff, H.K., Jahnsen, T., and Hansson, V., *Novel isozymes of cAMP-dependent protein kinase exist in human cells due to formation of RI alpha-RI beta heterodimeric complexes.* J Biol Chem, 1993. **268**(28): p. 21276-83.

31. Leon, D.A., Herberg, F.W., Banky, P., and Taylor, S.S., *A stable alpha-helical domain at the N terminus of the RIalpha subunits of cAMP-dependent protein kinase is a novel dimerization/docking motif.* J Biol Chem, 1997. **272**(45): p. 28431-7.

32. Banky, P., Huang, L.J., and Taylor, S.S., *Dimerization/docking domain of the type Ialpha regulatory subunit of cAMP-dependent protein kinase. Requirements for dimerization and docking are distinct but overlapping.* J Biol Chem, 1998. **273**(52): p. 35048-55.

33. Newlon, M.G., Roy, M., Morikis, D., Hausken, Z.E., Coghlan, V., Scott, J.D., and Jennings, P.A., *The molecular basis for protein kinase A anchoring revealed by solution NMR.* Nat Struct Biol, 1999. **6**(3): p. 222-7.

34. Brennan, J.P., Bardswell, S.C., Burgoyne, J.R., Fuller, W., Schroder, E., Wait, R., Begum, S., Kentish, J.C., and Eaton, P., *Oxidant-induced activation of type I protein kinase A is mediated by RI subunit interprotein disulfide bond formation.* J Biol Chem, 2006. **281**(31): p. 21827-36.

35. Gupte, R.S., Pozarowski, P., Grabarek, J., Traganos, F., Darzynkiewicz, Z., and Lee, M.Y., *RIalpha influences cellular proliferation in cancer cells by transporting RFC40 into the nucleus.* Cancer Biol Ther, 2005. **4**(4): p. 429-37.

36. Gupte, R.S., Weng, Y., Liu, L., and Lee, M.Y., *The second subunit of the replication factor C complex (RFC40) and the regulatory subunit (RIalpha) of protein kinase A form a protein complex promoting cell survival.* Cell Cycle, 2005. **4**(2): p. 323-9.

37. Beene, D.L. and Scott, J.D., *A-kinase anchoring proteins take shape.* Curr Opin Cell Biol, 2007. **19**(2): p. 192-8.

38. Huang, L.J., Durick, K., Weiner, J.A., Chun, J., and Taylor, S.S., *Identification of a novel protein kinase A anchoring protein that binds both type I and type II regulatory subunits.* J Biol Chem, 1997. **272**(12): p. 8057-64.

39. Huang, L.J., Durick, K., Weiner, J.A., Chun, J., and Taylor, S.S., *D-AKAP2, a novel protein kinase A anchoring protein with a putative RGS domain.* Proc Natl Acad Sci U S A, 1997. **94**(21): p. 11184-9.

40. Herberg, F.W., Maleszka, A., Eide, T., Vossebein, L., and Tasken, K., *Analysis of A-kinase anchoring protein (AKAP) interaction with protein kinase A (PKA) regulatory subunits: PKA isoform specificity in AKAP binding.* J Mol Biol, 2000. **298**(2): p. 329-39.

41. Burns-Hamuro, L.L., Ma, Y., Kammerer, S., Reineke, U., Self, C., Cook, C., Olson, G.L., Cantor, C.R., Braun, A., and Taylor, S.S., *Designing isoform-specific peptide disruptors of protein kinase A localization.* Proc Natl Acad Sci U S A, 2003. **100**(7): p. 4072-7.

42. Brandon, E.P., Zhuo, M., Huang, Y.Y., Qi, M., Gerhold, K.A., Burton, K.A., Kandel, E.R., McKnight, G.S., and Idzerda, R.L., *Hippocampal long-term depression and depotentiation are defective in mice carrying a targeted disruption of the gene encoding the RI beta subunit of cAMP-dependent protein kinase.* Proc Natl Acad Sci U S A, 1995. **92**(19): p. 8851-5.

43. Burton, K.A., Treash-Osio, B., Muller, C.H., Dunphy, E.L., and McKnight, G.S., *Deletion of type IIalpha regulatory subunit delocalizes protein kinase A*

in mouse sperm without affecting motility or fertilization. J Biol Chem, 1999. **274**(34): p. 24131-6.

44. McKnight, G.S., Cummings, D.E., Amieux, P.S., Sikorski, M.A., Brandon, E.P., Planas, J.V., Motamed, K., and Idzerda, R.L., *Cyclic AMP, PKA, and the physiological regulation of adiposity.* Recent Prog Horm Res, 1998. **53**: p. 139-59; discussion 160-1.

45. Amieux, P.S., Cummings, D.E., Motamed, K., Brandon, E.P., Wailes, L.A., Le, K., Idzerda, R.L., and McKnight, G.S., *Compensatory regulation of RIalpha protein levels in protein kinase A mutant mice.* J Biol Chem, 1997. **272**(7): p. 3993-8.

46. Thiele, T.E., Willis, B., Stadler, J., Reynolds, J.G., Bernstein, I.L., and McKnight, G.S., *High ethanol consumption and low sensitivity to ethanol-induced sedation in protein kinase A-mutant mice.* J Neurosci, 2000. **20**(10): p. RC75.

47. Amieux, P.S. and McKnight, G.S., *The essential role of RI alpha in the maintenance of regulated PKA activity.* Ann N Y Acad Sci, 2002. **968**: p. 75-95.

48. Uhler, M.D. and McKnight, G.S., *Expression of cDNAs for two isoforms of the catalytic subunit of cAMP-dependent protein kinase.* J Biol Chem, 1987. **262**(31): p. 15202-7.

49. Jones, K.W., Shapero, M.H., Chevrette, M., and Fournier, R.E., *Subtractive hybridization cloning of a tissue-specific extinguisher: TSE1 encodes a regulatory subunit of protein kinase A.* Cell, 1991. **66**(5): p. 861-72.

50. Boshart, M., Weih, F., Nichols, M., and Schutz, G., *The tissue-specific extinguisher locus TSE1 encodes a regulatory subunit of cAMP-dependent protein kinase.* Cell, 1991. **66**(5): p. 849-59.

51. Solberg, R., Sandberg, M., Natarajan, V., Torjesen, P.A., Hansson, V., Jahnsen, T., and Tasken, K., *The human gene for the regulatory subunit RI alpha of cyclic adenosine 3', 5'-monophosphate-dependent protein kinase: two*

distinct promoters provide differential regulation of alternately spliced messenger ribonucleic acids. Endocrinology, 1997. **138**(1): p. 169-81.

52. Su, A.I., Wiltshire, T., Batalov, S., Lapp, H., Ching, K.A., Block, D., Zhang, J., Soden, R., Hayakawa, M., Kreiman, G., Cooke, M.P., Walker, J.R., and Hogenesch, J.B., *A gene atlas of the mouse and human protein-encoding transcriptomes.* Proc Natl Acad Sci U S A, 2004. **101**(16): p. 6062-7.

53. Imaizumi-Scherrer, T., Faust, D.M., Barradeau, S., Hellio, R., and Weiss, M.C., *Type I protein kinase a is localized to interphase microtubules and strongly associated with the mitotic spindle.* Exp Cell Res, 2001. **264**(2): p. 250-65.

54. Tortora, G., Pepe, S., Bianco, C., Baldassarre, G., Budillon, A., Clair, T., Cho-Chung, Y.S., Bianco, A.R., and Ciardiello, F., *The RI alpha subunit of protein kinase A controls serum dependency and entry into cell cycle of human mammary epithelial cells.* Oncogene, 1994. **9**(11): p. 3233-40.

55. Tortora, G., Pepe, S., Bianco, C., Damiano, V., Ruggiero, A., Baldassarre, G., Corbo, C., Cho-Chung, Y.S., Bianco, A.R., and Ciardiello, F., *Differential effects of protein kinase A sub-units on Chinese-hamster-ovary cell cycle and proliferation.* Int J Cancer, 1994. **59**(5): p. 712-6.

56. Budovskaya, Y.V., Stephan, J.S., Deminoff, S.J., and Herman, P.K., *An evolutionary proteomics approach identifies substrates of the cAMP-dependent protein kinase.* Proc Natl Acad Sci U S A, 2005. **102**(39): p. 13933-8.

57. Budovskaya, Y.V., Stephan, J.S., Reggiori, F., Klionsky, D.J., and Herman, P.K., *The Ras/cAMP-dependent protein kinase signaling pathway regulates an early step of the autophagy process in Saccharomyces cerevisiae.* J Biol Chem, 2004. **279**(20): p. 20663-71.

58. Mavrakis, M., Lippincott-Schwartz, J., Stratakis, C.A., and Bossis, I., *Depletion of type IA regulatory subunit (RIalpha) of protein kinase A (PKA) in mammalian cells and tissues activates mTOR and causes autophagic deficiency.* Hum Mol Genet, 2006. **15**(19): p. 2962-71.

59. Casey, M., Vaughan, C.J., He, J., Hatcher, C.J., Winter, J.M., Weremowicz, S., Montgomery, K., Kucherlapati, R., Morton, C.C., and Basson, C.T., *Mutations in the protein kinase A R1alpha regulatory subunit cause familial cardiac myxomas and Carney complex.* J Clin Invest, 2000. **106**(5): p. R31-8.

60. Sandrini, F., Matyakhina, L., Sarlis, N.J., Kirschner, L.S., Farmakidis, C., Gimm, O., and Stratakis, C.A., *Regulatory subunit type I-alpha of protein kinase A (PRKAR1A): a tumor-suppressor gene for sporadic thyroid cancer.* Genes Chromosomes Cancer, 2002. **35**(2): p. 182-92.

61. Kammer, G.M., Khan, I.U., Kammer, J.A., Olorenshaw, I., and Mathis, D., *Deficient type I protein kinase A isozyme activity in systemic lupus erythematosus T lymphocytes: II. Abnormal isozyme kinetics.* J Immunol, 1996. **157**(6): p. 2690-8.

62. Miller, W.R., *Regulatory subunits of PKA and breast cancer.* Ann N Y Acad Sci, 2002. **968**: p. 37-48.

63. Nesterova, M.V. and Cho-Chung, Y.S., *Chemoprevention with protein kinase A RIalpha antisense in DMBA-mammary carcinogenesis.* Ann N Y Acad Sci, 2005. **1058**: p. 255-64.

64. Chen, H.X., Marshall, J.L., Ness, E., Martin, R.R., Dvorchik, B., Rizvi, N., Marquis, J., McKinlay, M., Dahut, W., and Hawkins, M.J., *A safety and pharmacokinetic study of a mixed-backbone oligonucleotide (GEM231) targeting the type I protein kinase A by two-hour infusions in patients with refractory solid tumors.* Clin Cancer Res, 2000. **6**(4): p. 1259-66.

65. Goel, S., Desai, K., Macapinlac, M., Wadler, S., Goldberg, G., Fields, A., Einstein, M., Volterra, F., Wong, B., Martin, R., and Mani, S., *A phase I safety and dose escalation trial of docetaxel combined with GEM231, a second generation antisense oligonucleotide targeting protein kinase A R1alpha in patients with advanced solid cancers.* Invest New Drugs, 2006. **24**(2): p. 125-34.

66. Kammer, G.M., Laxminarayana, D., and Khan, I.U., *Mechanisms of deficient type I protein kinase A activity in lupus T lymphocytes.* Int Rev Immunol, 2004. **23**(3-4): p. 225-44.

67. Kirschner, L.S., Carney, J.A., Pack, S.D., Taymans, S.E., Giatzakis, C., Cho, Y.S., Cho-Chung, Y.S., and Stratakis, C.A., *Mutations of the gene encoding the protein kinase A type I-alpha regulatory subunit in patients with the Carney complex.* Nat Genet, 2000. **26**(1): p. 89-92.

68. Boikos, S.A. and Stratakis, C.A., *Carney complex: the first 20 years.* Curr Opin Oncol, 2007. **19**(1): p. 24-9.

69. Thermann, R., Neu-Yilik, G., Deters, A., Frede, U., Wehr, K., Hagemeier, C., Hentze, M.W., and Kulozik, A.E., *Binary specification of nonsense codons by splicing and cytoplasmic translation.* EMBO J, 1998. **17**(12): p. 3484-94.

70. Bubis, J., Vedvick, T.S., and Taylor, S.S., *Antiparallel alignment of the two protomers of the regulatory subunit dimer of cAMP-dependent protein kinase I.* J Biol Chem, 1987. **262**(31): p. 14961-6.

71. Veugelers, M., Wilkes, D., Burton, K., McDermott, D.A., Song, Y., Goldstein, M.M., La Perle, K., Vaughan, C.J., O'Hagan, A., Bennett, K.R., Meyer, B.J., Legius, E., Karttunen, M., Norio, R., Kaariainen, H., Lavyne, M., Neau, J.P., Richter, G., Kirali, K., Farnsworth, A., Stapleton, K., Morelli, P., Takanashi, Y., Bamforth, J.S., Eitelberger, F., Noszian, I., Manfroi, W., Powers, J., Mochizuki, Y., Imai, T., Ko, G.T., Driscoll, D.A., Goldmuntz, E., Edelberg, J.M., Collins, A., Eccles, D., Irvine, A.D., McKnight, G.S., and Basson, C.T., *Comparative PRKAR1A genotype-phenotype analyses in humans with Carney complex and prkar1a haploinsufficient mice.* Proc Natl Acad Sci U S A, 2004. **101**(39): p. 14222-7.

72. Kirschner, L.S., Sandrini, F., Monbo, J., Lin, J.P., Carney, J.A., and Stratakis, C.A., *Genetic heterogeneity and spectrum of mutations of the PRKAR1A gene in patients with the carney complex.* Hum Mol Genet, 2000. **9**(20): p. 3037-46.

73. Greene, E.L., Horvath, A.D., Nesterova, M., Giatzakis, C., Bossis, I., and Stratakis, C.A., *In vitro functional studies of naturally occurring pathogenic PRKAR1A mutations that are not subject to nonsense mRNA decay.* Hum Mutat, 2008. **29**(5): p. 633-9.

74. Gangal, M., Cox, S., Lew, J., Clifford, T., Garrod, S.M., Aschbaher, M., Taylor, S.S., and Johnson, D.A., *Backbone flexibility of five sites on the*

catalytic subunit of cAMP-dependent protein kinase in the open and closed conformations. Biochemistry, 1998. **37**(39): p. 13728-35.

75. Varshavsky, A., *The N-end rule.* Cell, 1992. **69**(5): p. 725-35.

76. Potter, R.L. and Taylor, S.S., *The structural domains of cAMP-dependent protein kinase I. Characterization of two sites of proteolytic cleavage and homologies to cAMP-dependent protein kinase II.* J Biol Chem, 1980. **255**(20): p. 9706-12.

77. Skalhegg, B.S., Huang, Y., Su, T., Idzerda, R.L., McKnight, G.S., and Burton, K.A., *Mutation of the Calpha subunit of PKA leads to growth retardation and sperm dysfunction.* Mol Endocrinol, 2002. **16**(3): p. 630-9.

78. Carlson, C.R., Ruppelt, A., and Tasken, K., *A kinase anchoring protein (AKAP) interaction and dimerization of the RIalpha and RIbeta regulatory subunits of protein kinase a in vivo by the yeast two hybrid system.* J Mol Biol, 2003. **327**(3): p. 609-18.

79. Rubin, C.S., Erlichman, J., and Rosen, O.M., *Molecular forms and subunit composition of a cyclic adenosine 3',5'-monophosphate-dependent protein kinase purified from bovine heart muscle.* J Biol Chem, 1972. **247**(1): p. 36-44.

80. Miki, K. and Eddy, E.M., *Identification of tethering domains for protein kinase A type Ialpha regulatory subunits on sperm fibrous sheath protein FSC1.* J Biol Chem, 1998. **273**(51): p. 34384-90.

81. Brown, R.L., August, S.L., Williams, C.J., and Moss, S.B., *AKAP7gamma is a nuclear RI-binding AKAP.* Biochem Biophys Res Commun, 2003. **306**(2): p. 394-401.

82. Reinton, N., Collas, P., Haugen, T.B., Skalhegg, B.S., Hansson, V., Jahnsen, T., and Tasken, K., *Localization of a novel human A-kinase-anchoring protein, hAKAP220, during spermatogenesis.* Dev Biol, 2000. **223**(1): p. 194-204.

83. Li, H., Adamik, R., Pacheco-Rodriguez, G., Moss, J., and Vaughan, M., *Protein kinase A-anchoring (AKAP) domains in brefeldin A-inhibited guanine*

nucleotide-exchange protein 2 (BIG2). Proc Natl Acad Sci U S A, 2003. **100**(4): p. 1627-32.

84. Zimmermann, B., Chiorini, J.A., Ma, Y., Kotin, R.M., and Herberg, F.W., *PrKX is a novel catalytic subunit of the cAMP-dependent protein kinase regulated by the regulatory subunit type I.* J Biol Chem, 1999. **274**(9): p. 5370-8.

85. Kussel-Andermann, P., El-Amraoui, A., Safieddine, S., Hardelin, J.P., Nouaille, S., Camonis, J., and Petit, C., *Unconventional myosin VIIA is a novel A-kinase-anchoring protein.* J Biol Chem, 2000. **275**(38): p. 29654-9.

86. Lim, C.J., Han, J., Yousefi, N., Ma, Y., Amieux, P.S., McKnight, G.S., Taylor, S.S., and Ginsberg, M.H., *Alpha4 integrins are type I cAMP-dependent protein kinase-anchoring proteins.* Nat Cell Biol, 2007. **9**(4): p. 415-21.

87. Gupte, R.S., Traganos, F., Darzynkiewicz, Z., and Lee, M.Y., *Phosphorylation of RIalpha by cyclin-dependent kinase CDK 2/cyclin E modulates the dissociation of the RIalpha-RFC40 complex.* Cell Cycle, 2006. **5**(6): p. 653-60.

88. Foster, L.J., Rudich, A., Talior, I., Patel, N., Huang, X., Furtado, L.M., Bilan, P.J., Mann, M., and Klip, A., *Insulin-dependent interactions of proteins with GLUT4 revealed through stable isotope labeling by amino acids in cell culture (SILAC).* J Proteome Res, 2006. **5**(1): p. 64-75.

89. Yang, W.L., Iacono, L., Tang, W.M., and Chin, K.V., *Novel function of the regulatory subunit of protein kinase A: regulation of cytochrome c oxidase activity and cytochrome c release.* Biochemistry, 1998. **37**(40): p. 14175-80.

90. Pasqualucci, L., Kitaura, Y., Gu, H., and Dalla-Favera, R., *PKA-mediated phosphorylation regulates the function of activation-induced deaminase (AID) in B cells.* Proc Natl Acad Sci U S A, 2006. **103**(2): p. 395-400.

91. Rual, J.F., Venkatesan, K., Hao, T., Hirozane-Kishikawa, T., Dricot, A., Li, N., Berriz, G.F., Gibbons, F.D., Dreze, M., Ayivi-Guedehoussou, N., Klitgord, N., Simon, C., Boxem, M., Milstein, S., Rosenberg, J., Goldberg, D.S., Zhang, L.V., Wong, S.L., Franklin, G., Li, S., Albala, J.S., Lim, J., Fraughton, C., Llamosas, E., Cevik, S., Bex, C., Lamesch, P., Sikorski, R.S., Vandenhaute, J.,

Zoghbi, H.Y., Smolyar, A., Bosak, S., Sequerra, R., Doucette-Stamm, L., Cusick, M.E., Hill, D.E., Roth, F.P., and Vidal, M., *Towards a proteome-scale map of the human protein-protein interaction network.* Nature, 2005. **437**(7062): p. 1173-8.

92. Li, H., Degenhardt, B., Tobin, D., Yao, Z.X., Tasken, K., and Papadopoulos, V., *Identification, localization, and function in steroidogenesis of PAP7: a peripheral-type benzodiazepine receptor- and PKA (RIalpha)-associated protein.* Mol Endocrinol, 2001. **15**(12): p. 2211-28.

93. Ewing, R.M., Chu, P., Elisma, F., Li, H., Taylor, P., Climie, S., McBroom-Cerajewski, L., Robinson, M.D., O'Connor, L., Li, M., Taylor, R., Dharsee, M., Ho, Y., Heilbut, A., Moore, L., Zhang, S., Ornatsky, O., Bukhman, Y.V., Ethier, M., Sheng, Y., Vasilescu, J., Abu-Farha, M., Lambert, J.P., Duewel, H.S., Stewart, II, Kuehl, B., Hogue, K., Colwill, K., Gladwish, K., Muskat, B., Kinach, R., Adams, S.L., Moran, M.F., Morin, G.B., Topaloglou, T., and Figeys, D., *Large-scale mapping of human protein-protein interactions by mass spectrometry.* Mol Syst Biol, 2007. **3**: p. 89.

94. Chaturvedi, D., Poppleton, H.M., Stringfield, T., Barbier, A., and Patel, T.B., *Subcellular localization and biological actions of activated RSK1 are determined by its interactions with subunits of cyclic AMP-dependent protein kinase.* Mol Cell Biol, 2006. **26**(12): p. 4586-600.

95. Diskar, M., Zenn, H.M., Kaupisch, A., Prinz, A., and Herberg, F.W., *Molecular basis for isoform-specific autoregulation of protein kinase A.* Cell Signal, 2007. **19**(10): p. 2024-34.

96. Tanner, S., Shu, H., Frank, A., Wang, L.C., Zandi, E., Mumby, M., Pevzner, P.A., and Bafna, V., *InsPecT: identification of posttranslationally modified peptides from tandem mass spectra.* Anal Chem, 2005. **77**(14): p. 4626-39.

97. Schmidt, P.H., Dransfield, D.T., Claudio, J.O., Hawley, R.G., Trotter, K.W., Milgram, S.L., and Goldenring, J.R., *AKAP350, a multiply spliced protein kinase A-anchoring protein associated with centrosomes.* J Biol Chem, 1999. **274**(5): p. 3055-66.

98. Michel, J.J. and Scott, J.D., *AKAP mediated signal transduction.* Annu Rev Pharmacol Toxicol, 2002. **42**: p. 235-57.

99. Takahashi, M., Shibata, H., Shimakawa, M., Miyamoto, M., Mukai, H., and Ono, Y., *Characterization of a novel giant scaffolding protein, CG-NAP, that anchors multiple signaling enzymes to centrosome and the golgi apparatus.* J Biol Chem, 1999. **274**(24): p. 17267-74.

100. Keryer, G., Rios, R.M., Landmark, B.F., Skalhegg, B., Lohmann, S.M., and Bornens, M., *A high-affinity binding protein for the regulatory subunit of cAMP-dependent protein kinase II in the centrosome of human cells.* Exp Cell Res, 1993. **204**(2): p. 230-40.

101. Wang, H.Y., Tao, J., Shumay, E., and Malbon, C.C., *G-Protein-coupled receptor-associated A-kinase anchoring proteins: AKAP79 and AKAP250 (gravin).* Eur J Cell Biol, 2006. **85**(7): p. 643-50.

102. Neuberger, G., Schneider, G., and Eisenhaber, F., *pkaPS: prediction of protein kinase A phosphorylation sites with the simplified kinase-substrate binding model.* Biol Direct, 2007. **2**: p. 1.

103. Kukalev, A., Nord, Y., Palmberg, C., Bergman, T., and Percipalle, P., *Actin and hnRNP U cooperate for productive transcription by RNA polymerase II.* Nat Struct Mol Biol, 2005. **12**(3): p. 238-44.

104. Roshon, M.J. and Ruley, H.E., *Hypomorphic mutation in hnRNP U results in post-implantation lethality.* Transgenic Res, 2005. **14**(2): p. 179-92.

105. Pomerantz, A.H., Allfrey, V.G., Merrifield, R.B., and Johnson, E.M., *Studies on the mechanism of phosphorylation of synthetic polypeptides by a calf thymus cyclic AMP-dependent protein kinase.* Proc Natl Acad Sci U S A, 1977. **74**(10): p. 4261-5.

106. DeManno, D.A., Cottom, J.E., Kline, M.P., Peters, C.A., Maizels, E.T., and Hunzicker-Dunn, M., *Follicle-stimulating hormone promotes histone H3 phosphorylation on serine-10.* Mol Endocrinol, 1999. **13**(1): p. 91-105.

107. Frajnt, M. and Jakubowicz, T., *The effect of vanadate on Pichia pastoris growth, protein kinase A activity and ribosomal protein phosphorylation.*

108. Hashimoto, E., Takeda, M., Nishizuka, Y., Hamana, K., and Iwai, K., *Studies on the sites in histones phosphorylated by adenosine 3':5'-monophosphate-dependent and guanosine 3':5'-monophosphate-dependent protein kinases.* J Biol Chem, 1976. **251**(20): p. 6287-93.

109. Corbin, J.D., Keely, S.L., and Park, C.R., *The distribution and dissociation of cyclic adenosine 3':5'-monophosphate-dependent protein kinases in adipose, cardiac, and other tissues.* J Biol Chem, 1975. **250**(1): p. 218-25.

110. Kirchhof, P., Fabritz, L., Zwiener, M., Witt, H., Schafers, M., Zellerhoff, S., Paul, M., Athai, T., Hiller, K.H., Baba, H.A., Breithardt, G., Ruiz, P., Wichter, T., and Levkau, B., *Age- and training-dependent development of arrhythmogenic right ventricular cardiomyopathy in heterozygous plakoglobin-deficient mice.* Circulation, 2006. **114**(17): p. 1799-806.

111. Lester, L.B., Coghlan, V.M., Nauert, B., and Scott, J.D., *Cloning and characterization of a novel A-kinase anchoring protein. AKAP 220, association with testicular peroxisomes.* J Biol Chem, 1996. **271**(16): p. 9460-5.

112. Su, A.I., Cooke, M.P., Ching, K.A., Hakak, Y., Walker, J.R., Wiltshire, T., Orth, A.P., Vega, R.G., Sapinoso, L.M., Moqrich, A., Patapoutian, A., Hampton, G.M., Schultz, P.G., and Hogenesch, J.B., *Large-scale analysis of the human and mouse transcriptomes.* Proc Natl Acad Sci U S A, 2002. **99**(7): p. 4465-70.

113. Garnis, C., Rosin, M.P., Zhang, L., and Lam, W.L., *Alteration of AKAP220, an upstream component of the Rb pathway, in oral carcinogenesis.* Int J Cancer, 2005. **116**(5): p. 813-9.

114. Schillace, R.V. and Scott, J.D., *Association of the type 1 protein phosphatase PP1 with the A-kinase anchoring protein AKAP220.* Curr Biol, 1999. **9**(6): p. 321-4.

115. Schillace, R.V., Voltz, J.W., Sim, A.T., Shenolikar, S., and Scott, J.D., *Multiple interactions within the AKAP220 signaling complex contribute to protein phosphatase 1 regulation.* J Biol Chem, 2001. **276**(15): p. 12128-34.

116. Rubin, E., Tamrakar, S., and Ludlow, J.W., *Protein phosphatase type 1, the product of the retinoblastoma susceptibility gene, and cell cycle control.* Front Biosci, 1998. **3**: p. D1209-19.

117. Barradeau, S., Imaizumi-Scherrer, T., Weiss, M.C., and Faust, D.M., *Intracellular targeting of the type-I alpha regulatory subunit of cAMP-dependent protein kinase.* Trends Cardiovasc Med, 2002. **12**(6): p. 235-41.

118. Skalhegg, B.S., Tasken, K., Hansson, V., Huitfeldt, H.S., Jahnsen, T., and Lea, T., *Location of cAMP-dependent protein kinase type I with the TCR-CD3 complex.* Science, 1994. **263**(5143): p. 84-7.

119. Abramoff, M.D., Magelhaes, P.J., and Ram, S.J., *Image processing with ImageJ, Biophoton*. 2004, Int.

120. Herberg, F.W., Taylor, S.S., and Dostmann, W.R., *Active site mutations define the pathway for the cooperative activation of cAMP-dependent protein kinase.* Biochemistry, 1996. **35**(9): p. 2934-42.

121. Clague, M.J. and Urbe, S., *Multivesicular bodies.* Curr Biol, 2008. **18**(10): p. R402-4.

122. Woodman, P.G. and Futter, C.E., *Multivesicular bodies: co-ordinated progression to maturity.* Curr Opin Cell Biol, 2008. **20**(4): p. 408-14.

123. Di Franco, A., Russo, M., and Martelli, G.P., *Ultrastructure and Origin of Cytoplasmic Multivesicular Bodies Induced by Carnation Italian Ringspot Virus.* Journal of General Virology, 1984. **65**(7): p. 1233.

124. Iwata, J., Ezaki, J., Komatsu, M., Yokota, S., Ueno, T., Tanida, I., Chiba, T., Tanaka, K., and Kominami, E., *Excess peroxisomes are degraded by autophagic machinery in mammals.* J Biol Chem, 2006. **281**(7): p. 4035-41.

125. Filimonenko, M., Stuffers, S., Raiborg, C., Yamamoto, A., Malerod, L., Fisher, E.M., Isaacs, A., Brech, A., Stenmark, H., and Simonsen, A., *Functional multivesicular bodies are required for autophagic clearance of protein*

aggregates associated with neurodegenerative disease. J Cell Biol, 2007. **179**(3): p. 485-500.

126. Angelo, R.G. and Rubin, C.S., *Characterization of structural features that mediate the tethering of Caenorhabditis elegans protein kinase A to a novel A kinase anchor protein. Insights into the anchoring of PKAI isoforms.* J Biol Chem, 2000. **275**(6): p. 4351-62.

127. Weber, W. and Hilz, H., *cAMP-dependent protein kinases I and II: divergent turnover of subunits.* Biochemistry, 1986. **25**(19): p. 5661-7.